THE UNIVERSITY OF CALGARY

Solution-Gas Drive in Heavy Oil - Gas Mobility and Kinetics of Bubble Growth

by

Rajneesh Kumar

A THESIS

SUBMITTED TO THE FACULTY OF GRADUATE STUDIES IN PARTIAL FULFILLMENT OF THE REQUIREMENTS FOR THE DEGREE OF

MASTER OF SCIENCE IN CHEMICAL ENGINEERING

Department of Chemical and Petroleum Engineering

Calgary, Alberta

December, 1999

Abstract

Some of the heavy oil reservoirs in Canada and Venezuela under solution-gas drive show anomalous behaviour, when compared to conventional light oil reservoirs. Once below the bubble point pressure, producing GOR does not increase sharply and rate of pressure drop is low. Some wells show higher oil production rates than those predicted using conventional flow equations in radial coordinate. The overall recovery under solution-gas drive is higher than that expected from a similar conventional oil reservoir.

Research was initiated to study solution-gas drive in heavy oil reservoirs, and investigate the reasons for the favourable behaviour. In the first part of the research program, gas phase growth was studied by modelling bubble growth in bulk and comparing growth in light and heavy oil. The effect of step and gradual change in pressure was studied. Further, a model was developed to study gas phase growth, in a closed system, for constant volumetric rate depletion. Sensitivity of various parameters on behaviour of the system was studied. One of the findings of the study was that, the pressure in the system can fall even after generation of bubbles in the system. Thus, the bubble nucleation need not coincide with the minimum point on the P-V curve (known as "Critical Supersaturation"). A new term "Apparent Critical Supersaturation" was coined to represent minimum point on the P-V curve.

In the second part of the project, flow experiments were performed to measure the mobility of gas in heavy oil. Depletion was performed at various rates to study the effect of depletion rate on critical gas saturation and supersaturation. The experimental data was matched on Eclipse-100 black oil simulator to determine the gas relative permeability at various depletion rates.

Results indicate that the gas relative permeability under solution-gas drive in heavy oil is very low. This is attributed as one of the factors leading to favourable behaviour of heavy oil reservoirs.

Acknowledgement

This work was a result of continued support, guidance, encouragement, understanding and patience of many individuals and organisations. Although the efforts have been priceless, I would like to gratefully thank all of them for their contributions.

First of all, I would like to thank my supervisor, Dr. Mehran Pooladi-Darvish, for providing me an opportunity to pursue a Masters degree. His knowledge of the project and enthusiasm was infectious. He was always polite, encouraging and accessible any time of the day for fruitful discussions. He provided me opportunity to perform independence research; nonetheless being always there when I needed him. I also thank him for all the non-project related discussions we had. I was fortunate to have such an understanding supervisor and I can say that in this process I found a nice friend.

The experiments were carried out at the Imperial Oil Research Centre in Calgary. I consider myself fortunate enough to be associated with such an organisation and would cherish the memories I had here. I would like to thank Dr. Tadahiro Okazawa for providing guidance, support and valuable suggestions for this work.

I wish to acknowledge Ms. Kathleen Corry for her incessant efforts in making the experiments a success. I thank her for all the invaluable help and advice she offered in setting up the experiment. She was extremely instrumental in steering the project thorough, in some of the most difficult phases. I would also like to thank Mr. Brad Harkar for his technical expertise, and always coming out with some brilliant ideas in case of dire need. I also wish to acknowledge Mr. Mike Ruckdaeschel and Mr. Doug Rancier for their help in setting up the experiments.

I would like to thank Dr. Roland Leaute and Dr. Rick Kry for some insightful comments. Further, I would like to acknowledge the staff at Imperial Oil for their support during my stay and running the experiments.

I would also like to thank my committee members Dr. B. B. Maini and Dr. R. C. K. Wong for taking out time to read my thesis. They are undoubtedly among one of the most prolific and knowledgeable persons in this area. I consider myself fortunate enough to have them on my defence committee. I would like to thank Dr. B. B. Maini for his valuable advice during the experiments.

I would like to thank my wife, for understanding my desire to pursue higher studies. She has been extremely supportive and patient and has contributed in ways I would always appreciate. I would like to thank my parents, for their love, upbringing and sacrifice, and making me the person I am today.

In the end, I would like to thank the Natural Science Engineering and Research Council (NSERC), Alberta Department of Energy (ADOE) and Imperial Oil for providing funding for the project. I would also like to thank the Department of Chemical and Petroleum Engineering and all the fellow graduate students for their help during my studies at the university.

To,

my parents

From the unreal lead me to the real !
From darkness lead me to light !
From death lead me to immortality !

.....*Brihad-aranyaka Upnishad*

TABLE OF CONTENTS

LIST OF TABLES

LIST OF FIGURES

NOMENCLATURE

A	=	area, m^2
B	=	bubbles
c	=	rate of pressure drop, Pa/s
C	=	mass concentration, kg/m^3
Đ	=	diameter, m
D	=	diffusion coefficient, m^2/s
f	=	friction factor
G	=	dimensionless pressure parameter
Ja	=	jacob number
K	=	Henry's constant, $Pa./Kg/m^3$
k	=	permeability, m^2
L	=	length, m
M	=	molecular weight, Kg/KMol
P	=	fluid pressure, Pa.
ΔP	=	pressure drop, Pa.
q	=	flow rate, m^3/s
r	=	radial coordinate
R	=	bubble radius, m
T	=	temperature, ^oK
Re	=	reynolds number
R_s	=	solution gas-oil ratio, m^3/m^3
s	=	supersaturation, Pa.
S	=	saturation
Sc	=	schmidt number
t	=	time coordinate
u	=	velocity, m/s
V	=	volume, m^3
W	=	free energy
X	=	empirical constant

z	=	gas compressibility factor
β	=	formation volume factor, rm^3/m^3
μ	=	viscosity, Pa.s
τ	=	dimensionless time
ξ	=	dimensionless radius
Π	=	dimensionless pressure
η	=	dimensionless radial coordinate
ϕ	=	dimensionless surface tension parameter
ψ	=	boltzmann's constant
ρ	=	density, kg/m^3
ν	=	kinematic viscosity, m/s^2
σ	=	surface tension, N/m
γ	=	gas constant, Pa. m^3/KMol. ^oK.
κ	=	compressibility, Pa^{-1}
α	=	error in guess value of concentration in simulation
δ	=	error in guess value of radius in simulation

Subscripts

0	=	initial value
1	=	at the first grid point i.e. at the interface
c	=	capillary
do	=	dead oil
eff	=	effective
e	=	estimated value
f	=	final value
form	=	formation
G, g	=	gas
i	=	position in space grid
ini	=	initial (at bubble point)
l	=	previous value

L	=	liquid
no	=	number
o	=	oil
org	=	value at residual oil saturation
p	=	pore value
R	=	at bubble interface
r	=	relative value
sc	=	standard conditions
t	=	total
w	=	at the interface
∞	=	value at far away point

Superscript

0	=	end point value
$*$	=	dimensionless value
n	=	time step number
n_o, n_g	=	corey's exponent

Chapter 1

INTRODUCTION

1.1. Background

As the conventional light oil resources diminish, need to develop the heavier oil resources draws more attention. The total estimated resource of heavy oil and bitumen in the world is about 5 trillion barrels, of which Canada holds about 2.7 trillion barrels [Butler, (1991)]. The heavy oil, having a higher viscosity, does not flow out of the reservoir as readily as conventional light oil. This had initially been sighted as an unfavourable attribute, predicted to result in lower primary recovery based on application of conventional flow equations in radial geometry.

In some parts of Western Canada and Venezuela, anomalously high recovery of heavy oil under solution-gas drive was reported, thus contradicting the prediction using the conventional methods. This was accompanied by lower gas-oil ratio and pressure maintenance in the reservoirs. The heavy oil production in some areas in Canada has been accompanied by high sand cuts. A new term "Cold Production" was coined to represent such process. In mid 80's Smith (1988) pioneered the research on heavy oil recovery under solution-gas drive and brought this favourable behaviour of heavy oil reservoirs to the attention of the oil industry. His paper triggered off research in this field. Following his paper, various research projects were initiated; aiming to have a better understanding of the process and generating a model that could explain this behaviour of heavy oil systems. The model thus generated was intended to be used to predict performance of the reservoir and also to efficiently manage and produce the reservoir.

The high viscosity of heavy oil results in unfavourable mobility ratio during water flood, leading to low sweep efficiency and poor oil recovery. Thus

more expensive thermal methods have to be applied for higher recovery of heavy crude oils. The favourable behaviour of heavy oil reservoirs under solution-gas drive is an encouraging feature for the oil patch in Canada, where heavy oil makes up a larger portion of total oil produced year after year [AEUB (1997)]. With better understanding and proper modelling of solution-gas drive in heavy oil, higher initial oil recovery can be achieved at much lower cost. Further, the reservoir can be optimally produced in such a way that subsequent application of thermal processes are more effective. Efficient primary production has more significance to some of the thin reservoirs in Canada where a lot of heat is lost, to the under and over lying formations, should thermal processes such as cyclic steam stimulation (CSS) and steam drive be used.

This research is in continuation of the efforts being made to have a better grasp of the cardinal principles underlying the solution-gas drive process in heavy oil. Theoretical and experimental techniques are employed. Modelling efforts concentrate on more fundamental aspects of the process. Experiments have been designed such that conclusions can be drawn regarding the process under field conditions. Comparisons have been made with the rapidly expanding body of the literature on the subject.

1.2. Layout

The thesis starts with literature review (chapter 2) with specific application to solution-gas drive process in heavy oil. This is done keeping in view the anomalies observed in heavy oil reservoirs and various works done on that. Following literature review the objectives of the thesis are stated in chapter 3. Chapter 4 presents the bubble growth model developed for solution-gas drive process. In chapter 5, experimental work on gas mobility measurement is presented and results discussed. Chapter 6 concludes the study with summary and recommendation for future work.

Chapter 2

LITERATURE REVIEW

2.1. What is Solution-gas drive?

When the pressure of an originally undersaturated reservoir is lowered below the bubble point, the gas phase is generated. The gas phase, being compressible, helps maintaining the pressure in the reservoir and hence provides the driving force for primary production. The gas does not flow as an independent phase until it reaches certain saturation known as the *Critical Gas Saturation*. After this, the gas flows as an independent phase. Since, the gas mobility is significantly greater than that of oil, the gas production rate is much higher than that of oil. Conventionally, this results in a high producing GOR (Gas-Oil Ratio). The high gas production rate results in rapid decline in reservoir pressure. This mode of primary recovery is known as the *Solution-gas drive*. The process of solution-gas drive involves supersaturation, which results in nucleation of the gas bubbles, followed by bubble growth and coalescence and finally flow of gas as an independent phase.

Sections (2.1.1-2.1.6) present the literature review on the various steps involved in solution-gas drive process, with specific application to solution-gas drive in heavy oil. Next, the anomalous behaviour of heavy oil reservoirs is stated (2.2). This is followed by a brief review of the various models proposed to explain this behaviour (2.3). One of the aims of the study is to measure gas relative permeability under solution-gas drive in heavy oil. A brief review on relative permeability is presented in section 2.4. This includes introduction, various methods for measurement of relative permeability, relative permeability measurement under solution-gas drive process, discussion and selection of

experimental method for measuring the relative permeability under solution-gas drive.

2.1.1. Supersaturation

When the pressure is lowered below bubble point in an undersaturated reservoir, gas bubbles are expected to be generated as per the equilibrium PVT properties. A certain supersaturation is required for nucleation of bubbles. So, the pressure in the system falls below bubble point without generation of gas phase. The system in this state, is said to be supersaturated.

Supersaturation can be defined as the difference between actual oil pressure and the saturation pressure corresponding to the amount of gas dissolved in the oil [Kamath and Boyer (1995)]. The system may remain supersaturated even after nucleation has taken place, for various reasons.

Kennedy and Olson (1952) observed supersaturation as high as 770 psi (5307 KPa), during fast depletion rates on methane in kerosene solution, before nucleation was detected. At supersaturation of 30 psi (207 KPa) no bubble was found to nucleate, even when the liquid was kept for 138 hours. They found that supersaturation affected the nucleation rate, and evaluated a function for nucleation rate as a function of supersaturation.

Various factors have been reported to affect supersaturation. Presence of asphaltenes has been reported to increase supersaturation [Bora and Maini (1997)]. Bora and Maini (1997), carrying out pressure depletion test in glass micromodel found out that higher oil viscosity gives higher supersaturation.

Higher depletion rates resulting in higher supersaturation has been reported by several researchers [Stewart *et al.* (1954), Dumore (1970), Moulu (1989), Wall and Khurana (1972), Hunt and Berry (1956)]. Hunt and Berry (1956) reported a supersaturation of 10 psi (69 KPa) after carrying out depletion experiments for 40 days, even though the depletion rate was extremely low (1 psi/day (6.9 KPa/day)) and gas bubbles were generated on the 20th day. Recent experimental results [Pooladi-Darvish and Firoozabadi (1999), Guo-Quig and

Firoozabadi (1999)], at comparatively higher depletion rate, indicate no supersaturation, after certain time (20-30 days) following nucleation of bubbles.

The degree of supersaturation was related to pore structure by Firoozabadi *et al.* (1992). They conducted constant volumetric rate depletion experiments on two different types of rock samples and concluded that smaller grain size may lead to lower supersaturation.

Supersaturation is a driving force for nucleation and bubble growth and is affected by various parameters. The intricate influence of these variables and supersaturation on solution-gas drive is an area of further research.

2.1.2. Nucleation

Cavitation and boiling are the two ways in which bubble formation can occur in liquid phase. The formation of gas bubble due to lowering of pressure, at constant temperature, below bubble point is known as cavitation. On the other hand, boiling involves raising the temperature above boiling point, at constant pressure. Cavitation is the nucleation mechanism taking place in reservoir under solution-gas drive and shall be discussed here.

In a recent study, Jones *et al.* (1999) presented a novel classification for nucleation:

1. classical homogeneous nucleation
2. classical heterogeneous nucleation
3. pseudo classical nucleation
4. non-classical nucleation

In classical homogeneous nucleation the bubbles are generated in the bulk. Nucleation starts by formation of embryo, which grow to nuclei and then to bubbles. Very high supersaturation is required in this class of nucleation [Hemmingsen (1975)]. For homogeneous nucleation, the expression for rate of nucleation, was given by Brennen (1995) as:

$$J = Z\exp\left(\frac{-W}{\psi T}\right) = Z\exp\left[\frac{-16\pi\sigma^3}{3\psi T s^2}\right] \qquad (2.1)$$

where Z is the total number of gas molecules present in the system, W is the driving free energy needed to create a cluster, ψ is Boltzmann's constant, T is the temperature in Kelvin, σ is the interfacial tension and s is the supersaturation. The critical radius formed is given by:

$$R_{critical} = \frac{2\sigma}{s} \tag{2.2}$$

The above equation implies that, higher supersaturation leads to formation of smaller bubbles.

The classical heterogeneous nucleation is catalysed by presence of impurities or rough surface. The surface energy is lowered, that in turn lowers the supersaturation required for nucleation. In heterogeneous nucleation the bubbles nucleate on foreign particles, thus the work done to create a bubble is several orders of magnitude less than that required for homogeneous nucleation. Heterogeneous nucleation has been suggested as one of the more probable mechanisms taking place in porous medium [Firoozabadi *et al.* (1992)]. The nucleation rate expression for heterogeneous nucleation is given by Moulu (1989) as

$$J = Z\exp\left(\frac{A}{s^2}\right) \tag{2.3}$$

The values for constants Z and A were experimentally determined, for crude oil system in porous media [Moulu (1989)]. The equation is written as

$$J = 9X10^{-3}\exp\left(\frac{-16.5}{s^2}\right) \tag{2.4}$$

The last two classifications involve presence of pre-existing bubbles. In pseudo classical nucleation the pre-existing bubble radii are smaller than the critical radius and have to overcome capillary barrier to grow, whereas, in non-classical nucleation, the bubbles radius is larger than the critical radius and all of them grow since there is no activation energy required.

The other classification of nucleation, is related to the duration of nucleation. Nucleation can be divided into two categories, which are

a) instantaneous nucleation

b) progressive nucleation

Instantaneous nucleation theory states that all the bubbles are nucleated at a single value of supersaturation. No further nucleation of bubbles takes place as the depletion proceeds. Whereas, in progressive nucleation, the bubbles nucleate at all values of supersaturation, as depletion progresses. The debate, that the nucleation in porous medium during cavitation is instantaneous or progressive, has been going on for a long time now. Kashchiev and Firoozabadi (1993) proposed instantaneous nucleation to be taking place in the reservoir. Geilikman *et al.* (1995) said that majority of the bubbles nucleate at maximum supersaturation. He defined this process as "explosive foaming or bubbling". Bora and Maini (1997) observed nucleation of bubbles even after other bubbles had nucleated. They thus concluded that nucleation in porous media is not instantaneous but progressive.

Bora and Maini (1997) observed two types of nucleation processes. In the first type, the nucleation site became inactive after generating bubble. This could be due to trapped gas, which is a non-classical type of nucleation. In the second type, the site produced a string of bubbles. This could be due to capillary pressure criteria being met at the crevice. The impurities were observed to assist nucleation. They also observed that nucleation mostly occurred at pore walls. However, asphaltenes were not found to assist nucleation. Danesh *et al.* (1987) stated that the presence of connate water can delay the formation of vapour phase. Bora and Maini (1997) also reported similar results. However, Kennedy and Olson (1952) observed no effect of water on frequency of bubble formation. Kamath and Boyer (1995) mentioned that nucleation might be facilitated due to presence of connate water.

Hunt and Berry (1956) realised the discrepancy observed in pressure data, for nucleation of first bubble, when similar experiments are carried out, for reproducibility of results. They presented a probability function to explain this discrepancy. They also presented results for number of bubbles formed at various pressure decline rate and stated that the number of bubbles nucleated increase with increase in pressure decline rate. The oil recovery has been

reported [Stewart *et al.* (1954)] to depend on the number of bubbles formed during the solution-gas drive process. Several other researchers [Danesh *et al.* (1987), Moulu (1989), Bora and Maini (1997), Wall and Khurana (1972)] have also reported that faster depletion rate leads to nucleation of more bubbles. Kennedy and Olson (1952) quantified this and presented values for bubble density at different depletion rates. They said that one bubble is formed in every million pore even at very high depletion rates. They also concluded that the nucleation rate was a function of supersaturation only, and evaluated a function for nucleation rate as a function of supersaturation. Comparing nucleation on calcite and silica, they concluded that both are equally effective in promoting formation of bubbles.

Wong *et al.* (1999) concluded that the number of bubbles formed is not affected by fluid viscosity. Considering that, diffusion coefficient is a function of oil viscosity, the lower diffusion coefficient may lead to generation of more number of bubbles. Pooladi-Darvish and Firoozabadi (1999) and later on Guo-Quig and Firoozabadi (1999) reported more number of bubbles, when conducting experiments with heavier oil as compared to that observed when using lighter oil. Similar results have been reported elsewhere [Bora and Maini (1997), Maini (1999)].

There seems to be several different classifications for bubble nucleation. The nucleation appears to be a strong function of the mode and conditions under which experiment is carried out. Minute variation in experimental process and condition can lead to different results. Experiments should be carried out carefully and under exactly similar conditions to achieve satisfactory duplicate results.

2.1.3. Bubble growth

Once the bubbles nucleate, they start growing. The rate of growth of bubble determines the gas phase growth in porous media, and hence is of particular interest for solution-gas drive process.

It has been reported [Scriven (1959), Szekely and Martins (1971), Szekely and Fang (1973), Rosner and Epstein (1972), Patel (1980)] that a number of parameters viz. viscosity, surface tension, diffusivity and initial bubble radius play a significant role in determining the rate of growth of a bubble. The forces that govern the growth of a bubble can be broadly classified into two categories. One being the hydrodynamic (inertial, pressure and viscous) forces and the other being the diffusional force. The inertial, pressure and the diffusional forces are the forces assisting growth, whereas the viscous forces resist growth. This problem has been extensively studied in the chemical engineering literature, especially when the process is dominated by one of the forces, only. Scriven (1959) simplified the bubble growth problem by neglecting the hydrodynamic forces and presented an analytical solution for the diffusional growth problem for a particular range of mass transfer driving force. Later on, the effect of other parameters was included by others [Szekely and Martins (1971), Szekely and Fang (1973), Rosner and Epstein (1972), Patel (1980), Li and Yortsos (1995)]. Rosner and Epstein (1972), Patel (1980) and Szekely and Martins (1971) concluded that at early times of bubble growth in a bulk liquid, the inertial forces limit bubble growth, but at later times it is limited by diffusional forces. Szekely and Martins (1971) and Patel (1980) showed that increase in viscous forces lead to lower rate of bubble growth at early time.

The above bubble growth studies in bulk considered the case when the pressure was dropped in a step. The bubble growth for gradual decline in pressure is of particular interest, since it more closely simulates reservoir conditions.

Kashchiev and Firoozabadi (1993) reviewed many of the limiting models when either hydrodynamic forces or mass transfer forces dominate bubble growth. It was shown that in some cases, bubble growth can be modelled by $R(t) = at^b$, where R and t are bubble radius and time, and a and b are constants.

Danesh *et al.* (1987) carried out depletion experiments in glass micromodel and observed that the growth of bubbles in porous media was controlled by capillary force. They observed no effect of gravity and direction of

flow on the pattern of growth. However, later on, contradicting their earlier statement, they said that gas may not always occupy the largest pores and leave oil behind in tighter pores. They observed gas entering and displacing oil in tight pores instead of entering the larger pores.

The approach, to model gas phase growth in porous media should incorporate capillary pressure terms. Moulu (1989) and Hunt and Berry (1956) neglected the hydrodynamic and capillary forces in treatment of the bubble growth problem in porous media. Moulu (1989) developed a comprehensive theoretical model for heterogeneous bubble nucleation, followed by growth and then attainment of critical gas saturation. He was successful in matching the experimental results quiet well, even while neglecting capillary forces. However, looking at the diffusion growth equation, it seems he neglected the moving boundary term, caused by the expansion of bubble. His model has been used by other researchers [Sheng *et al.* (1999)], while modelling solution-gas drive process in porous media.

Hunt and Berry (1956) presented an analytical solution for the diffusional growth equation for a set of initial and boundary condition. However it is not clear in their analysis how the pressure at the far boundary is changing.

Li and Yortsos (1995) presented a detailed theoretical network model for multiple bubble growth in porous media including the terms for capillary forces. They presented several scenarios for bubble growth and critical gas saturation.

Modelling solution-gas drive process, Firoozabadi and Kashchiev (1996), assumed instantaneous nucleation to take place at maximum supersaturation. They used the at^b model for growth and were able to match experimental data of gas phase growth during the solution-gas drive process. They considered nucleation to occur at the lowest point on the P-V curve.

Bubble growth is one of the key parameter in modelling solution-gas drive. The forces governing the growth need to be delineated and properly accounted for while modelling the growth. Further, the applicability and validity of the empirical growth models need to be ascertained before usage.

2.1.4 Coalescence

Coalescence occurs when the two bubbles come close to each other. This is followed by thinning of liquid lamella separating the bubbles which involves flow from between the bubble surfaces towards its periphery. Coalescence, has been reported to be affected by a number of factors, including bubble size, liquid property, porous media etc.

Geilikman *et al.* (1995), in their analysis showed that small bubbles turn out to be strongly compressed by capillary forces and do not coalesce. This, they said, is because there is no gain in surface energy due to coalescence. Whereas the larger bubbles, coalesce rapidly, as coalescence leads to reduction in surface energy. As stated earlier, higher supersaturation, which is due to faster depletion rate, leads to smaller bubbles. Hence, higher depletion rate leads to formation of smaller and more stable bubbles.

Coalescence was reported to happen more readily in light oil than in heavy oil, in experimental results of Pooladi-Darvish and Firoozabadi (1999). This might be an indication of effect of viscous forces on coalescence. Dusseault (1993) stated that the bubbles formed in heavy oil do not readily coalesce due to high viscosity of oil and capillary forces. Studies have shown that presence of asphaltenes hinders coalescence and stabilizes the gas bubbles [Bora and Maini (1997)]. From their pressure depletion tests in glass micromodel, Bora and Maini (1997) also concluded that coalescence is more likely to occur at low liquid velocity (lower depletion rate).

Islam and Chakma (1990) stated that there is distinct impact of presence of asphaltenes on gas bearing capacity of oil. They showed that the entrained gas content of oil increases with increase in asphaltene content. This can be due to formation of more stable bubbles that lead to dispersed gas flow. Pooladi-Darvish and Firoozabadi (1999) and Guo-Quig and Firoozabadi (1999) reported that the bubbles do not remain isolated in heavy oil in porous media, but coalesce to form a bigger gas phase before flowing.

Ward *et al.* (1982) and Ward and Levart (1984) showed that small bubbles can be stable due to presence of impurities. Ward *et al.* (1982) also showed that increase in number of bubbles in closed volume reduces the size of the bubble required for equilibrium. Thus it can be inferred that presence of asphaltene in a reservoir can lead to smaller and more stable bubbles.

The presence of porous media on stability of bubbles has been discussed in detail by Kovscek and Radke (1994). They stated that in the bulk, the larger bubbles grow at the expense of smaller bubbles. This is because the bubble size and radius of curvature are directly proportional to each other. However, in porous media, lamella curvature depends on pore dimension and location within pore space. They concluded that, in porous media, coalescence happens only when the lamella reaches the same pore throat.

Coalescence is a complex process and one that is not well understood and modelled. It is of importance because it determines the number of lamella and gas saturation morphology in porous media. This in effect is a measure of the resistance to gas flow and hence a factor affecting gas relative permeability.

2.1.5 Critical gas saturation

The gas phase under solution-gas drive is not mobile at low saturations. As the depletion progresses, the gas phase grows due to diffusion, pressure reduction and coalescence. A certain saturation of gas is required before a mobile gas phase can be realised. This gas saturation is known as critical gas saturation. The importance of critical gas saturation stems from the fact that it signals the onset of free gas flow, thus depleting the reservoir of the driving force for primary production.

Wall and Khurana (1972) defined critical gas saturation as minimum gas saturation which must exist before any flow of gas may occur.

Firoozabadi *et al.* (1992) gave a similar definition for critical gas saturation. A very low critical gas saturation value has been reported in their work (0.5 - 1.5%). They related critical gas saturation to supersaturation and

pore structure. They concluded that critical gas saturation decreases with decrease in supersaturation.

Very high values of critical gas saturation have also been reported in literature, especially for solution-gas drive in heavy oil [Loughead and Saltuklaroglu (1992), Sarma and Maini (1992), Islam and Chakma (1990)].

Kamath and Boyer (1995) defined critical gas saturation as minimum saturation for continuous gas flow through porous medium. They discussed critical gas saturation in external and internal gas drive and showed that the values are very different in the two cases. They reported critical gas saturations of 1 and 10% under external and solution-gas drive processes, respectively.

Li and Yortsos (1995) defined critical gas saturation as formation of a sample-spanning cluster. Pooladi-Darvish and Firoozabadi (1999) defined critical gas saturation as the minimum gas saturation at which the gas flow can be sustained. Here, in this study, we define critical gas saturation as the gas saturation at which a sustained, though intermittent, gas flow can occur.

Numerous researchers [Hunt and Berry (1956), Firoozabadi et al. (1992), Kamath and Boyer (1995)] have studied the effect of depletion rate on critical gas saturation. A unanimous conclusion has been that critical gas saturation increases with increase in depletion rate.

Li and Yortsos (1995) developed a model for multiple bubble growth in porous media and concluded that for instantaneous nucleation with constant nucleation fraction the critical gas saturation is independent of depletion rate. However, the critical gas saturation was reported to increase with nucleation fraction for case of instantaneous nucleation. Whereas, for progressive nucleation (sequential activation), the critical gas saturation increases with depletion rate.

Critical gas saturation is one of the factors affecting recovery under solution-gas drive, provided other parameters remain the same. A high critical gas saturation delays gas production and hence increases recovery. The dependence of critical gas saturation on so many factors warrants that properly

designed experiments, simulating field conditions, be carried out to have a reasonably accurate value.

2.1.6 Gas flow

Once critical gas saturation is reached, gas starts flowing as an independent phase, thus depleting the reservoir of the driving force for primary production. The gas flow can mainly be in two forms

1. dispersed gas flow
2. continuous gas flow through gas channels

The former represents low gas phase mobility whereas the gas mobility in the later case is comparatively higher (this shall be justified later). The later case is undesired during solution-gas drive process, since it leads to rapid loss of gas from the reservoir. Several microscopic and macroscopic studies have been conducted to understand and model this part of the process, since it is affected by so many parameters.

Bora and Maini (1997) observed that in slow depletion tests the bubbles do not vacate the original pore and migrate towards the outlet. Thus the slow depletion tests displayed classical solution–gas drive behaviour. Contrary to this, in faster depletion tests, the bubbles were observed to nucleate, grow and then move towards the outlet end. In this process the bubbles would split. The split bubbles would then grow and split again as they moved towards the outlet. This was referred to as dispersed gas flow. They concluded that high viscosity coupled with high velocity leads to dispersed gas flow. In earlier work, Sarma and Maini (1992) said that the heavy oil/gas mixture flows in form of oil continuous foam. Snap-off phenomenon was observed in solution-gas drive experiments conducted by Danesh *et al.* (1987) in glass micromodel. They reported that snap-off is promoted by higher velocity and structure of the porous media (high pore body to pore throat ratio).

Wall and Khurana (1972) stated that during slower pressure decline, gas flows intermittently. There is a period of gas saturation build-up during which

no gas flow occurs. This is followed by period of gas flow. Similar behaviour was observed in slow depletion experiments of Pooladi-Darvish and Firoozabadi (1999).

Wall and Khurana (1972) conducted pressure depletion experiments and reported that increase in flow rate from one value to another leads to intermittent gas flow at higher equilibrium saturation. They concluded that the final gas saturation increases with pressure decline rate.

Wong *et al.* (1999) carried out pressure depletion tests on bitumen. They said that the gas flows through free gas channels after reaching critical gas saturation. A constant increasing GOR (Gas-Oil Ratio) should be observed if gas flows through channels. However, the produced GOR results indicate fluctuating values of produced GOR. This may be due to intermittent flow of gas, which happens when dispersed gas flow occurs in the porous media.

Dumore (1970), from solution-gas drive experiment in transparent porous media, concluded that dispersed gas flow results in higher gas saturation; an observation that holds true for the results of Pooladi-Darvish and Firoozabadi (1999). He also stated that dispersed gas flow in a porous media is a function of the pore structure of the porous media. He found a value, for transition from dispersed to non-dispersed flow, from his external gas drive experiments. The study concluded that high capillary pressure leads to non-dispersed flow whereas low capillary pressure leads to dispersed flow.

The modelling of gas flow is quite complex at microscopic level. At macroscopic levels Darcy's equation is used to represent the flow. The parameter most often changed to represent flow at a particular gas saturation is gas relative permeability and viscosity.

Modelling of each of the individual processes in solution-gas drive presents a unique challenge, as it depends on so many parameters and is affected by so many process variables. A proper comprehensive modelling should take into account non-equilibrium phenomenon (supersaturation), nucleation (type of nucleation, rate etc.), growth of gas phase (including hydrodynamic, diffusive and capillary forces), coalescence, gas flow (dynamic

effect of change in gas saturation distribution on gas flow), effect of porous media among other parameters.

2.2 Anomalous behaviour of heavy oil reservoirs

The heavy oil reservoirs in Western Canada and Venezuela under solution-gas drive show anomalous behaviour when compared to conventional light oil reservoirs. Once below the bubble point pressure, producing GOR does not increase sharply and rate of pressure drop is low. Some wells show higher oil production rates than those predicted using conventional flow equations in radial co-ordinate. The overall recovery under solution-gas drive is higher than that expected from a conventional oil reservoir. Visual field observations reveal presence of "chocolate like mousse" in storage tanks. These reservoirs are often termed as *"Foamy Oil"* reservoirs. Here, in this study, the usage of this termed is deliberately avoided. If we look at the anomalies observed, all of them indicate that somehow the gas is remaining inside the reservoir and is not able to flow out.

In a study on Celtic heavy oil field in Lloydminster, Loughead and Saltuklaroglu (1992) reported production rates in excess to that which can be predicted using Darcy's law in radial flow. Primary recovery, as high as 14%, was reported. This is in contrast to conventional light oil reservoir where solution-gas drive leads to much lower oil recovery. Mirabal *et al.* (1997) reported high production rates from heavy oil reservoirs in Hamaca region in Venezuela. The initial high productivity index of this reservoir yielded unexpected cold production flow rates of 500 STB/day (vertical well) and 2500 STB/day (horizontal well). The average pressure in the reservoir dropped by 100 psi (689 KPa) only, after 12 years of production. Until 1996 158 MMSTB of oil has been produced. History matching revealed that, high gas retention exhibited cannot be justified by conventional techniques. Compaction/subsidence effect, which was thought of as the mechanism responsible mechanism for favourable behaviour, was studied. The study

indicated that compaction/subsidence effect could only result in recovery of 3% OOIP under a threshold pressure of 580 psi (3997 KPa). Modelling the reservoir and simulation revealed that 13 % OOIP can be recovered under primary production.

High initial sand cuts have been observed in oil field producing under solution-gas drive in western canada, which later on tapers off to 1-3% sand cut [Loughead and Saltuklaroglu (1992), Metwally and Solanki (1995)]. It has been reported that blocking sand production in Lloydminster and Primrose fields results in drastic reduction (upto 10 times) in heavy oil production [Dusseault (1993)].

Abnormal behaviour has also been observed in Lindbergh and Frog Lake heavy oil fields [Metwally and Solanki (1995), Huang *et al.* (1997)]. Metwally and Solanki (1995) reported that high production rates are sustained for long period of time in absence of any external mechanism such as aquifer, compaction etc. They stated that the primary production in a reservoir should increase until the pressure effect reaches the far boundary after which the pressure and hence the production rate should drop depending on the *in-situ* mobility. They inferred that some kind of pressure maintenance mechanism was present. Metwally and Solanki (1995) conducted several field tests in Frog lake and carried out simulation to history match the field production and pressure data. They found that this behaviour of heavy oil reservoirs can not be solely attributed to permeability enhancement due to sand production or dispersed gas phase flow. They simulated the pressure maintenance at the far boundary by assigning an infinite aquifer. This alone was also not sufficient to history match the field results.

The behaviour of heavy oil reservoirs under solution-gas drive has intrigued the oil industry for over a decade now [Smith (1988), Loughhead and Saltuklaroglu (1992)]. Extensive research, from microscopic to macroscopic level, has been carried out to explain this anomalous behaviour. The flow mechanism under solution-gas drive in heavy oil is quite complex and involves a myriad of factors, many of which contribute towards the favourable

behaviour. Understanding the mechanism and modelling the solution-gas drive process in heavy oil reservoir would help better planning of recovery of heavy oil.

2.3 Models proposed

The favourable behaviour of heavy oil reservoirs has generated a lot of interest in researchers to explore what abnormal mechanism is taking place in a heavy oil system or reservoir that is not taking place in conventional light oil reservoir. Several theories have been proposed and models put forward to explain this unusual behaviour.

2.3.1. Presence of microbubbles

Smith (1988), in one of the first works on solution-gas drive in heavy oil, postulated that gas flows in form of tiny bubbles with the oil. He hypothised that the size of the bubbles is so small that they flow through the pore throats with the oil. He termed them as *"microbubbles"*. He further stated that these gas bubbles do not coalesce to form a continuous gas phase. This study provided impetus for further research in this field. In a recent study, Islam and Paddock (1999) presented a new time dependent equation of state for PVT properties of oil with microbubbles and asphaltenes. The parameters in the equations were identified to be a function of viscosity, density etc.

Treinen *et al.* (1997) in their solution-gas drive experiments observed reduction in GOR of the produced oil before start of free gas flow. They thus concluded that, below critical gas saturation, small gas bubbles or fine foam does not flow with the oil phase. They argued that the produced GOR should remain constant if gas flows in form of small bubbles entrained in oil.

Bora and Maini (1997) could not verify the presence of large number of micro bubbles during the depletion experiments in their glass micromodel. Later on, more precise experiments [Bora (1998)], confirmed the presence of

microbubbles was demonstrated by showing that, the compressibility of the oil below bubble point is much greater than the compressibility of single-phase live oil above bubble point.

The theory of presence microbubbles or tiny bubbles is of immense interest in the present context. Many theories that have been proposed to explain the anomalous behaviour of heavy oil reservoirs, revolve around this main theory.

2.3.2. Lowering of viscosity

By simple application of Darcy's law, the enhanced oil production rate can be modelled by lowering the oil phase viscosity. This principle was investigated in several studies, which measured the oil phase viscosity after generation of gas bubbles.

Smith (1988) was probably the first to propose a correlation for the gas-oil mixture viscosity for two-phase flow, for this application. He used modified build-up analysis data from field to infer apparent *in-situ* viscosities for oil. He said that the mixture viscosity was much below the viscosity of oil and above that of gas. This reduced viscosity was proposed to partially account for enhanced production in heavy oil reservoirs.

Poon and Kisman (1992) demonstrated the non-newtonian behaviour of heavy oil and concluded that the dilatant behaviour of heavy oil results in lower effective viscosity at low shear stress. This could explain enhanced oil flow in region far from well, but lack of explanation of GOR data poses a few questions.

Islam and Chakma (1990) proposed a mathematical model to describe the peculiar pressure dependent multiphase flow properties. They concluded that the gas-oil mixture viscosity is lowered during solution-gas drive. They carried out several flow experiments on capillary tube and core. The microbubbles were generated elsewhere and then injected into the core. This external approach as opposed to internal drive experiments may pose some

doubt on direct interpretation of the results. Average velocity of microbubbles was estimated to be 1.2 times higher than the liquid velocity.

Clarigde and Prats (1995) supported the theory of Simth (1988) and said that the gas bubbles are stabilised due to accumulation of asphaltenes at the bubble interface. This further leads to lowering of *in-situ* oil viscosity. They showed that the viscosity of live oil, on asphaltenes removal, could be lowered by as much as 10 times. They, performed numerical simulation to explain the higher production rates and lower GOR observed in field. However, laboratory experiments not showing any difference in behaviour of solution-gas drive process with or without asphaltenes [Sheng *et al.* (1999), Maini (1999)], poses a serious question on this hypothesis. More so, when Claridge and Prats (1995) did not support their theory with experimental results.

Sheng *et al.* (1997) did not report any significant effect of asphaltene on *"foamy oil"* stability. Later on, Maini (1999) also reported no effect on recovery factor due to presence of asphaltene for high rate solution-gas drive experiments.

Shen and Batycky (1999) also proposed a correlation for effective viscosity with lubrication effects. However, they used this correlation to prove that the favourable behaviour of heavy oil reservoirs is due to increased oil mobility due to nucleation of gas bubbles at pore walls.

Different studies have shown results in favour and against this theory. The effect of presence of asphaltenes is presently debated and needs further investigation. This theory should be carefully examined while studying and modelling solution-gas drive process in heavy oil.

2.3.3. Foamy oil flow

The "*Foamy Oil*" flow mechanism [Maini *et al.* (1993), Bora and Maini (1997), Maini (1999)] is an extension of the dispersed gas flow model proposed by Smith (1988). Bora and Maini (1997) studied the effect of rate of depletion on the bubble nucleation and subsequent flow in a micromodel. They

concluded that higher rate of pressure drop results in nucleation of more number of bubble and more dispersed gas flow. They termed this as *"foamy oil"* flow. They concluded that the enhanced oil recovery under solution-gas drive in heavy oil can be explained by this flow behaviour of heavy oil. Earlier, Mirabal *et al.* (1996) reported that the enhanced oil recovery was due to *in-situ* formation of non-aqueous foam. In a recent work, Maini (1999) described *"foamy oil"* flow as two-phase gas-oil flow at high capillary number. He further explained that high viscous force is required to mobilize the gas ganglia in this process. He also indicated that a critical rate of pressure drop, that increased sharply with decreasing viscosity, is required to maintain *"foamy flow"*.

Guo-Quig and Firoozabadi (1999) from their experiments on a visual core-holder concluded that characterizing the solution-gas drive in heavy oil as *"foamy"* is inappropriate. They conducted slow constant volumetric rate depletion experiments and did not report any *"foamy oil"* flow.

Wong *et al.* (1999) from pressure depletion tests on core observed high recovery of bitumen even under slow depletion tests. They performed pressure depletion tests in steps and measured production of bitumen and gas. Observing the GOR results they concluded that the *"foamy oil"* flow occurred below bubble point and above critical gas saturation. They argued that since GOR did not decrease below bubble point, the gas flowed with the oil. They also observed very brief transient period of foamy behaviour below bubble point, when the pressure was dropped in a step, after which the pressure at the upstream and downstream became equal. They related this to time-dependent volumetric expansion behaviour of foamy bitumen-gas mixture. Based on high bitumen recovery under slow depletion test they inferred that factors other than *"foamy oil"* flow may be responsible for high oil recovery. Wong *et al.* (1999), from their pressure depletion tests, did not report any enhancement of bitumen recovery due to temperature.

Zhang (1999) studied the effect of temperature on *"foamy"* solution-gas drive process. The results can also be viewed as the effect of viscosity on solution-gas drive process. Most of the other parameters during the

experimentation were similar in all the runs. It was concluded that there is an optimum temperature for maximum recovery condition, which essentially is a trade off between increased mobility from lower viscosity at higher temperature and increased dispersed gas flow (lower coalescence) due to higher viscosity at lower temperatures. However, Maini (1999) stated that recovery factors in fast depletion tests are independent of oil viscosity.

Sheng *et al.* (1997) studied the *"foamy oil"* stability in bulk by carrying out pressure depletion in live oil liquid column and measuring the height of liquid column with time. They found that higher viscosity leads to higher foam stability. This may be one of reasons for more stable heavy oil column observed by Pooladi-Darvish and Firoozabadi (1999). Later on, Sheng *et al.* (1999) formulated a dynamic model for *"foamy oil"* flow in porous media. The model was more successful in modelling the flow under high depletion rates, when the *"foamy"* effect is most present, as against the equilibrium model. For the slower depletion tests (131 psi/day (903 KPa/day)) the dynamic model was quite close to the equilibrium model. This slow rate is much higher than the pressure decline rate present in the field and even at this fast rate equilibrium model gives satisfactory results. Hence, the inevitable question that "are high pressure gradients available in field to induce *"foamy oil"* flow or is it just the dispersed gas flow even at low pressure gradient responsible for favourable behaviour of heavy oil reservoirs?" comes up.

Maini (1996) said that a threshold pressure drawdown is required for the onset of *"foamy solution-gas drive"* mechanism. He further stated that slow depletion test are similar to conventional solution-gas drive mechanism. From the field data it is observed that the pressure drawdown is very slow [Mirabal *et al.* (1997)]. This implies that the mechanism in field cases cannot be *"foamy solution-gas drive"*. Maini (1996) said that the formation of "wormholes" may induce high pressure gradient and hence formation of *in-situ foam*. This can be explained in the near well-bore region but applicability of this at point far form well-bore is unlikely [Smith (1988)]. Additionally, mechanism for heavy oil wells

exhibiting high recovery in absence of sand production, cannot be explained by this theory alone.

2.3.4. Pseudo-bubble point model

The aspect of delay in gas production in heavy oil reservoirs has been modelled in several different ways. On of the ways is to define a pseudo-bubble point pressure, that is much below equilibrium bubble point pressure.

Kraus *et al.* (1993) proposed a pseudo-bubble point model to account for this favourable behaviour of heavy oil reservoirs. The authors stated that, solution-gas, after getting liberated at equilibrium bubble point, is entrained in oil and does not form a continuous free phase until pseudo-bubble point pressure is reached. They defined new functions to calculate PVT properties for this model. Although he could justify the high production rates, low GOR and pressure maintenance with his model, the lack of comparison with field or experimental data may raise several doubts on practical application of this theory.

Geilikman *et al.* (1995) stated that the foamy state of heavy oils occurs not at the equilibrium bubble point pressure but at some pressure below actual (kinetic) bubble point. They further said that this kinetic bubble point depends on gas diffusivity and rate of pressure drop.

The pseudo-bubble point model in-effect, seems to be an alternate expression for the tiny immobile entrained gas bubbles present in heavy oil under solution-gas drive.

2.3.5. High critical gas saturation

The basic mass balance calculations indicating presence of high gas saturation lead to the theory that, high critical gas saturation is responsible for this favourable behaviour of heavy oil reservoirs.

Treinen *et al.* (1997) performed flow experiments on unconsolidated sand-pack having a pore volume of 200 cc. The experiments simulated field conditions that were equivalent to flow in a reservoir 1000 ft. from a vertical well with 125 ft of net pay, producing at 400 BPD. CT scanning of the core was done which indicated pockets having local gas saturation as high as 70%. However, the critical gas saturation was reported at 9%. Huerta *et al.* (1996), conducting similar experiments, reported a critical gas saturation of 10%. Additionally, they attributed this favourable behaviour to *in-situ* formation of non-aqueous foam which contributes for recovery of 10% OOIP. They finally concluded that the high recovery under solution-gas drive was due to high critical gas saturation.

Loughead and Saltuklaroglu (1992), from their study on the unusual behaviour of Lloydminster field, concluded that the trapped gas saturation has to be as high as 35% for this behaviour to be justified. Additionally, they said that the oil phase relative permeability decreases by less than 5% in the gas phase saturation range of 0-35%.

Sarma and Maini (1992) and Maini *et al.* (1993) conducted blow down experiments on sand-packs. Observing the high recovery, they concluded that a mechanism is present to increase the critical gas saturation. They reported a critical gas saturation of 40%. They attributed formation of oil continuous foam, for high critical gas saturation. However, it seems they referred critical gas saturation to be formation of continuous gas phase and discounted any intermittent gas production due to production of *"oil continuous foam"*.

Islam and Chakma (1990) suggested a relative permeability curve for heavy oil in which they assigned the critical gas saturation to be near 45-50%.

However, in some of the recent solution-gas drive studies on heavy oil [Pooladi-Darvish and Firoozabadi (1999), Guo-Quig and Firoozabadi (1999)], the critical gas saturation was found to be low (1.1 – 5.5%). Even in the simulation studies of Claridge and Prats (1995) a critical gas saturation of 3% was considered with their low viscosity model to show enhanced oil production.

2.3.6. Geo-mechanical effects

The large amount of sand cut observed in some of the heavy oil reservoirs in western Canada have lead to theories based on enhanced permeability due to sand production.

The geo-mechanical effect, i.e. compaction and formation of "wormholes", which are essentially high permeability channels, has also been proposed as a possible mechanism leading to enhanced primary recovery.

Dusseault (1993), discussing why heavy oil production is higher if low sand cut is allowed in the well, proposed four major factors responsible for enhanced production. He listed the following four factors: enhanced drainage radius, grain movement, gas bubble expansion and continuous pore debottlenecking. He stated that the bubbles formed do not coalesce due to high viscosity of oil and capillary forces. The bubbles, instead of blocking the pores, move with the oil due to movement of sand grains and provide internal driving force through expansion. Further, the movement of grains provides debottlenecking mechanism in the pore throats, which is caused by blockage due to fines or gas.

Geilikman *et al.* (1995) delineated the radial reservoir into near well-bore *"foamy"* and distant *"non-foamy"* zones. At the boundary of these zones they applied continuity of radial stress and fluid pressure relationship. Using the general solutions for stresses they found expression for radial stress at the boundary between foamy and non-foamy zone. Hence, they found condition for tensile failure to occur at the boundary and expression for propagation of *"foamy"* front.

Smith (1988) argued that presence of "wormholes" can only affect the production in the near well-bore region. The far away point, which contributes to bulk of production, is not affected by the "wormholes". He also stated that the fines migration in reservoir leads to plugging, not cleaning. However, Loughead and Saltuklaroglu (1992) used this mechanism to model the flow in the altered matrix.

Treinen *et al.* (1997) presented arguments similar to Smith (1988) and said that stress reduction and fluid shear that leads to formation of wormholes and sand dilation is highest near the well-bore but diminishes rapidly at greater distance from well. Although wormholes and dilated sand can explain the high production rates near the well-bore, recovery of oil is dominated by mechanism controlling oil flow away from well-bore.

The current study investigates the anomalous behaviour of heavy oil reservoirs in absence of geo-mechanical effects.

2.3.7. Increased oil mobility

In absence of reduction of effective oil viscosity, the high oil production rates from heavy oil reservoirs can be explained by increase in oil phase mobility.

Shen and Batycky (1999) suggested increase in oil mobility due to lubrication caused by nucleation of bubbles at pore walls. They used the experimental results of Sarma and Maini (1992) and Maini *et al.* (1993) to prove their hypothesis. Sarma and Maini (1992) and Maini *et al.* (1993) had concluded that oil phase mobility decreases due to formation of gas bubbles. Shen and Batycky (1999) said that although the overall oil mobility might have decreased but the local oil mobility increased with nucleation of bubbles. They assumed a pseudo single-phase flow and presented a correlation for effective oil viscosity that included a slip parameter. The slip parameter was stated to be a function of pressure drop and depletion rate; increasing with increase in depletion rate. In order to match the pressure gradients at the near-outlet region they had to increase the oil mobility by 10-40%. This is low compared to the increase in production observed in field under solution-gas drive [Loughhead and Saltuklaroglu (1992)].

Earlier, Loughead and Saltuklaroglu (1992), in a similar context, stated that the presence of microbubles does not impede oil flow and postulated that it may enhance oil mobility.

Huerta *et al.* (1996) from their experiments on long slim tube found that the oil phase mobility does not increase as the pressure is lowered during the solution-gas drive process.

Pooladi-Darvish and Firoozabadi (1999), in their experimental work observed increased pressure drop at constant oil production rate as gas saturation increased from zero, and concluded that there is no increase in oil phase mobility due to nucleation of bubbles. Rather, the oil phase mobility decreases due to formation of gas phase.

2.3.8. Lower gas mobility

As stated earlier that all the anomalies in heavy oil reservoir indicate that the gas is retained in the reservoir and is not able to flow out. One of the reasons could be that the gas mobility is low in heavy oil resulting in gas retention in the reservoir.

Pooladi-Darvish and Firoozabadi (1999) attributed the favourable behaviour of heavy oil reservoir under solution-gas drive to low gas phase mobility in heavy oil. The low gas mobility implies lower gas velocity which results in gas retention and hence pressure maintenance in the reservoir. Finally, all these factors lead to higher oil recovery. They suggested that this low gas phase mobility might be due to dispersed gas flow and increased number of bubbles. This theory was supported by Gou-Quig and Firoozabadi (1999), who performed similar experiment. Guo-Quig and Firoozabadi (1999) reported recoveries in excess of 13% under solution-gas drive experiments. This recovery is in line with the field results.

Claridge and Prats (1995) also indicated in their study that the gas mobility is lowered due to presence of stabilised bubbles. This could be due to dispersed gas flow. Dispersed gas flow was later on proposed by Pooladi-Darviah and Firoozabadi (1999) and Gou-Quig and Firoozabadi (1999)

Dumore (1970) from solution-gas drive experiment in transparent porous media concluded that dispersed gas flow results in higher gas saturation, an

observation that can be applied to results of Pooladi-Darvish and Firoozabadi (1999).

One major objective of the present study is to investigate the above theory, by measuring gas relative permeability under highly controlled conditions with low experimental errors. The following section presents a review on relative permeability. An additional aim is to study the effect of depletion rate on the solution-gas drive process.

2.4. Relative permeability

2.4.1 Introduction

Flow of a single-phase fluid through a horizontal1-D porous medium can be described by Darcy's law, which is stated as

$$q = -\frac{k}{\mu} A \frac{dP}{dL} \tag{2.5}$$

here, q is the flow rate, μ is the viscosity, A is the flow area, dP/dL is the pressure gradient and k is the absolute permeability of the porous media.

The recovery of oil from a reservoir is seldom a single-phase flow. There is always a second phase present in the system except when undersaturated oil is flowing in presence of connate water, in which case water can be considered as a part of the rock matrix. In all the other cases, whether it is solution-gas drive, water drive, cyclic steam stimulation, polymer injection etc., there is always multiphase flow present. In solution-gas drive, once pressure is below bubble point and for gas saturation above the critical value, the flow is governed by Darcy's equation for two-phase flow incorporating the relative permeability term. So it becomes imperative to determine the effective permeability of one phase in presence of the other phase to predict the recovery.

The two-phase flow in the porous media is given by the equation

$$q_l = -\frac{k_{effl}}{\mu_l} A \frac{dP_l}{dL} \tag{2.6}$$

Here k_{eff1} is the effective permeability of phase *1*. If we divide the effective permeability by absolute permeability then we get a term, which is called relative permeability

$$k_{r1} = \frac{k_{eff1}}{k} \tag{2.7}$$

Where k_{r1} is the relative permeability of phase *1*. Relative permeability is a measure of relative ease of flow of one fluid in presence of another fluid.

2.4.2. Measurement of relative permeability

It has been extensively studied [Honarpour *et al.* (1994)] and well known that relative permeability depends on a number of factors. One of the most important factors is phase saturation.

The measurement of relative permeability mainly involves measurement of gas-oil flow rates along with the saturation. Measurement of two-phase relative permeability has been carried out since long. Flow experiments are performed on the core to determine relative permeability. The flow experiments usually involve flow of two-phases simultaneously, until steady state is reached (Steady State Method) [Osaba *et al.* (1951), Richardson *et al.* (1952)]. In other methods [Civan and Donaldson (1987), Sarma and Bentsen (1989, 90), Johnson *et al.* (1959), Chardaire (1989), Helset *et al.* (1998), Watson *et al.* (1988)], unsteady state data obtained from displacement of one phase by another is used to calculate relative permeability. All the above techniques require external injection of fluids. In practice, the relative permeability obtained by performing these experiments is used to predict performance and recovery under solution-gas drive. Stewart *et al.* (1953, 54) showed that relative permeability under external and solution-gas drive are quite different. Very limited literature is available on the measurement of relative permeability under solution-gas drive, especially for heavy oil.

Efforts have also been made to correlate relative permeability to properties of either the porous medium or the fluid [Taxler and Baum (1936),

Leverett (1939, 41), Carman (1937), Rose (1949)]. All these models were developed based on data from external drive experiments and may not be valid for predicting relative permeability under solution-gas drive.

Several other efforts have been made to model relative permeability. Fatt and Dykstra (1951) presented a formulation for calculating relative permeability by assuming that porous media can be represented by a bundle of capillary tubes. They introduced a tortuosity factor in their formulation. Rapoport and Leas (1951) also presented an analytical expression for calculation of relative permeability as a function of saturation.

The above analysis considered the Buckley-Leverett solution and hence saturation profile was obtained from theory (Bentsen (1978) proved that Buckley-Leverett solution is indeed the steady state solution to the two-phase flow, when capillary pressure is small). The assumptions and boundary conditions inherent in Buckley-Leverett (B-L) solution are not at all valid for solution-gas drive process. Hence, relative permeability calculated from unsteady state experiments assuming Buckley-Leverett solution can be refused *in-toto* for solution-gas drive process.

From the above argument, we can conclude that expressions to correlate relative permeability to some property of porous medium may not be valid as relative permeability depends on a myriad of other factors other than the rock.

Other important parameter to be measured while measuring relative permeability is the phase saturation. Several methods have been used to measure saturation in the core. Earlier methods involved core weighing [Osaba *et al.* (1951), Leas *et al.* (1950), Richardson *et al.* (1952)] and material balance [Fatt and Dykstra (1951), Rapoport and Leas (1951)] for estimation of average gas saturation. Electrical resistance [Bail and Marsden (1957)], X-ray [Oak *et al.* (1990), Oak and Ehrlich (1998), Laird and Putnam (1951, 59), Morgan *et al.* (1950), Boyer *et al.* (1947), Geffen and Gladfelter (1952)], Microwave [Sarma and Bentsen (1989, 90), Parsons (1975)], Ultrasound [Hoyos *et al.* (1990), Kalaydjian (1992)] and gamma ray [Chardaire (1989)] are non-intrusive techniques and have been used to determine the *in-situ* saturation.

Muskat (1949) in his work stated that solution-gas drive process was equivalent to external gas drive process. Thus, he measured the relative permeability by performing external gas drive experiments and concluded that these were applicable for solution-gas drive process as well.

Handy (1958) from his studies on solution-gas drive concluded that at lower rates, the recoveries are independent of rate and could be predicted by Muskat's theory; applying relative permeability data from external gas drive experiments.

Stewart *et al.* (1953, 54) measured the relative permeability under external and solution-gas drive and showed that they were quite different. Similar results were reported by Handy (1958). The process of external and solution-gas drive is principally not the same. This is because, in external drive experiments, gas, being the non-wetting phase, traverses through the largest pores and is only present in the largest pores. In contrast, in solution-gas drive, as we lower the pressure, the gas bubble may nucleate in the smaller pores and grow. Although it may travel through the largest pores once mobile gas saturation is reached but it is present in the pores of all sizes. Hence, the saturation distribution in the two cases may be different [Handy (1958)]. Higher numbers of lamellae denote more dispersed gas phase flow. During solution-gas drive process, we may end up with a more dispersed gas flow than that due to external gas drive. Kennedy and Olson (1952) stated that the gas distribution in porous media is one of the factors that may account for different gas relative permeability for same gas saturation. Studies [Falls *et al.* (1988)] indicate that different bubble density results in different resistance to flow. As the number of bubbles formed are a function of rate of pressure drop [Stewart *et al.* (1954), Bora and Maini (1997)], inference can be drawn that the relative permeability might depend on rate of depletion in solution-gas drive process.

Stewart *et al.* (1954), from his work on solution-gas drive concluded that oil recoveries can not be predicted for all rates using the same set of relative permeability values. This is in line with our inference earlier that relative permeability depends on depletion rate. The study [Stewart (1954)] implies that

for the same value of saturation, the relative permeability value may be different for different rates of pressure drop. In the process of external drive there is no such term as rate of pressure drop hence this effect is absent. There is only pressure drop across the core, which is related to velocity (or injection rate). Moreover, in early works [Osaba *et al.* (1951), Richardson *et al.* (1952)], the relative permeability in external drive process was shown to be independent of rate.

The above review suggests that the relative permeability due to solution-gas drive is different from that due to external gas drive. The important factors affecting the relative permeability in solution-gas drive are the pressure drop rate, viscosity etc. Capillary end effect [Richardson *et al.* (1952)] and saturation gradients are important factors to be addressed during experiments and subsequent modelling.

Maini (1995) in his paper argued about the futility of measuring the relative permeability for heavy oil reservoirs. Several factors ranging form effect of viscosity, viscous fingering, condition and size of the core sample, experimental techniques and possible errors were discussed. He concluded that accuracy of the measurement is determined by the "lowest common denominator of the skill of the levels of the users and providers of the data". However, the importance of measurement of relative permeability cannot be discounted and it is the closest we can get to the real behaviour of multiphase flow in porous media.

Having established that gas phase distribution and hence relative permeability during solution-gas drive is principally different than in external gas drive, the next objective was to study the relative permeability under solution-gas drive and factors affecting it.

2.4.3 Relative permeability under solution-gas drive

As discussed above, the processes of external and solution-gas drive are principally not the same. The solution-gas drive process cannot be represented

by external drive. The number of bubbles and hence the number of lamella may be different in the two cases [Pooladi-Darvish and Firoozabadi (1999)], resulting in different resistances in flow [Holm (1968)] and hence different relative permeability.

The dependence of relative permeability under solution-gas drive on depletion rate has been discussed earlier. Stewart *et al.* (1954) showed that the gas-oil relative permeability ratio decreased with increase in depletion rate. Guo-Quig and Firoozabadi (1999) reported no change in relative permeability when depletion rate was changed. The change in rate in their experiments was very small (2 times) and it is possible for the relative permeability not to change for such small changes in depletion rate. However, it is expected that the relative permeability would change if the depletion rate is changed several folds.

Wall and Khurana (1972) showed the effect of viscosity on relative permeability to gas in their study. They showed that the gas relative permeability decreases with increase in viscosity. The effect of oil viscosity on relative permeability to gas has been debated for long time now. Stewart *et al.* (1954) enlisted viscosity as one of the factors affecting relative permeability. From the gas relative permeability results of Guo-Quig and Firoozabadi (1999) we can observe that the gas phase relative permeability for the lighter oil (8500 cp) is about one order of magnitude higher than that in heavier oil (32,000 cp), other conditions remaining similar. The recovery was also reported to be higher for heavier oil.

The effect of viscosity ratio on relative permeability was studied by Odeh (1959). He concluded that the relative permeability to the non-wetting phase increases with increase in viscosity ratio whereas the relative permeability of the wetting phase is unaffected. He also concluded that, above an absolute permeability of 1 Darcy, the effect of viscosity ratio on relative permeability vanishes. Handy (1958) stated that reduction in relative permeability ratio was a function of oil viscosity.

A time-based behaviour of heavy oil under solution-gas drive, put forward by Sheng *et al.* (1997), introduces an additional factor on which relative

permeability depends; i.e. time. Infact, it is the gas phase morphology that changes with time which brings in this effect. The gas phase is initially dispersed during solution-gas drive process. Due to coalescence of gas phase the morphology changes in the porous medium and hence the resistance to flow. This leads to a different value of relative permeability. However, the study of Sheng *et al.* (1997) mostly considered cases when the pressure was dropped in a step or dropped at a very fast rate (6-12 psi/min (41-82 KPa/min)or 8640-17280 psi/day). These depletion rates are unpractical and unlikely to exist in field. It would be interesting to study the time-dependent behaviour of heavy oil under very slow pressure decline rates (5-10 psi/day (34-68 KPa/day)).

In this project an attempt is being made to measure relative permeability under solution-gas drive and study the effect of depletion rate on relative permeability. Experimental setup has been designed to measure the same.

2.4.4. Discussion

Maini (1996, 99) stated that dispersed gas flow is possible under high pressure gradients. It has been observed in experiments of Pooladi-Darvish and Firoozabadi (1999) that even under slow depletion rates more number of bubbles are formed in heavy oil compared to that in light oil. This might be explained by lower diffusion coefficient in heavy oil (We shall discuss this in chapter 4). The diffusion coefficient is an inverse function of viscosity of oil. So, more viscous oil could generate more number of bubbles and more dispersed gas flow [Pooladi-Darvish and Firoozabadi (1999)]. Dispersed gas flow has also been shown to result in higher gas saturation [Dumore (1970)], which leads to higher recovery. Similar results were obtained by Handy (1958). Thus, a heavier oil may result in more dispersed gas flow and higher gas saturation even in absence of high pressure gradient.

The data from the field for heavy oil has reported recoveries as high as 5-14% under solution-gas drive. However, the high recoveries obtained under laboratory experiments for fast depletion rates [Maini (1999)] of 23-25% seem

unrealistically high for field conditions. Even in the behaviour of pressure and cumulative gas produced [Maini (1999)], it is observed that 90% of the pressure is depleted and equivalent amount of gas produced in first 1000 minutes, after which there is very little driving force left for primary production. Whereas, in slow depletion rate results, pressure is maintained and cumulative gas produced is low for a long time. Although ultimate recovery is low in slow depletion but is in line with field results. Guo-Quig and Firoozabadi (1999) reported recovery in the range of 13% even for slow depletion tests (≈ 5 psi/day (34 KPa/day)after generation of gas phase). This is in line with the figure observed in field. They observed intermittent gas production and concluded that the flow was in the form of dispersed gas flow. By running experiments on transparent core, they could observe coalescence of bubbles which is characteristic of conventional solution-gas drive. Thus they attributed favourable behaviour of heavy oil reservoirs to low gas phase mobility. Similar results were previously reported [Pooladi-Darvish and Firoozabadi (1999)].

Stewart *et al.* (1954) accepted that the lab recovery results were rather optimistic due to high pressure decline rates used. They further said that the recovery in field is expected to be lower under solution-gas drive as the number of bubbles expected to nucleate are less at slower depletion rates. He quantified the number of bubbles expected to nucleate per unit volume of reservoir as a function of pressure decline rate. These results may be a function of viscosity of oil (which affects the diffusion coefficient) and the applicability of their correlation for oils of all viscosity is questionable.

Wong *et al.* (1999) stated that, for step decline in pressure, a high supersaturation is generated which leads to formation of more gas bubbles and high recovery. However, such high supersaturation cannot be generated in field except near well-bore. So, experiments in the lab should be designed to simulate field conditions.

Islam and Chakma (1990) stated that since laboratory results are carried out at much faster depletion rates compared to field, hence they result in much higher recoveries. Maini (1999) argued that although pressure gradient applied

in the lab is much higher than that existing in field, the existence of *"foamy oil"* flow in field is reflected by low GOR, which is not possible under conventional solution-gas drive. He said that high pressure gradients are induced in the reservoir due to sand production and propagation of sharp front away from the well. Considering the field case of Hamaca where geo-mechanical effects are absent and pressure has dropped only 100 psi (689 KPa) in 12 years of production, it might be argued that *"foamy flow"* is unlikely to be the factor contributing to enhanced recovery.

The above argument poses a serious question on the conclusions from high pressure depletion rate tests. Can the mechanism defined from high depletion rate and the results generated apply to the field situation?.

Although most of the theories seem to be different; on a closer analysis it seems they relate to the same principle. Essentially all of them try to somehow address two major issues:

1. Gas retention in porous media (low gas mobility, *"foamy oil"* flow, pseudo-bubble point, high critical gas saturation), and
2. High oil flow rate (lowering of viscosity, increase in oil mobility, non-newtonian effects, geo-mechanical effects)

After an extensive review it seems that flow behaviour in a heavy oil reservoir is quite complex and cannot be explained with a single theory. A combination of some or all of the theories would be required to totally address all the aspects of this favourable behaviour of heavy oil reservoir.

2.4.5. Selection of experimental method

Having established that gas phase distribution and hence relative permeability during solution-gas drive is principally different than in external gas drive, it was desired to design experiment to measure relative permeability which is representative of solution-gas drive process.

The relative permeability under solution-gas drive as discussed, depends on a number of factors. For measurement of relative permeability

representative of the field condition, it is necessary that properly designed and scaled experiments are carried out [Maini (1995)].

There are few published data [Pooladi-Darvish and Firoozabadi (1999), Guo-Quig and Firoozabadi (1999)] of gas relative permeability in the presence of heavy oil, especially using the depletion techniques. The above studies have used the core depletion set-up to represent the solution-gas drive process. In this study, a similar setup was designed to conduct the desired experiments. Certain improvements and modifications were made for better control and monitoring of the experiments. The detail of the setup shall be given in chapter-5.

Chapter 3

OBJECTIVE

3.1. Scope of the study

Following a thorough study of the solution-gas drive process and favourable behaviour of heavy oil reservoirs under solution-gas drive, it was decided to investigate why heavy oil reservoirs exhibit behaviour unlike conventional light oil reservoirs.

As mentioned previously, the process of solution-gas drive involves supersaturation resulting in bubble nucleation that is followed by gas phase growth, coalescence and finally flow. This study looks at two steps in the process of solution-gas drive viz. gas phase growth and flow. Thus the research was divided into two parts. In the first part a theoretical study was undertaken to model the gas phase growth during the solution-gas drive process. In the second part, depletion experiments were carried out to study the effect of depletion rate on gas mobility under solution-gas drive process.

3.1.1. Kinetics of bubble growth

In some of the previous studies [Pooladi-Darvish and Firoozabadi (1999)], the P-V graph during the constant volumetric rate depletion process was observed to exhibit different behaviour, under similar experimental conditions, for light and heavy oil. The supersaturation in lighter oil was found to be lower than that in heavy oil. The supersaturation, in the experimental run, as mentioned earlier, occurs much before critical gas saturation is reached. At this time the bubbles may have nucleated and are growing. Since

this is the early time during the solution-gas drive process, the gas bubbles may be isolated and not coalescing.

In this part of the thesis, a theoretical model was developed for gas phase growth. Both, hydrodynamic and diffusive forces were accounted for in the model. At first, a single bubble growth is studied in infinite domain for gradual decline in pressure. One of the main objectives of the study was to compare the bubble growth from step decline in pressure to that from gradual decline in pressure. In the next step a no-flow boundary condition is introduced which more closely resembles real reservoir condition. Finally, the model is modified for growth of several bubbles in a closed region coupled with constant volumetric rate depletion. This represents the desired gas phase growth model during solution-gas drive process. The results from this model were used to explain the unlike behaviour of heavy oil system from conventional light oil system. The sensitivity of gas phase growth to various parameters was studied. Finally, we wanted to find the range of applicability and validity of the diffusional growth model (at^b) which has been used quite extensively [Kashchiev and Firoozabadi (1993, 96), Sheng (1995)] to predict the gas saturation build up in a reservoir.

3.1.2. Gas mobility measurement

To investigate the favourable behaviour of heavy oil reservoirs, depletion experiments were performed on a sand-pack. Observations were made, with particular relevance to the various models that exist, to explain the anomaly observed in heavy oil reservoirs. One of the specific objectives was to investigate one of the theories [Pooladi-Darvish and Firoozabadi (1999), Guo-Quig and Firoozabadi (1999)], which attributes this behaviour to low gas relative permeability in heavy oil under solution-gas drive.

The depletion experiments were performed at various rates to study the effect of depletion rate on the solution-gas drive process and observe the various parameters that are affected by depletion rate. Several improvements

were made to overcome the shortcomings of the previous works. Pressure was measured at different points along the length of the sand-pack to model the flow accurately. The core-holder was rotated to negate the gravity affects during experimental run. Overburden and Axial pressure was applied during the experiments. A connate water saturation was established in the sand-pack for experiments. Further, more accurate pressure transducers were used for data acquisition.

The experimental data were simulated on Eclipse-100 black oil simulator to determine gas relative permeability. Further the experimental results were analysed, in light of experimental observations, to examine some of the existing theories.

Chapter 4

KINETICS OF BUBBLE GROWTH

4.1. Introduction

The process of solution-gas drive involves nucleation of bubbles in oil as the pressure falls below the bubblepoint pressure, following which the bubbles grow. During growth, the bubbles come in contact with each other and with the breaking of the lamella coalesce to form interconnected gas bubbles, often with multiple branches.

As mentioned earlier, the process of solution-gas drive in heavy oil reservoirs shows a number of anomalies when compared to that in a light oil reservoir. A number of theories [Smith (1986), Claridge and Prats (1995), Shen and Batycky (1999), Islam and Chakma (1990), Geilikman *et al.* (1995), Bora and Maini (1997), Pooladi-Darvish and Firoozabadi (1999)] have been proposed to explain this behaviour of the heavy oil reservoir. However, only a few look at the basic physics of the problem to find out reasons for these anomalies. In this chapter an attempt has been made to study the aspect of bubble growth with specific application to the solution-gas drive process by looking at the physics of bubble growth and study the effect of viscosity, diffusion coefficient and other parameters on growth. As a first step, growth of a single bubble in bulk is considered and the effect of porous medium is not included. The bubble growth in light oil is compared with that in heavy oil and the reason for the differences sought.

The previous bubble growth studies in bulk [Scriven (1959), Patel (1980), Szekely and Martins (1971), Szekely and Fang (1973)] considered the case

when the pressure was dropped in a step. In this chapter, the bubble growth for gradual decline in pressure is studied, which more closely simulates reservoir conditions. The results from gradual decline in pressure are compared with step decline in pressure case.

Kashchiev and Firoozabadi (1993) reviewed many of the limiting models when either hydrodynamic forces or mass transfer forces dominate bubble growth. It was shown that in some cases, bubble growth can be modelled by $R(t) = at^b$, where R and t are bubble radius and time, and a and b are constants. In this study, we incorporate both hydrodynamic and diffusion terms, and examine the range of applicability and validity of this model that has been used quite extensively [Firoozabadi and Kashchiev (1996), Sheng *et al.* (1999), Hunt and Berry (1956)] to predict the gas saturation build up in porous media. Further, the applicability of this power-law model is verified at different rates of pressure decline and effect of initial bubble radius on growth is also investigated.

In the next step, growth in infinite domain is compared with that in a closed domain (no-flow boundary), which more closely simulates multiple bubble growth in porous media. Results clearly show significant difference between bubble growth in infinite and finite domains.

Finally, our numerical bubble growth model is used to simulate the gas phase growth during solution-gas drive experiments, neglecting effect of porous media. Growth of several bubbles in a limited domain, with no-flow boundary, at constant volumetric depletion rate is studied. Simulation was done to match the experimental data of Pooladi-Darvish and Firoozabadi (1999). The effect of rate of depletion, viscosity and diffusion coefficient is studied.

4.2. Statement of the problem

Consider oil that is saturated with gas and is in equilibrium with a gas bubble. At this time, pressure in the liquid is reduced, either in a step or gradually, leading to growth of the bubble. The equations governing the bubble

growth were written following Szekely and Martins (1971) and are given below. These equations can be broadly classified into two categories viz. Hydrodynamic and Diffusional growth equation as mentioned earlier. The derivation of these equations is given in Appendix - I. The schematic representation of the problem is shown in Figure 4.1.

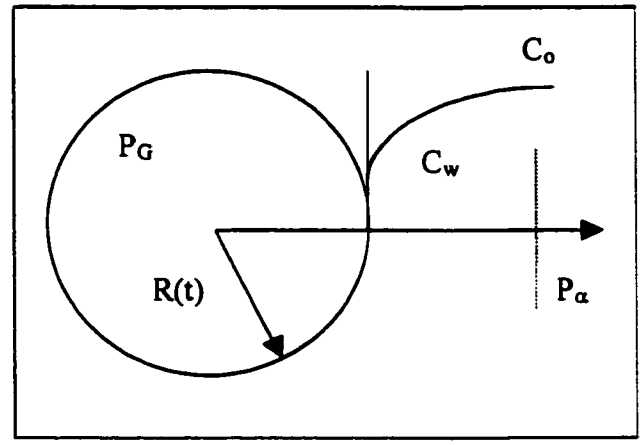

Figure 4.1: Schematic representation of the problem

4.2.1. Hydrodynamic growth model

Equation 4.1, which essentially is a combination of equation of continuity, motion and continuity of normal stress at bubble surface, with initial conditions 4.2 and 4.3 constitutes the hydrodynamic growth model.

$$R\frac{d^2R}{dt^2}+\frac{3}{2}\left(\frac{dR}{dt}\right)^2=\frac{1}{\rho_L}\left[P_{G,R}-\frac{2\sigma}{R}-4\mu\frac{(dR/dt)}{R}-P_{L,\infty}\right] \tag{4.1}$$

$$R=R_0,\quad t=0 \tag{4.2}$$

$$\frac{dR}{dt}=0,\quad t=0, \tag{4.3}$$

Equation 4.1 states that rate of growth is controlled by the pressure difference between the bubble and liquid, viscous momentum transfer, inertia of the liquid and rate of work done against surface tension forces. The liquid is

assumed to be incompressible. $P_{L,\infty}$ is the pressure at the far boundary. For step drop in pressure, $P_{L,\infty}$ has a constant value throughout the solution. Whereas, in gradual pressure decline case, it is replaced by a pressure-function, decreasing linearly with time. Any other desired correlation may also be substituted for $P_{L,\infty}$.

4.2.2. Diffusional growth model

Equation 4.4, which is essentially the mass conservation equation in spherical co-ordinates, with initial condition 4.5 and boundary condition 4.6 and 4.7, makes up the diffusional growth model.

$$\frac{\partial C}{\partial t} = D\left[\frac{\partial^2 C}{\partial r^2} + \frac{2}{r}\frac{\partial C}{\partial r}\right] - \left(\frac{R}{r}\right)^2 \frac{dR}{dt}\frac{\partial C}{\partial r}, \quad r > R \tag{4.4}$$

$$C = C_0, \quad t = 0, \quad r \geq R \tag{4.5}$$

$$C = C_0, \quad r \to \infty \tag{4.6}$$

$$P_G = f(C), \quad r = R \tag{4.7}$$

The boundary condition 4.6 is valid for an infinite domain. The finite domain boundary condition shall be presented later. Equation 4.7 is the equilibrium assumption at the interface. Henry's law defined as

$$P_G = KC_w \tag{4.8}$$

is used as an equilibrium correlation. Here, C_w is the concentration at the interface and K is the Henry's constant.

For diffusion limited growth, it is assumed that there is no pressure drop in the liquid phase i.e. pressure inside bubble = pressure at far boundary + capillary pressure ($P_G = P_{L,\infty} + P_c$), at the same fluid level and the solute concentration is in thermodynamic equilibrium with the gas contained in the bubble (Szekely and Fang (1973)). So,

$$C_w = \frac{P_{L,\infty} + P_c}{K}$$

The system pressure is approximately 600 psi and the capillary pressure is 6 psi. Neglecting capillary pressure will introduce and error of 1%. It is to be further noted that as the bubble grows the capillary pressure will go on decreasing and hence the error will also diminish (when the bubble grows 100 times, the error shall be approximately 0.01%). To simplify the above formulation the capillary pressure term can be neglected within acceptable error limits. The above equation simplifies to

$$C_w = \frac{P_{L,\infty}}{K} \tag{4.9}$$

4.2.3. General growth model

When both forces are important, i.e. for "general case", the two equations (Equation 4.1 and 4.4) are solved simultaneously along with the connecting boundary condition 4.10 and equilibrium condition (Equation 4.7). The connecting boundary condition relates mass flux to the increase in bubble size. It states that diffusional flux is equal to rate of increase of mass of bubble.

$$3DR^2 \frac{\partial C}{\partial r} = \frac{d(\rho_G R^3)}{dt}; \quad r = R \tag{4.10}$$

For solution of the general growth model, Equations 4.2, 4.3 and 4.5 are considered as the initial conditions. The bubble growth due to hydrodynamic and diffusional forces can be studied separately, by solving the corresponding equations independently with the appropriate boundary conditions. The general case is solved subsequently. Change in gas density in the bubble (Equation 4.10) is included in the growth model, which was neglected in some of the previous studies [Szekely and Martins (1971), Szekely and Fang (1973)]. When the pressure at the far boundary changes and bubble grows, the pressure inside the bubble changes and hence the gas density changes.

Bubble growth in infinite domain and in a closed system is modelled using a constant concentration and a zero concentration gradient at the far boundary, respectively. As, the bubble grows, the gas-oil interface moves

outwards. Hence, the location of the interface boundary condition, with respect to the radial co-ordinates changes with bubble growth. So, bubble growth is a moving boundary problem. A special co-ordinate is defined that transforms the position of the gas-oil interface to the reference position. The set of equations is solved in a co-ordinate system that moves with the liquid-bubble interface. Special care was given to properly account for the no-flow boundary condition for the finite domain problem, which moves inward in this new co-ordinate system. Details on this treatment shall be given later when defining finite domain model.

4.2.4. Dimensionless formulation

For the solution of the bubble growth problem, all the equations were first put in dimensionless form and then solved. Since the previous studies [Szekely and Martins (1971)] considered bubble growth when the pressure was dropped in a step, the dimensionless parameters defined in their study cannot be used. This is because, for our treatment, i.e. gradually changing pressure at the far away boundary, the dimensionless parameters as defined in previous studies would change with time. So, a new set of dimensionless parameters were defined that are given in Table 4.1.

Care was taken to define dimensionless parameters that do not change with time. All the equations, from 4.1 to 4.10, were put in dimensionless form. The detailed treatment and derivation is given in Appendix - I. The final form of the equations is as follows:

(i) Hydrodynamic Growth Model

$$\xi\frac{d^2\xi}{d\tau^2}+\frac{3}{2}\left(\frac{d\xi}{d\tau}\right)^2+\frac{4Sc}{\xi}\frac{d\xi}{d\tau}=G\left[\Pi-\frac{\phi}{\xi}\right]-\frac{G}{P_o}\left[P_{L,\infty}\right] \tag{4.11}$$

Initial Condition

$$\xi=1,\quad \tau=0 \tag{4.12}$$

$$\frac{d\xi}{d\tau}=0, \quad \tau=0 \tag{4.13}$$

(ii) Diffusion Growth Model

$$\frac{\partial C^*}{\partial \tau}=\frac{\partial^2 C^*}{\partial \eta^2}+\frac{d\xi}{d\tau}\left[1-\frac{1}{(1+\eta/\xi)^2}\right]\frac{\partial C^*}{\partial \eta}+\frac{2}{\xi(1+\eta/\xi)}\frac{\partial C^*}{\partial \eta} \tag{4.14}$$

Initial and Boundary Condition

$$C^*(0,\eta)=1 \tag{4.15}$$

$$C^*(\tau,\infty)=1 \tag{4.16}$$

(iii) Boundary condition - General growth model

Conservation of mass at the bubble interface (Equation 4.10) becomes

$$\left(\frac{\partial C^*}{\partial \eta}\right)_{\eta=0}=Ja\left(\Pi\frac{d\xi}{d\tau}+\frac{\xi}{3}\frac{d\Pi}{d\tau}\right) \tag{4.17}$$

(iv) Equilibrium Assumption at the gas-liquid interface - Henry's law

For general growth model

$$\Pi=C_w^* \tag{4.18}$$

For hydrodynamic limited growth asymptote since, $C_w=C_0$

$$\Pi=1 \tag{4.19}$$

For diffusion limited growth asymptote since, $P_{L,\infty}=P_G$

$$C_w^*=\frac{P_{L,\infty}}{KC_0} \tag{4.20}$$

Table 4.1: Dimensionless parameters

Dimensionless Parameter	Definition
τ	$\frac{Dt}{R_0^2}$
ξ	$\frac{R}{R_0}$
ϕ	$\frac{2\sigma}{R_0 P_0}$
Π	$\frac{P_G}{P_0}$
Sc	$\frac{\mu}{\rho_L D} = \frac{\nu}{D}$
C^*	$\frac{C}{C_0}$
η	$\frac{r}{R_0} - \xi$
G	$\frac{R_0^2 P_0}{\rho_L D^2}$
Ja	$\frac{\rho_{G,0}}{C_0}$

4.2.5. Gradual decline in pressure model

For gradual decline in pressure, $P_{L,\infty}$ is substituted into equation 4.11 as the following function of time:

$$P_{L,\infty} = P_o - ct \tag{4.21}$$

where, c is the rate of pressure decline.

4.2.6. Finite domain model

Most of the previous solutions available for bubble growth consider infinite domain for mass transfer. In real situation, the mass transfer domain and hence the solute available for bubble growth is limited. The following far away boundary condition, which implies zero mass flux at the outer boundary, is used for finite domain mass transfer model:

$$\frac{\partial C^*}{\partial \eta} = 0 \qquad \textit{at far boundary} \tag{4.22}$$

Since there is limited domain for mass transfer, the physical space available for growth of bubble is shrinking as the bubble is growing. It can best be visualised by bubble growing inside a closed spherical ball. This is represented in Figure 4.2.

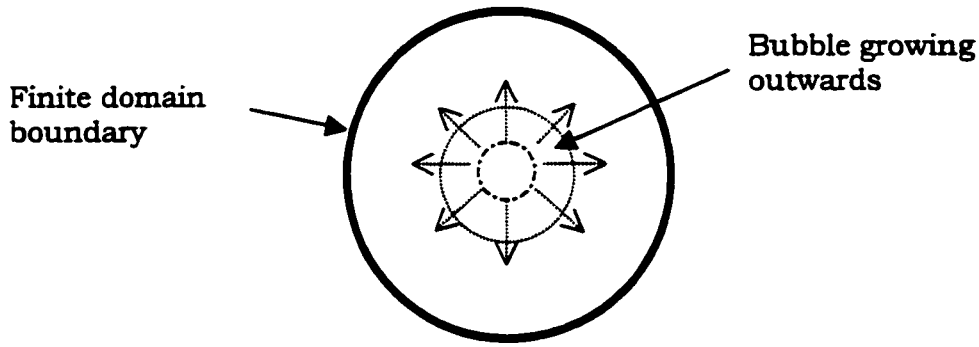

Figure 4.2: Representation of bubble growing in finite domain

The outer boundary is fixed and the bubble surface is moving outwards. As a result the physical space is reducing with time. Since, in numerical solution scheme, the space outside the bubble is divided into a number of equally spaced grid, this results in modification of the space grids as the bubble grows. If the size of the grid blocks in numerical solution of the problem is kept constant, then this situation translates into reducing number of grid block with time. During numerical simulation, the space available for solute diffusion is calculated at the end of each time step. This is done from

the knowledge of solution for bubble radius. The resultant space available is used to calculate the number of grid block, based on the spacing assumed during initialisation of the solution. These number of grid blocks are then used while considering solute transfer in the next time step.

A solute balance was done at the end of each time step to calculate the error in solute balance. Since this technique involves deleting grid blocks, we end up with some error in solute balance. It was expected that the maximum error in solute balance, when the bubble grows 3000 times, shall be 2-3%. In the run the error observed was as predicted. This value is within the acceptable error limit.

4.2.7. Modelling solution-gas drive process

While simulating the solution-gas drive process (constant volumetric rate depletion), a certain number of bubbles are considered to be growing in a specified domain. The growth of the bubble is coupled with the liquid withdrawn to determine final pressure in the system.

Consider constant volumetric rate production from a porous media saturated with live oil. During single phase, the average pressure is dropping at a constant rate determined by single-phase compressibility. At some point below the bubblepoint pressure, bubbles nucleate and start growing. Before critical gas saturation, the system pressure is not only a function of rate of production but also rate of bubble growth and bubble pressure. In a constant-volume system, rate of volume expansion of bubbles partly compensates for the produced liquid and the bubble pressure acts similar to internal pressure boundary condition, pushing against the liquid.

The following additional equations were used in conjunction with Equations 4.11 - 4.20 and 4.22 to find the solution for the constant volumetric rate depletion process.

$$\kappa_o = -\frac{1}{V}\frac{\partial V}{\partial P} \tag{4.23}$$

$$V_o = V_p - \left(\frac{4}{3}\pi(\xi R_0)^3\right)B_{no} \tag{4.24}$$

Where, κ_o is compressibility of the oil phase, V_o volume of oil, V_p pore volume and B_{no} number of bubbles. Equation 4.23 is the system compressibility expression. Equation 4.24 states that volume of oil at any time is equal to pore volume minus the volume of gas.

The assumption in equation 4.11 was that the liquid is incompressible, whereas, in equation 4.23 we consider it slightly compressible. It would be seen later in the results section that hydrodynamic forces play an insignificant role in bubble growth and hence can be neglected; the hydrodynamic growth equation can be omitted. Hence the incompressible assumption involved in derivation of equation 4.11 will not change the growth results.

Equation 4.23 is used to calculate the average pressure of the system after each time step, for constant volumetric rate depletion process. The calculated average pressure is designated as $P_{L,\infty}$. This is a good assumption since in the spherical coordinates, the bulk of the fluid is near the far boundary.

4.2.8. Physical parameters used in simulation

In this study, oil viscosity values ranging from 30 cp to 40,000 cp were considered. Diffusivity values were taken from AOSTRA handbook and are given when the results are presented. The diffusivity for oil of other viscosities was calculated using the following correlation (AOSTRA (1989))

$$D = 1.4x10^{-8}\frac{T(XM)^{0.5}}{\mu V^{0.6}} \tag{4.25}$$

where X is an empirical constant, V is the molar volume and M is the molecular weight. Once diffusivity value for oil of a certain viscosity is known, X is calculated and then equation 4.25 can be used to calculate diffusivity values for any other oil viscosity. The initial bubble radius in all cases was 1

micron (except while simulating the experiment where it was taken as 0.5 micron). Sensitivity studies were performed on initial bubble radius. Table 4.2 lists the properties that were used in the simulation.

Table 4.2: Parameters used in simulation of bubble growth

Parameter	Value
Initial Radius	1 micron
Specific gravity of Oil	0.995
Surface tension	0.02 N/m
Initial solution GOR	6.5 v/v
Henry's constant	549.5 KPa.m^3/Kg
Temperature	298 ^oK
Initial no.of space grids	100

4.3. Results

All the above equations, for various cases, were solved numerically. Since the growth equations are non-linear, they were first linearised using Newton's method [Hoffman (1992)]. Once linearised, the growth equations with boundary conditions were put into finite difference form. A set of linear algebraic equations were formed, which were then put in the form of a matrix and solved using LU decomposition.

The details of calculations, formulation and treatment of the equations and matrix is given in Appendix - I.

4.3.1. Gradual decline in pressure

4.3.1.1. Infinite domain results

In the simulation run, we started with oil 6 psi (41.36 Kpa) below the bubblepoint pressure of 600 psi (4136 Kpa) and a gas bubble in equilibrium with the oil. Accounting for capillary pressure, gas pressure is 600 psi (4136

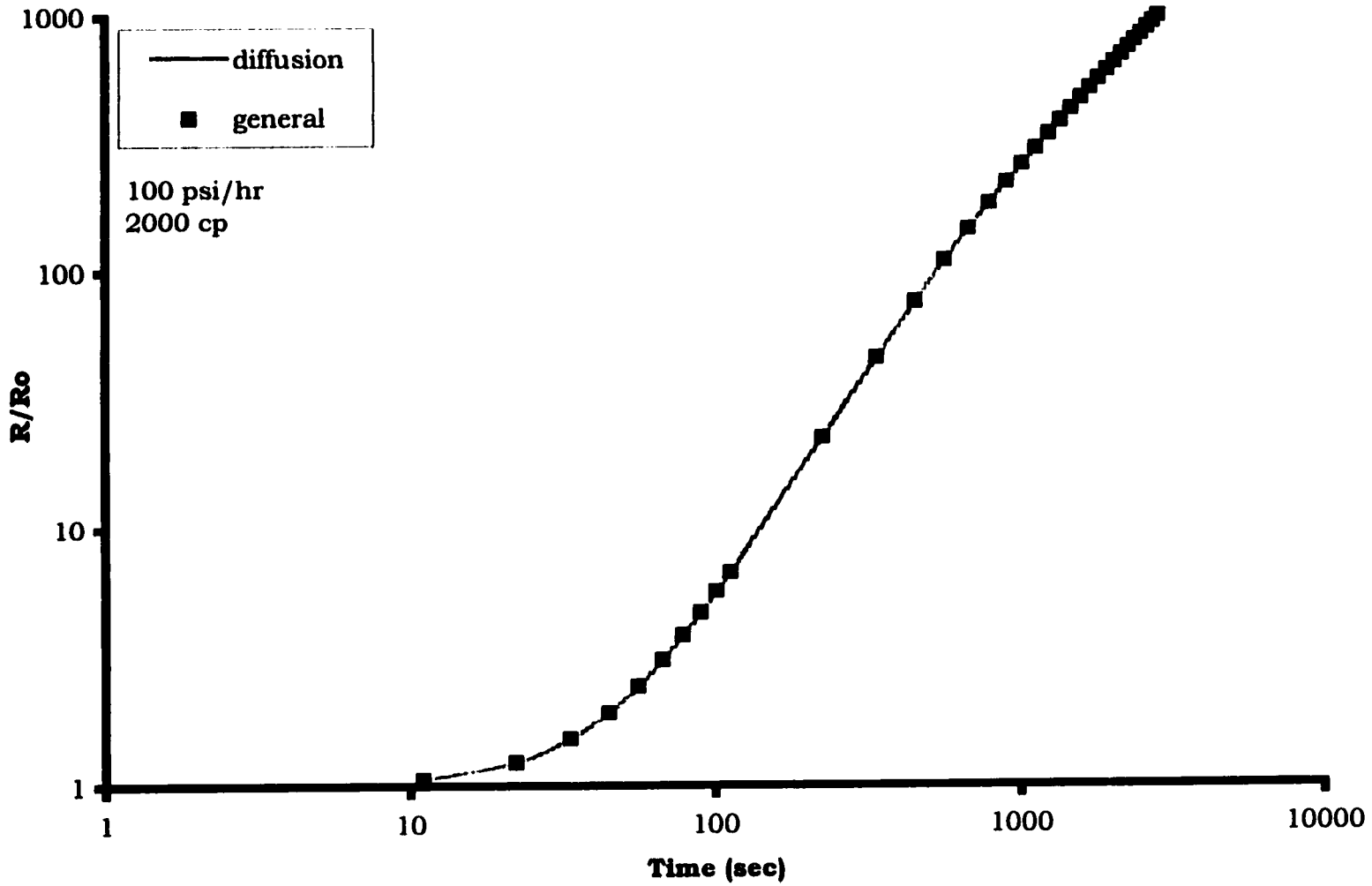

Figure 4.3: Diffusion limited vs General growth : gradual decline in pressure

Kpa) , and the liquid at the bubble interface is at equilibrium with the gas. Hence, no concentration gradient exists in the liquid and the bubble and liquid are in mechanical and chemical equilibrium. Here we have neglected change in partial molar volume, hence chemical potential of the gas in solution with pressure. The surface tension of the oil was taken as 0.02 N/m. In the simulation runs, the gradual decline case was modelled by decreasing the pressure boundary condition at the far boundary with time (Equation 4.21).

The preliminary results indicated that except for unrealistically small bubble diameters, the surface tension forces did not have any significant effect on bubble growth in the heavy and light oil. Szekely and Martins (1971) reported similar results. Surface tension force, although accounted for in the initial equilibrium of the bubble and liquid, is hence neglected in the growth process.

Figure 4.3 compares the general growth case, including both hydrodynamic and diffusive forces, to diffusion-limited asymptote, for pressure decline at rate of 100 psi/hr (689.3 Kpa/hr). The two results match each other exactly. This is in line with some previous conclusions [Szekely and Martins (1971), Szekely and Fang (1973)] that, except for very early times, the hydrodynamic forces do not play a significant role in bubble growth, and the model considering diffusive forces alone can be sufficient to predict the gas phase growth. Throughout this study and for generality of conclusions, calculations are performed using the general growth model.

The results shown in Figure 4.4 are for the growth of bubble for three oils of viscosities 30 cp, 2000 cp and 40,000 cp, when the pressure drop rate is 100 psi/hr (689.3 Kpa/hr). It may be noted that for light oil (30 cp) we observe the bubble grows by about an order of magnitude in the first minute whereas for a heavy oil of 2000 cp and 40,000 cp we may not see a considerable change in the size of the bubble in the first 2 and 100 minutes, respectively. In simulation runs of figure 4.4 diffusion coefficient was changed alongwith viscosity based on equation 4.25. It is still desired to investigate if the different results in Figure 4.4 for different oils is due to oil viscosity or diffusion

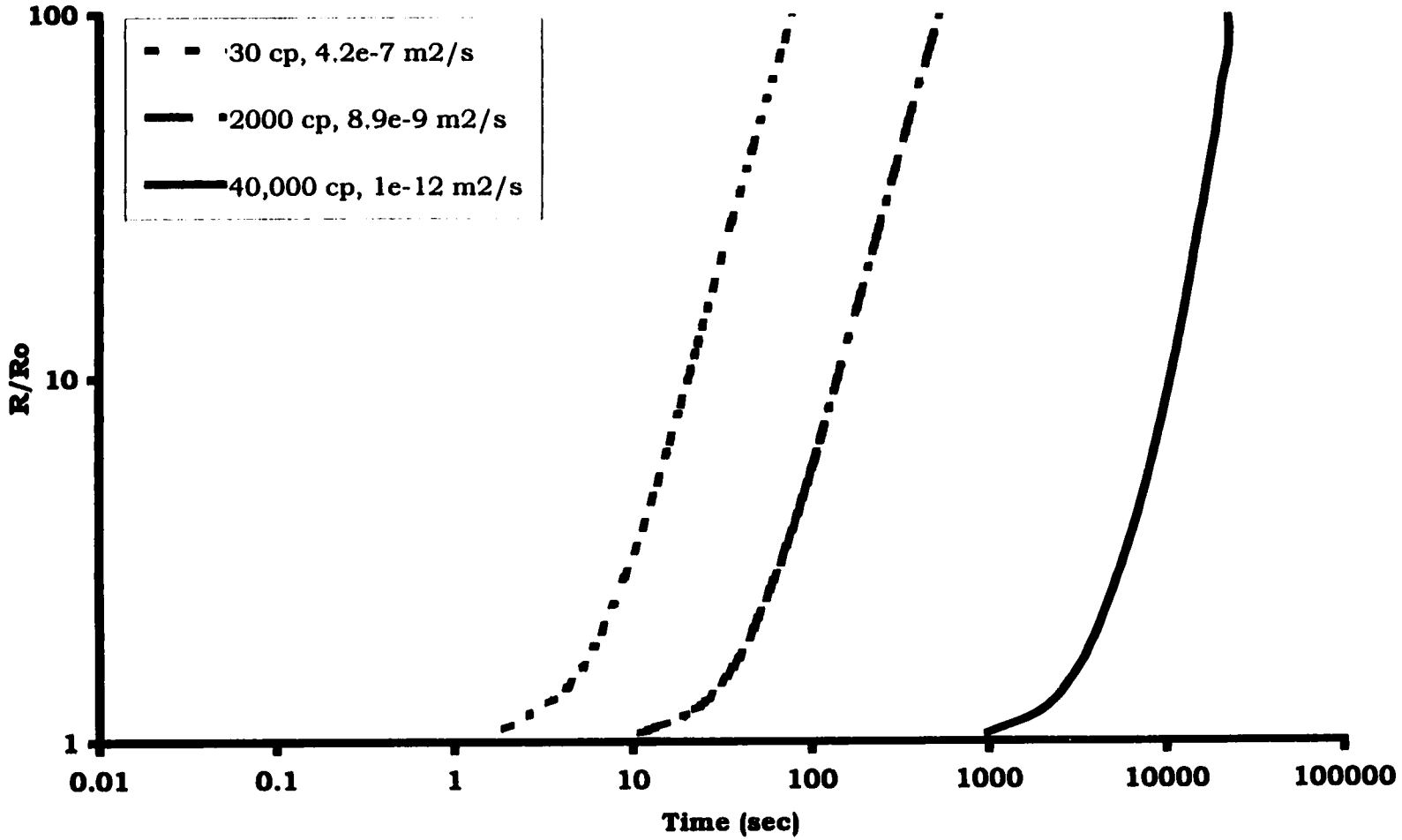

Figure 4.4: Comparison of bubble growth for gradual decline in pressure (100 psi/hr) for various cases

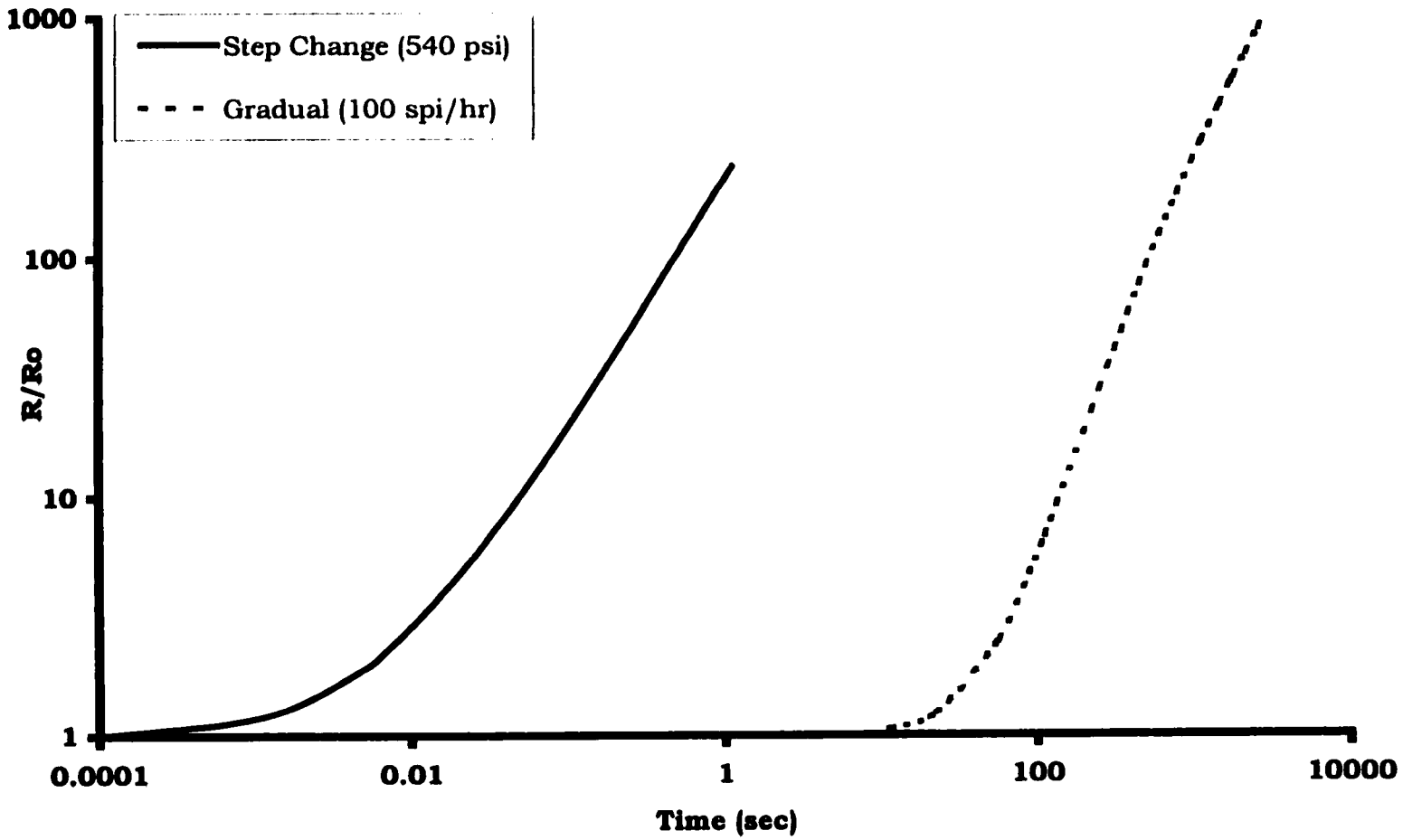

Figure 4.5: Comparison of bubble growth: step change vs. gradual change in pressure

coefficient. The results for the effect of diffusion coefficient shall be presented later.

It can also be seen in the Figure 4.4 that once the bubble growth starts, it almost follows a straight line on a log-log plot for all the cases. We can deduce that the bubble growth may be modelled by the relationship $R(t) = at^b$ for $R > R_0$. The constant a determines the initial delay observed in Figure 4.4. This delay plays an important role in the pressure behaviour of the two-phase system, as we shall see later. The above power-law model was previously suggested for the cases when the process was limited by one of the forces only [Kashchiev and Firoozabadi (1993)]. Here, its applicability is demonstrated for the general case where both hydrodynamic and diffusion terms are considered and pressure is gradually decreasing in an infinite domain, although it has already been shown that the process is governed by diffusive forces. The results depicted in Figure 4.4 suggest that the constant a is a function of oil type, for the same rate of pressure drop.

The simulations were done for the case when the pressure depletion rate was taken to be 100 psi/hr (689.3 KPa/hr). This, when compared to the field pressure depletion rate, is quite high. Cases with lower rate of pressure drop are discussed later (see Figures 4.6 and 4.11).

In Figure 4.5, bubble growth is compared for the two cases of step change and gradual decline in pressure. The step decline in pressure is simulated by dropping the pressure at the far away boundary suddenly by 540 psi (3722 KPa), from 600 psi (4136 KPa) initial pressure. The initial bubble growth in case of step decline in pressure is much greater than in the case when the pressure is lowered gradually. This is because, in step decrease in pressure, the concentration and the pressure driving forces are much greater than that in case of gradual decline of pressure, where the concentration and pressure driving forces increase slowly with time.

Results of Figure 4.5 indicate that for the same oil, constant b is rather insensitive to method of pressure drop, for example the exponent b is estimated to be 1.04 and 1.32 for the step decline and the gradual decline cases,

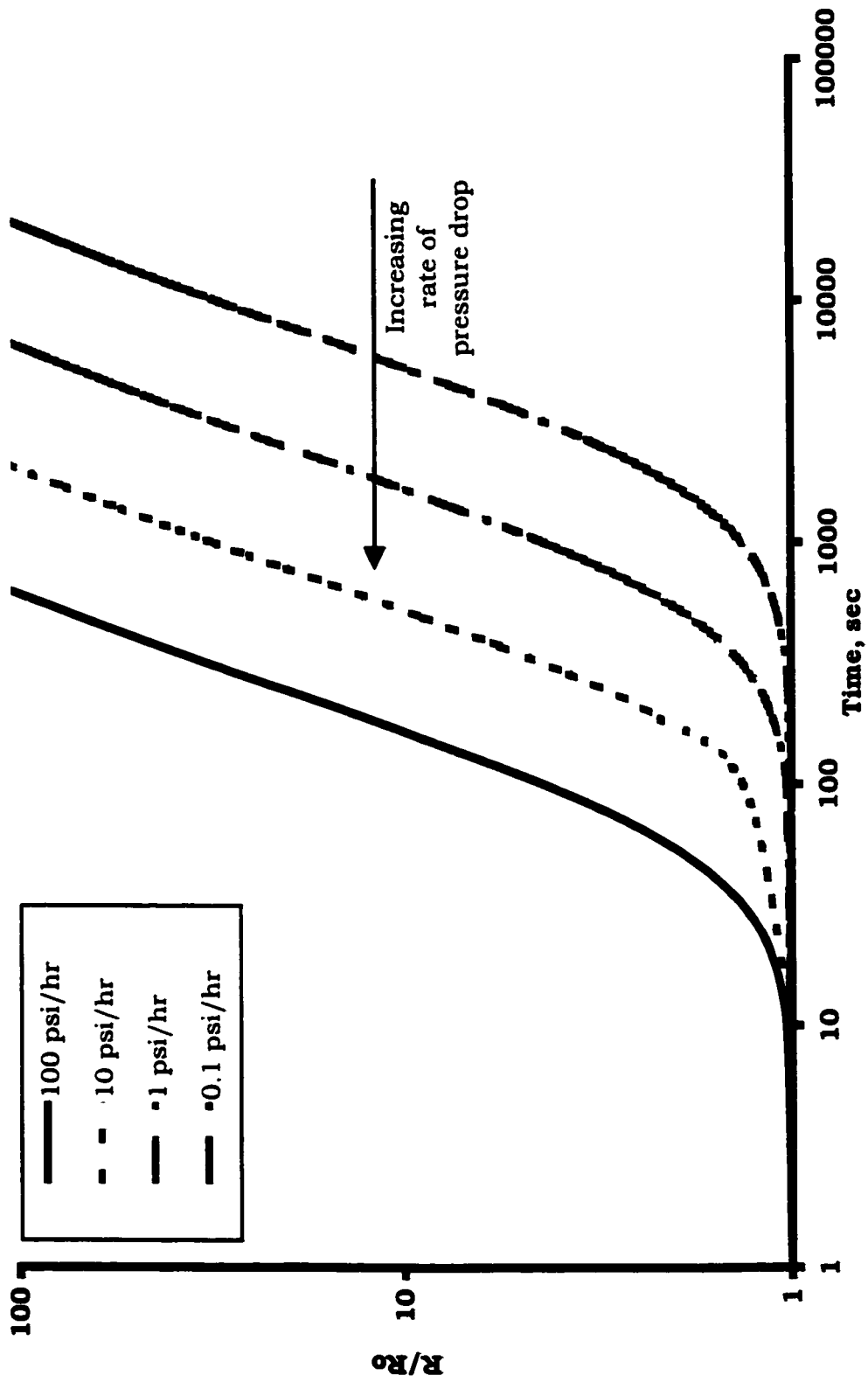

Figure 4.6: Effect of depletion rate on bubble growth

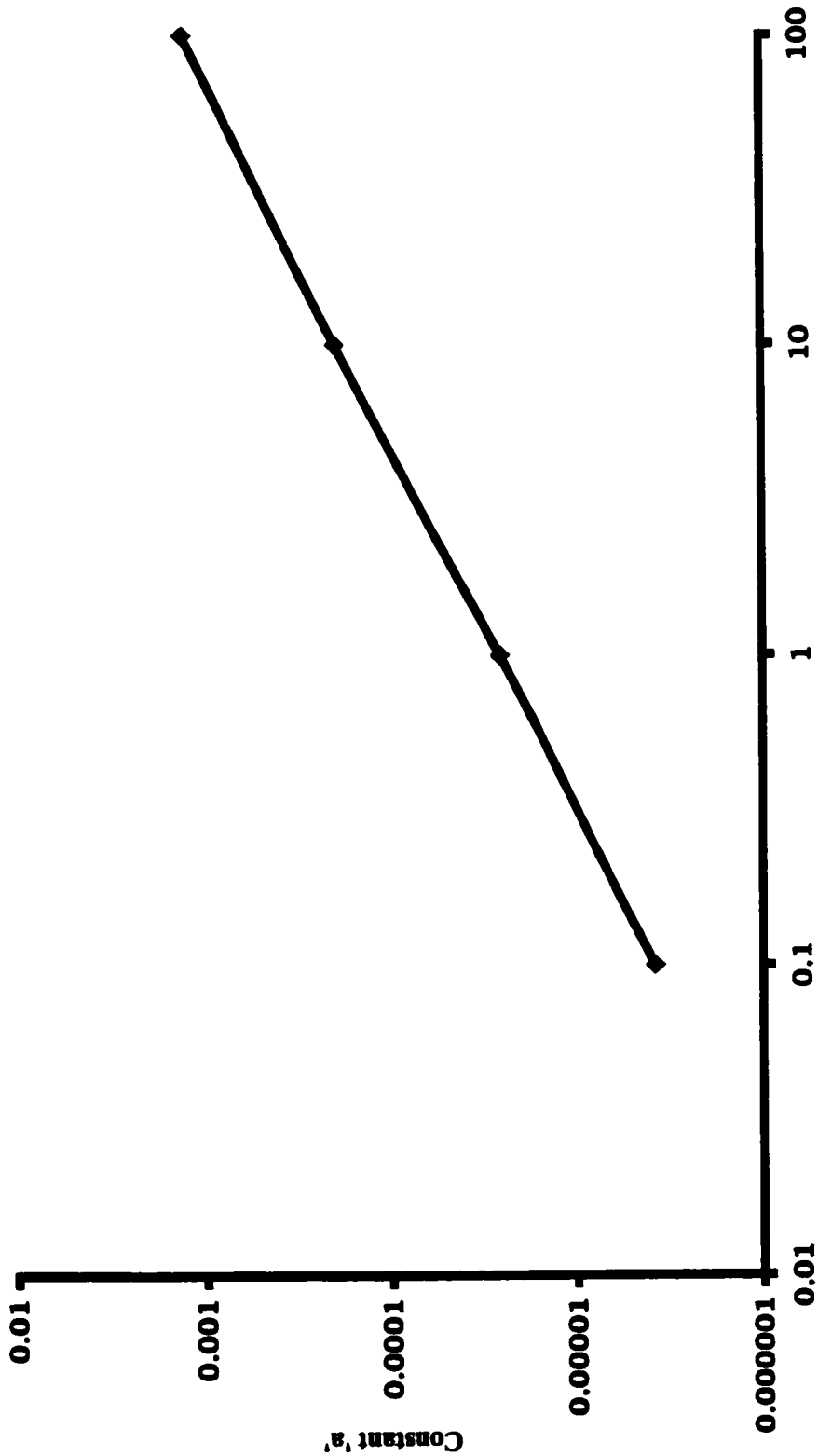

Figure 4.7: Constant "a" for growth model

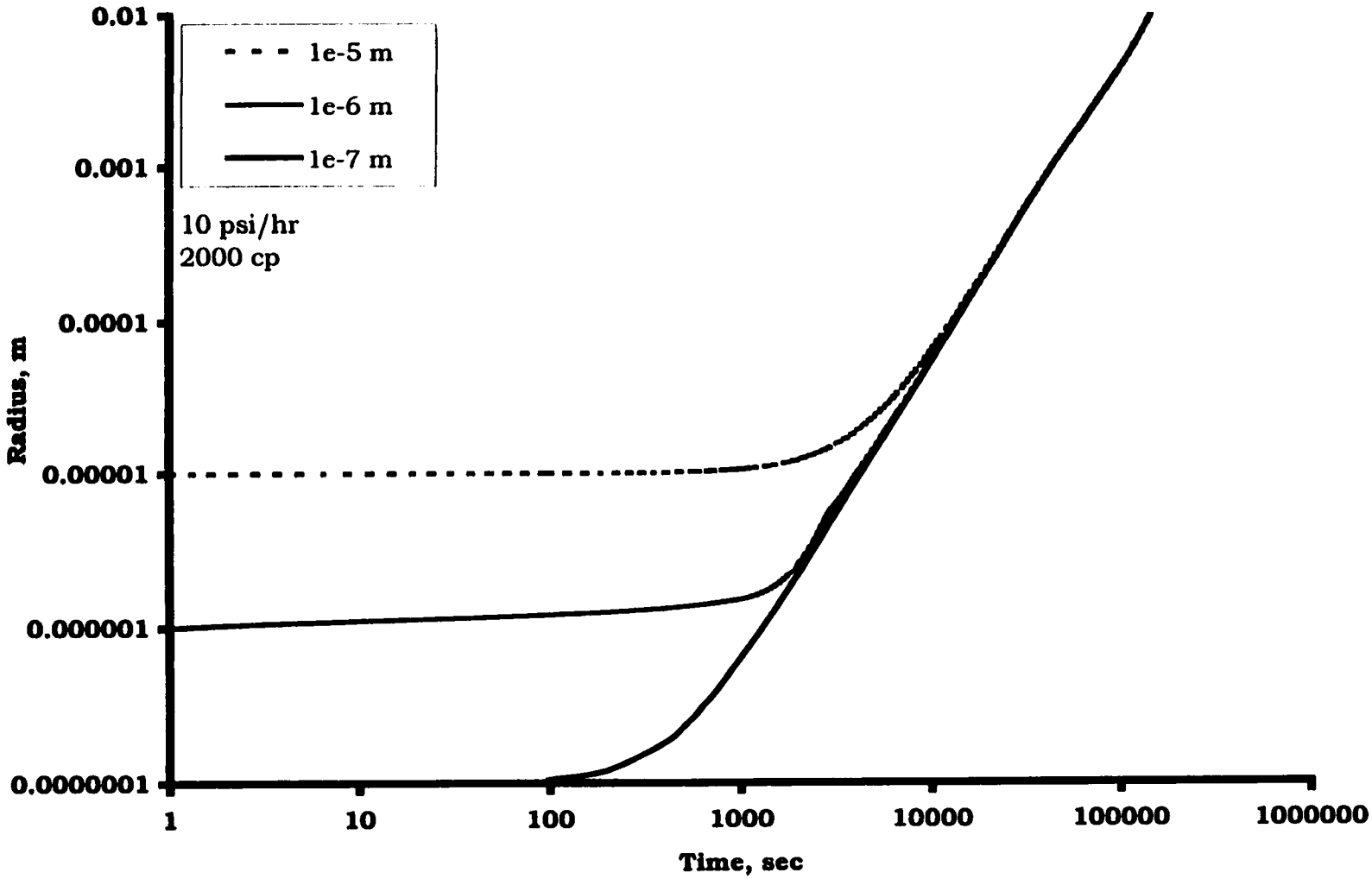

Figure 4.8 : Effect of initial bubble radius on bubble growth

respectively. The value of a which is a measure of the "delay", varies with change in depletion rate; increasing with increase in depletion rate, i.e., reduced delay.

The effect of pressure decline rate on the growth is shown in Figure 4.6. It is observed that for all the cases the slope is same. Hence it can be concluded that the constant b is independent of rate of pressure decline for the same oil. Further, it is apparent from the graph that constant a is a function of pressure decline rate. The constant a follows a logarithmic trend with pressure depletion rate as shown in Figure 4.7. A similar behaviour for a and b had been suggested in other studies [Firoozabadi and Kashchiev (1996)] on bubble growth.

The effect of initial bubble radius on bubble growth is shown in Figure 4.8. It is evident that at late time all the radii converge to a single value asymptotically. This is in conformance with the experimental study of Yousfi *et al.*(1997), where the bubble radius, with respect to time, was reported to be independent of initial bubble radius. Hence, the parameter a and b are insensitive to initial bubble size for the range of time studied.

The significance of results of Figures 4.4 - 4.8 is to show that if bubble growth experiments are used to develop empirical correlation of the type of at^b, experiments should be properly scaled because these constants are functions of oil properties, rate of pressure drop etc. Laboratory experiments with rates of pressure drop much higher than those observed in the field [Sheng *et al.* (1999)] and under different conditions can not be used for field predictions. Further, this single at^b model for all times is valid only for infinite domain - not finite domain as we shall see below.

4.3.1.2. Effect of no-flow boundary

In the simulation run, this was done by assigning a closed domain for mass transfer and a zero concentration gradient at the far boundary. This was shown in the mathematical formulation earlier (Equation 4.22) and is given in

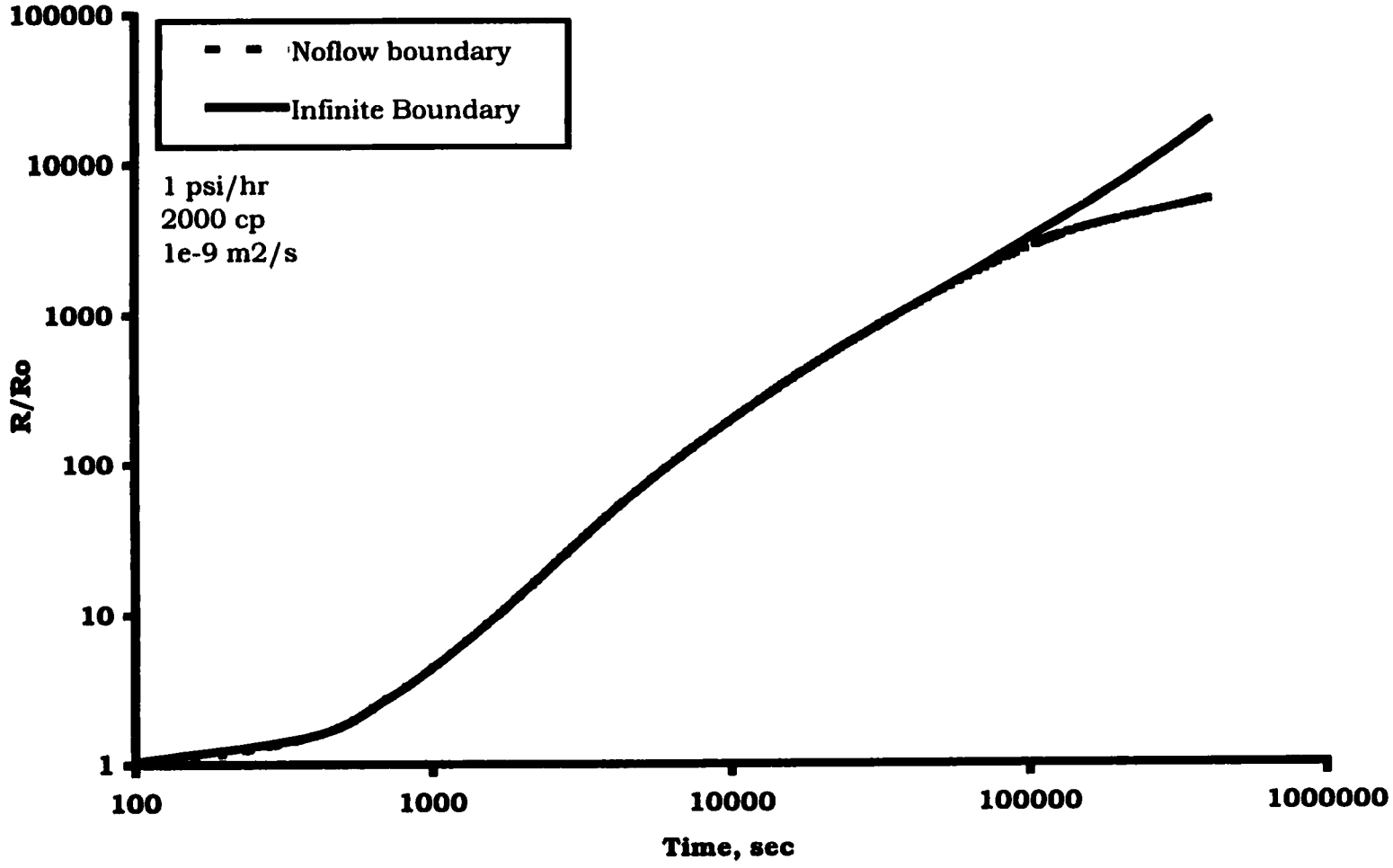

Figure 4.9: No-flow boundary vs. infinite boundary solution

detail in Appendix -I. What this translates to in the transformed co-ordinate, which moves with the bubble-interface, is that, although the bubble boundary remains stationary the outer boundary moves inwards with time. In Figure 4.9 comparison is done for cases of bubble growth in infinite and finite domain. It is clearly evident from the figure that, at late times, the model for bubble growth in infinite domain is different from that of no-flow boundary. The discrepancy starts when the concentration disturbance reaches the outer boundary in no-flow boundary case. Looking at the trend, it might be inferred that the no-flow boundary growth does not follow the at^b model. More results on bubble growth behaviour in a closed system are presented in the following.

4.3.2. Gas phase build-up during solution-gas drive

In this section, we report the results obtained from the application of the growth model thus developed, to the above physical problem. During early stages of gas evolution, and much before critical gas saturation is reached, bubbles are neither in contact nor flowing – conditions pertinent to our mathematical model. We have used the above model to study the pressure behaviour observed in constant rate of depletion experiments [Pooladi-Darvish and Firoozabadi (1999)], in particular, the sequence of increasing supersaturation below bubblepoint pressure, bounce in system pressure and the final reduced supersaturation. Similar behaviour has been reported in some of the other studies [Firoozabadi and Kashchiev (1996), Guo-Quig and Firoozabadi (1999)]. One assumption in extending our growth model to the above problem is that the effect of porous media on growth is neglected and the bubbles are assumed spherical. Also we have assumed that all bubbles nucleate at the same time below bubble point pressure, and no further bubbles nucleate afterwards. More on this assumption is given in Section 4.4. The simulation starts at the pressure where the bubbles are assumed to be nucleated. The P-V behaviour before nucleation is calculated separately using the single phase system compressibility.

The results discussed below, show that the system supersaturation increases even after bubbles have nucleated. This provides more driving force for further nucleation, violating the above assumption. Here, we ignore the short time when supersaturation is increasing and assume that instantaneous nucleation is a valid assumption [Kashchiev and Firoozabadi (1993)].

4.3.2.1. Results

In Figure 4.10, we show predictions of our numerical model for the experimental conditions of Pooladi-Darvish and Firoozabadi (1999). The bubblepoint of the oil in the above study was determined as 363 psig (2502 KPa) (by extrapolating equilibrium line backwards). In the model developed it has been assumed that the bubbles generated at 351 psig (2419 KPa) (a supersaturation of 12 psi (82.7 KPa), which corresponds to an initial bubble size of 0.5 micron). 250 bubbles were assumed, corresponding to roughly 1 bubble per cm^3 of pore volume. This approximate value of number of bubbles is in line, with that predicted by Kennedy and Olson (1952). The growth of the bubble and the system pressure were studied with respect to volume of fluid withdrawn. Table 4.3 lists the parameter and properties that were used in simulation.

Table 4.3: Parameter used in simulating experimental data of Pooladi-Darvish and Firoozabadi (1999)

Parameter	Value
Viscosity	34,000 cp
Depletion rate	1cc/day
Number of bubbles	250
Initial bubble size	0.5 micron
Pore volume	245 cc
Diffusivity coefficient	5×10^{-10} m^2/s
Initial GOR	6.5 v/v

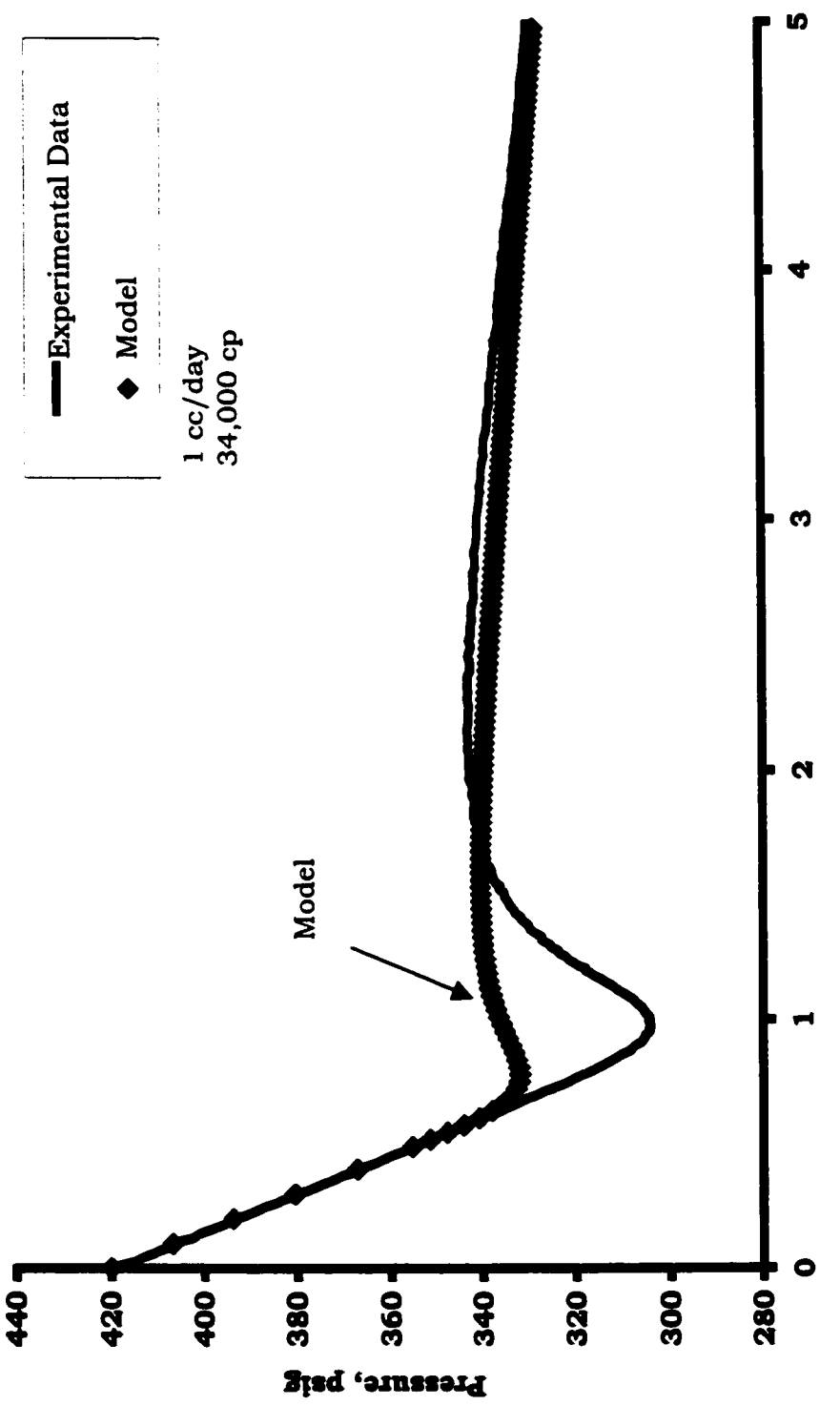

Figure 4.10: Comparison of model with experimental results

The data are those given by Pooladi-Darvish and Firoozabadi (1999) except the initial bubble size and diffusivity coefficient, which were not reported in the original reference. All other parameters were the same as those listed in Table 4.2.

Figure 4.10 shows that although the bubbles had nucleated at 351 psig (2419 KPa), the pressure continued to fall at the same rate. This means that the system compressibility, defined earlier as:

$$\kappa_o = -\frac{1}{V}\left(\frac{\partial V}{\partial P}\right)_T \tag{4.26}$$

is equal to single-phase compressibility even after bubble generation. In some of the previous works [Pooladi-Darvish and Firoozabadi (1999), Firoozabadi and Kashchiev (1996)] it was implied that the bubbles do not nucleate until we reach the lowest point in the depletion P-V curve. The authors argued that earlier nucleation of bubbles would have been reflected by the change in system compressibility and hence change in the slope of P-V graph. Here the results from our model show that even after generating bubbles, the pressure in the system can drop and can follow the single-phase compressibility curve. This might be explained by the delay present in the early times of bubble growth, evidenced in Figures 4.4 and 4.6. During the early time, rate of bubble growth is negligible so the rate of pressure drop is the same as that for the case of single-phase fluid. This early time behaviour, in part, can be attributed to smaller surface area available for mass transfer at early times when the bubble is smaller. This is abetted by the fact that the diffusivity coefficient is low for heavy oils. Later, when the P-V curve approaches the lower most part, the pressure drop line becomes more gradual as the growth of gas phase increases.

The time delay in bubble growth, which is the time after which the at^b model is valid, is not apparent in the gas phase growth model put forward by Firoozabadi and Kashchiev (1996). They apply this model as soon as the bubbles nucleate. Thus the pressure in their system rises as soon as bubbles nucleate.

Our model does not dip as much as the experimental results and does not match the data when the system pressure starts recovering. This might be due to the assumptions in the model: neglecting effect of porous media on growth and instantaneous nucleation. Sensitivity studies were performed to accurately fit the experimental data with the current model. The variable parameters were number of bubbles, diffusion coefficient and nucleation point. It was observed that lowering the nucleation point or diffusion coefficient or number of bubbles would dip the curve further down, but then the rebounding would take a long time. No significant improvement in the quality of the model was observed.

During the later stage of the process the model matches well with the experimental result. This is because an equilibrium state with respect to mass transfer has been attained and there is negligible mass transfer driving force in liquid phase. The negligible mass transfer driving force was evident in the concentration results, where the solute concentration at gas-oil interface was equal to that at the far boundary. It is the continual pressure drop at the far boundary that makes more gas available for bubble growth. Further, the two-phase compressibility, assuming equilibrium condition, as given by the following equation [Ramey (1964)]

$$\kappa_t = -\frac{S_o}{\beta_o}\left[\left(\frac{\partial \beta_t}{\partial p}\right)\right]_T + \kappa_{form} \tag{4.27}$$

where, β_t is the total, or two phase (gas and oil) formation volume factor:

$$\beta_t = \beta_o + (R_{sini} - R_s)\beta_g \tag{4.28}$$

is found to be 8.31 x 10^{-4} psi^{-1} (1.2 x 10^{-4} KPa^{-1}). This equals the experimentally observed two-phase compressibility of the system, which is 7.54 x 10^{-4} psi^{-1} (1.1 x 10^{-4} KPa^{-1}). This equality of the two values may indicate state of equilibrium.

Here, our intention was not to match the experimental data, which is governed by nucleation and growth physics in porous media. The arbitrary numbers chosen for matching purposes, i.e. nucleation supersaturation of 12 psi (82.7 KPa) and bubble density of 1 per cm^3, might be modified once a better

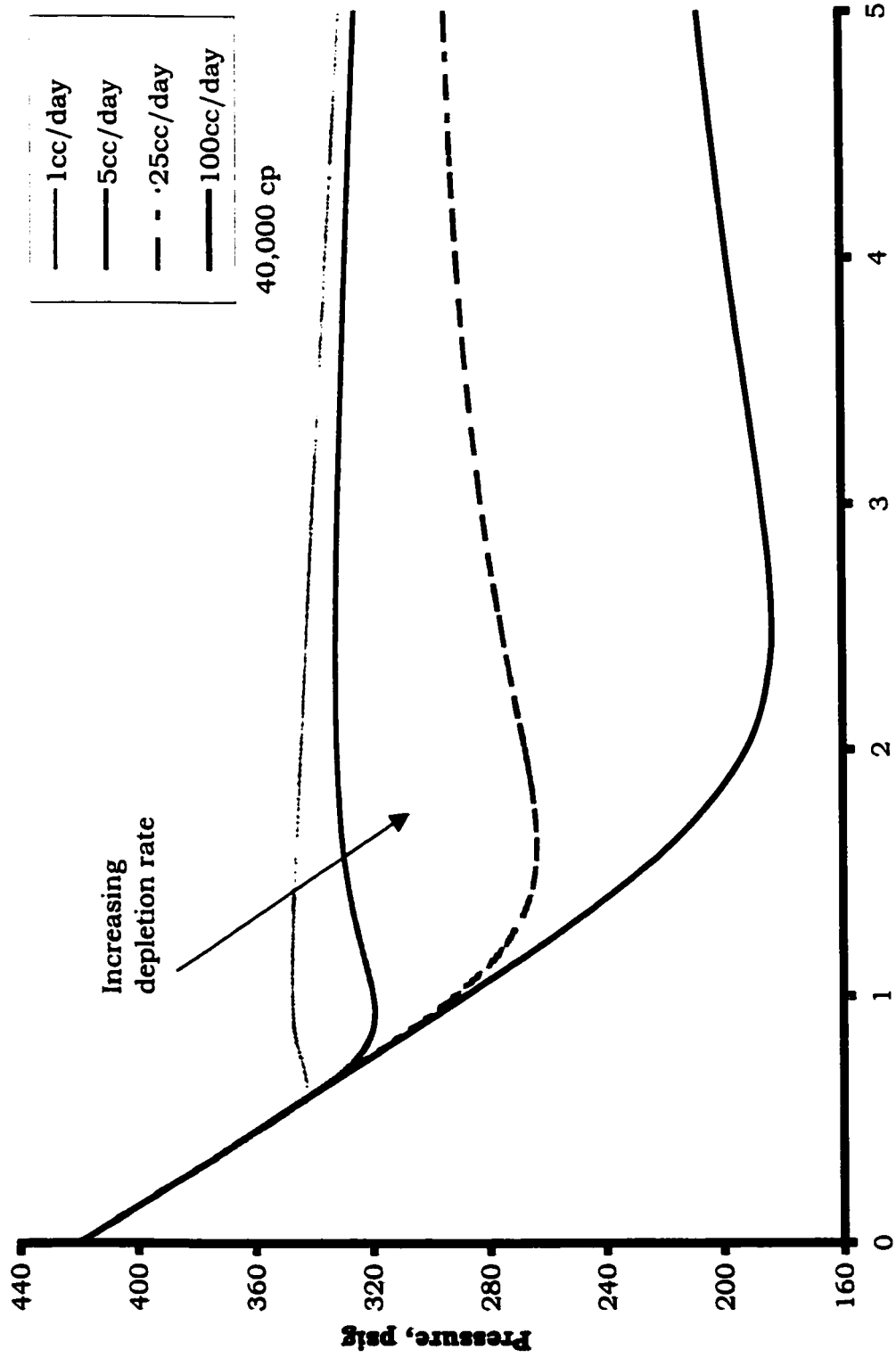

Figure 4.11 : Effect of depletion rate on system pressure

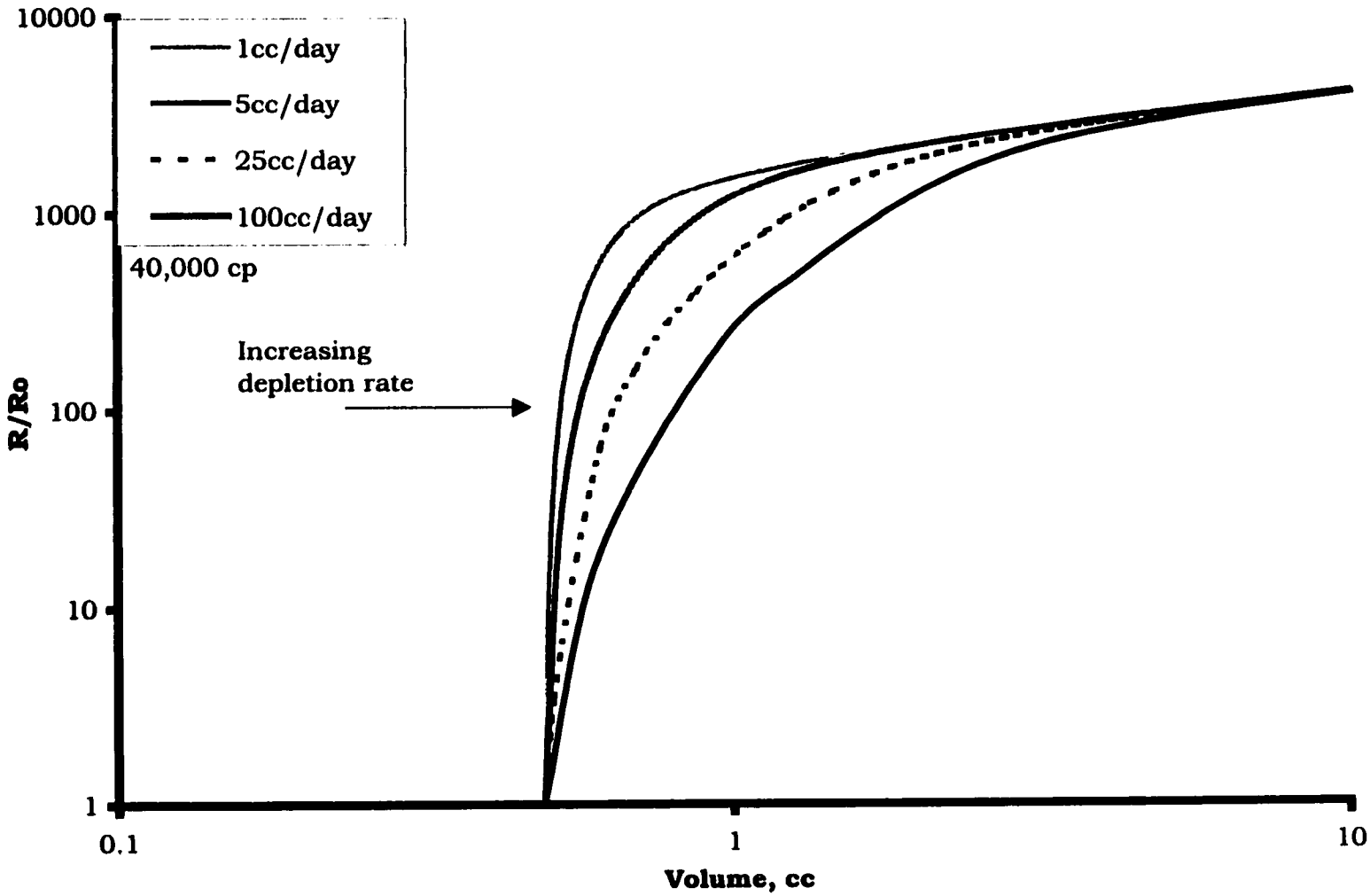

Figure 4.12: Effect of depletion rate on bubble radius

understanding of nucleation physics and the effect of porous media on nucleation and growth is known. The intention was to show that system compressibility might remain unchanged for some time even while bubbles are growing.

4.3.2.2. Sensitivity studies

4.3.2.2.1 Effect of depletion rate

The effect of rate of depletion is shown in Figures 4.11-4.12. It is evident that as the depletion rate increases, the pressure dips further down. This, in earlier studies [Kennedy and Olson (1952)], was assumed to be an indication of the increase in critical supersaturation before bubbles nucleated. Here we again show that, even though the bubbles nucleate much earlier at 351 psig (2419 KPa), the pressure keeps on dropping. The results clearly indicate that with increase in depletion rate, a lower pressure is obtained before pressure starts retrieving. A pressure difference that can be termed as "Apparent Critical Supersaturation".

Many of the previous studies had observed higher apparent critical supersaturation at higher rates of pressure drop. Our results suggest that, could be partly explained by the growth physics in contrast with nucleation physics.

Finite vs. Infinite:

Figure 4.12 shows the bubble radius as a function of produced volume (which is a multiple of time). It is observed in this graph as well as in Figures 4.14 and 4.16 that bubble growth behaviour is different than that observed in an infinite medium. Hence, the results of bubble growth studies in infinite domain [Scriven (1959), Szekely and Martins (1971), Szekely and Fang (1973), Rosner and Epstein (1972), Patel (1980)], which were used in growth studies in porous media [Kashchiev and Firooabadi (1993), Firoozabadi and Kashchiev

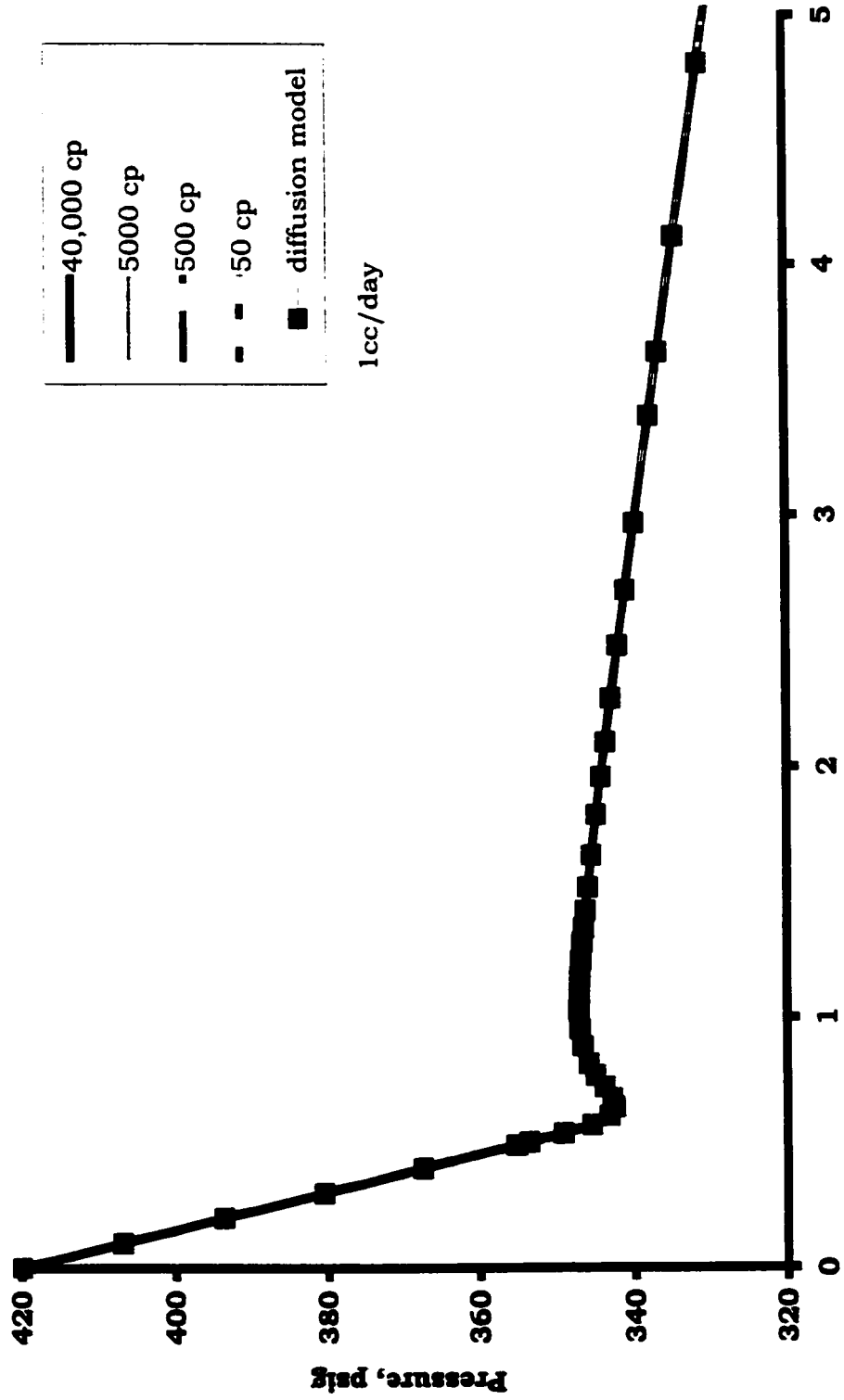

Figure 4.13: Effect of viscosity on system pressure

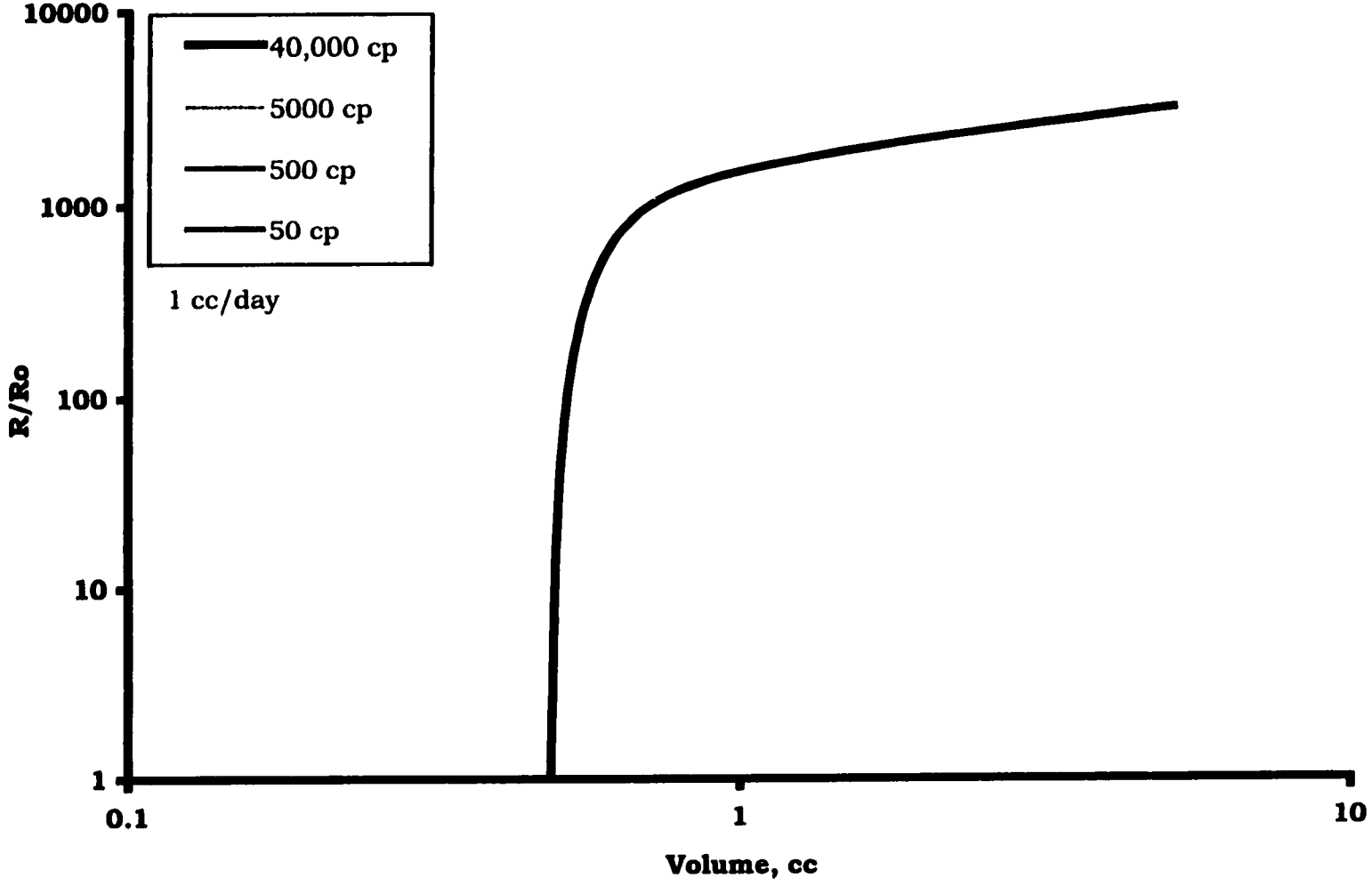

Figure 4.14: Effect of viscosity on bubble radius

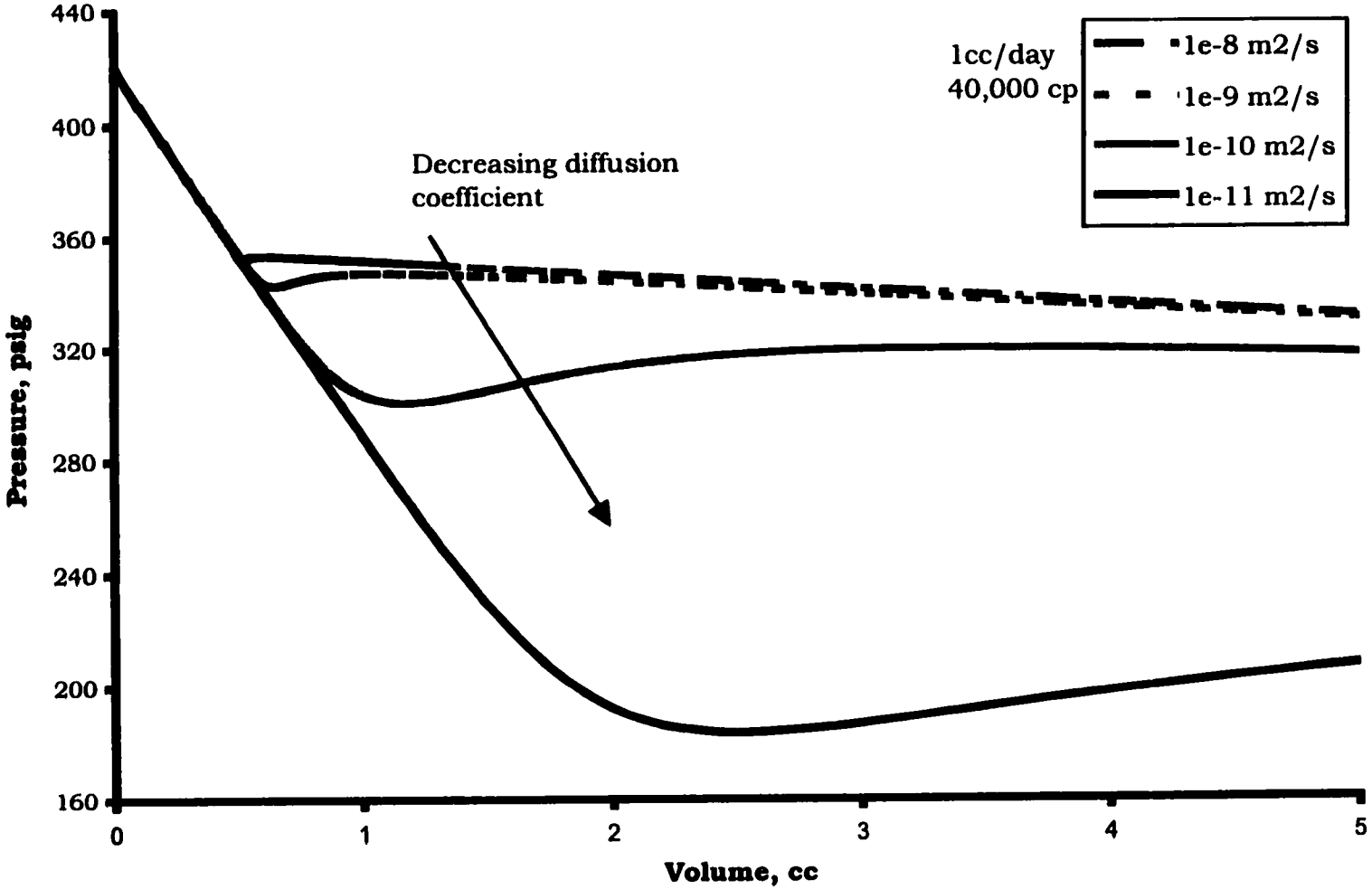

Figure 4.15: Effect of diffusion coefficient on system pressure

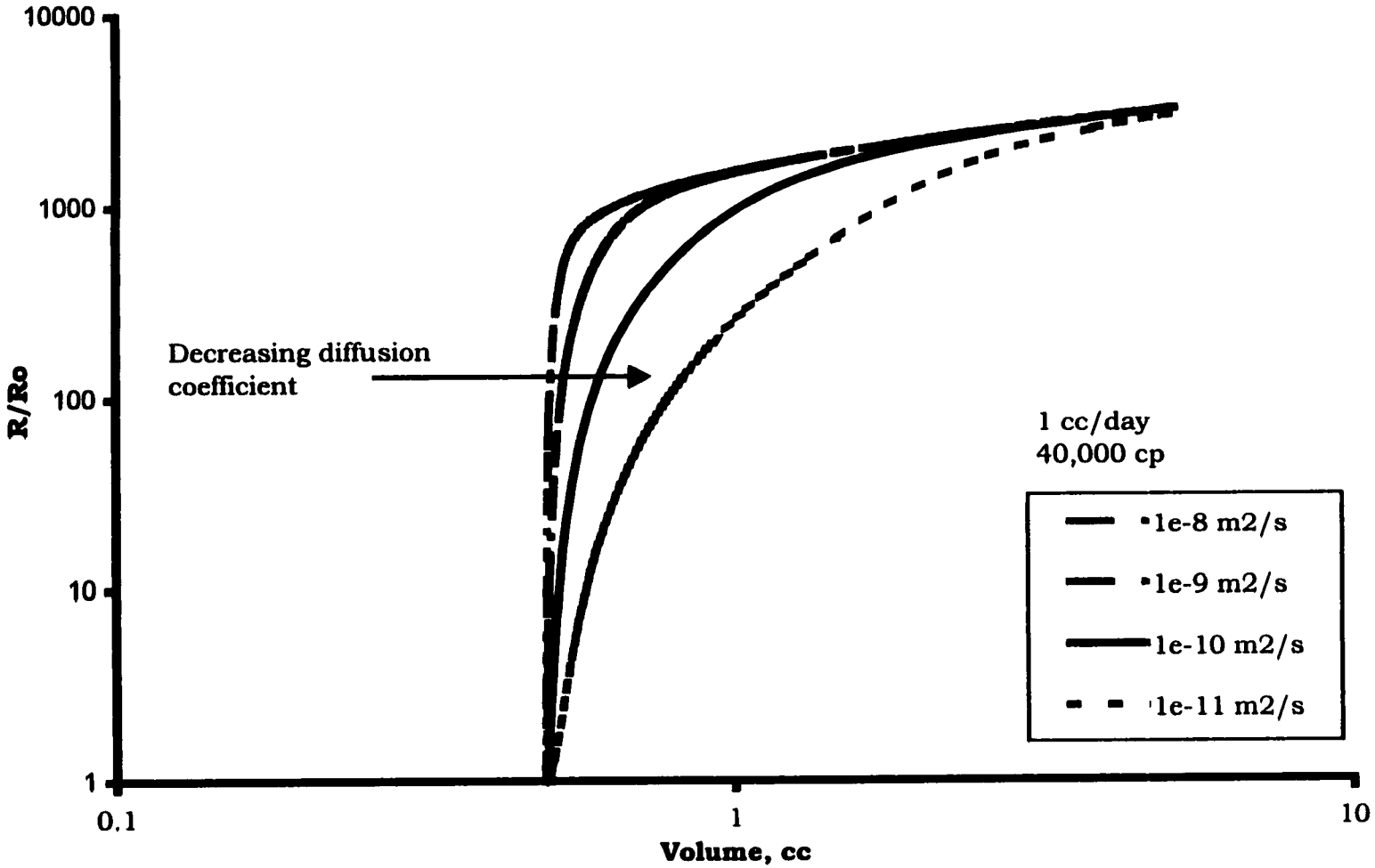

Figure 4.16: Effect of diffusion coefficient on bubble growth

(1996)] might be valid only before the effect of concentration at the far boundary in felt.

Once again considering the model growth of at^b, Figure 4.12, 4.14 and 4.16 suggests that after an early time of large b, where the concentration at the far boundary has not been affected, the exponent decreases and all the graphs converge to a single lower value of b, which is approximately equal to 0.5.

4.3.2.2.2. Effect of viscosity

The effect of oil viscosity is shown in Figures 4.13-4.14. For a large range of viscosity of oil, with similar diffusion coefficient, it is observed that all the results are same i.e there is no effect of viscosity. For further verification of the viscosity results shown in Figure 4.13, a model was run with only diffusional term and the results were compared. As can be seen in Figure 4.13, the diffusion model lies on top of all other cases. This clearly demonstrates that diffusional forces dominate the process of bubble growth in the real field time scales.

4.3.2.2.3. Effect of diffusion coefficient

The effect of diffusion coefficient on depletion process is shown in Figures 4.15 and 4.16. The higher diffusion coefficient leads to faster retrieval of pressure and lesser "Apparent Critical Supersaturation". This can be explained by the fact that initially the bubble grows faster in case of oil with higher diffusion coefficient (shown in Figure 4.16). At later time the bubble radius for all the cases starts reaching an asymptotic value but the amount of gas in bubble is different. This leads to different bubble pressure, which is being exerted on the liquid. Although bubble radii approaches the same value after some time, pressure is lower in lower diffusivity oils. So for the same rate of depletion in light and heavy oil, the higher "Apparent Critical

Supersaturation" in heavy oil can be attributed, in part, to the lower diffusivity coefficient of heavy oil.

4.4. Discussion

In a recent study [Tremblay *et al.* (1998)] no bubble was observed to form for about 3 hours after the pressure in a 30,000 cp live oil system was decreased from 780 psi (5170 KPa) to 500 psi (3446 KPa) in one step (P_b = 750 psi (5170 KPa)). One of the possible explanations for this anomaly could be that the supersaturation effects were large and no bubble could nucleate. A second explanation can be provided using the model of this study. The model was used for the above oil and it was found that the bubble, if nucleated, would grow to a size of about only 10 μm, starting from initial bubble size calculated for supersaturation of 250 psi (1723 KPa) [Brennen (1995)], in about 3 hours. Our model applies to growth in bulk, and it is expected that the porous media would further restrict the growth of bubbles. Our results suggest that the time frames might have been insufficient for noticeable growth of the bubbles and gas bubbles were possibly very small.

One assumption in our study is that nucleation is instantaneous. A number of researchers [Firoozabadi and Kashchiev (1996), Yousfi *et al.* (1997), Crum (1982), Wilt (1989), Coles (1974), Stewart *et al.* (1954)] have studied this phenomenon. Yousfi *et al.*(1997) studied the nucleation in micro-model and concluded that the nucleation is not progressive after a brief initial time since the number of bubbles reach a plateau after some initial time and the rate of bubble generation becomes zero. Further, in line with their observance of increasing number of bubbles at initial time, they concluded that the theory of instantaneous nucleation does not hold at early times. The same is also evident from the study of Stewart *et al.* (1954). Conversely, with the theory of pre-existing bubbles [Wilt (1989), Coles (1974)], due to presence of stabilized bubbles, the process of nucleation can be assumed to be instantaneous. Wilt (1989) in his study showed that the progressive process could result in very

small size of the bubbles and hence nucleation can be considered instantaneous. Yousfi *et al.* (1997) from their study concluded that if we disregard the initial time when the bubbles are being generated, which is negligible compared to field times, the assumption of instantaneous nucleation is valid. In our modelling we have adopted the instantaneous nucleation assumption.

4.5. One possible scenario of bubble generation

When the pressure is lowered below the bubblepoint pressure and there is no formation of free gas phase, the oil becomes supersaturated. When supersaturation becomes large enough bubbles nucleate and those larger than a critical radius start to grow. The growth of the bubble can be dominated by hydrodynamic forces, mass transfer forces or both, at least at early time. Since the diffusion coefficient is typically low in heavy oil, the rate of increase of supersaturation due to pressure decrease could initially be more than the decrease in supersaturation due to diffusion of gas into the bubble. This is due to the fact that the concentration disturbance has not reached the far boundary. As a result the supersaturation at a point far away from the bubble goes on increasing. This is especially true, before system pressure starts the upward trend. Due to further increase in supersaturation, the threshold value required for the nucleation to occur may be met at the far away point. Thus a new bubble nucleates which starts lowering down the local supersaturation. The time required for this process may be small compared to the field time and hence instantaneous nucleation may be a good assumption [Yousfi *et al.* (1997)] for all practical purposes, whereas in reality and microscopic sense the nucleation process may be progressive. Since the diffusion coefficient in light oil is greater than in heavy oil, it is expected that decrease of supersaturation shall be more in light oil than in heavy oil. This leads to conclude that the number of nucleated bubbles shall be more in heavy oil than in light oil. This is in line with the experimental results of Pooladi-Darvish and Firoozabadi

(1999), where a larger number of bubbles were observed in their heavy oil experiments than that in light oil experiments.

The increase in the number of bubbles during solution gas drive has been shown to increase the recovery factor [Stewart *et al.* (1954)]. This could also be one of the factors responsible for the favourable behaviour of heavy oil reservoirs.

Whether supersaturation and the kinetics of nucleation and growth are important under field condition is still unresolved. Batycky *et al.* (1997) in their work gave clear evidence of significant supersaturation in the reservoir.

Solution gas drive in porous media involves nucleation, bubble growth and flow. Further studies would clarify the interaction of these phenomena and the effect of presence of porous medium on the process.

4.6. Conclusion

A numerical model was developed for growth of a single bubble in heavy oil and light oil for gradual decline in pressure. The results for the cases studied indicated that:

1. Viscous forces, and in general hydrodynamic forces, have little or no effect on bubble growth in heavy oils at late times. Modelling bubble growth in heavy oil using diffusion equation only, can be a valid approximation after an early time of the order of seconds to minutes. Rate of growth of a bubble in heavy oil is much less than that in light oil.

2. For bubble growth in infinite domain, the application of the growth model of $R(t) = at^b$ for $R>R_0$ could be extended to the cases where both diffusional and hydrodynamic forces are acting. However, if experiments are conducted to determine constants a and b, these need to be properly designed to represent the actual case of interest. It was shown that the constants depend on numerous parameters such as diffusion coefficient and rate of pressure drop. More over, modelling of bubble growth in closed domain

showed that this simple power law model might not adequately describe bubble growth behaviour.

3. By applying growth model to one set of solution gas drive experiment it was shown that even though the bubbles nucleated earlier, the system pressure decreased before retrieving after reaching the "apparent critical supersaturation" pressure. Hence, the assumption that bubbles nucleate at the apparent critical supersaturation might not be correct. The apparent critical supersaturation depends on bubble nucleation as well as bubble growth kinetics.

4. It was found that higher depletion rate and lower diffusion coefficient result in a larger difference between nucleation pressure and the apparent critical supersaturation pressure. This could explain higher supersaturation obtained in heavy oil experiments (lower diffusivity) and those with higher rate of pressure drop.

Chapter 5

GAS MOBILITY MEASUREMENT

5.1. Introduction

The process of solution gas drive involves nucleation of the gas bubbles followed by bubble growth and coalescence and finally flow of gas.

As mentioned previously, the heavy oil reservoirs in Alberta and Western Saskatchewan under solution gas drive show anomalous behaviour when compared to conventional light oil reservoirs. At least one of the theories [Pooladi-Darvish and Firoozabadi (1999), Guo-Quig and Firoozabadi (1999)] attributes this favourable behaviour to low gas phase mobility in heavy oil. The low gas mobility implies lower gas velocity that results in gas retention and pressure maintenance in the reservoir. Finally, all these factors lead to higher oil recovery.

In this part of the thesis, experiments were done on unconsolidated sand-pack at various depletion rates and the effect of rate of depletion on critical gas saturation and supersaturation was studied. Further, the experimental results were used to determine mobility of gas phase at various depletion rates. Production and pressure data obtained from depletion was matched on a commercial reservoir simulator by adjusting critical gas saturation and gas relative permeability values.

The chapter starts by describing the experimental setup and procedure. Next, the experimental results are presented. Simulation of the experiment and analysis of the results follow the results. Towards the end of the chapter, a brief discussion is presented which is followed by conclusion.

5.2. Experimental setup

The experimental setup consists of an Isco syringe pump, a multiple pressure port core holder with viton sleeve that encases the sand pack, gas-liquid separator (Visual cell), overburden and axial pressure system, piston cylinder for transfer of live oil, a recombiner for preparation of live oil, constant temperature air baths and a vacuum pump. The instruments used for data acquisition are pressure transducers and thermocouples. A LabTech (1994) notebook is used to record data from various instruments during the experimental run. The schematic of the experimental setup is shown in Figure 5.1.

The core holder is made of titanium and encases the Viton sleeve that contains 60 cm long sand-pack. There are 3 pressure taps in the core-holder, connected to pressure transducers to measure the differential pressure in the various sections of the sand-pack. The reading accuracy of the differential pressure transducers is ± 0.025 psi (0.17 KPa). The picture of the core-holder is given in Figure 5.2.

To avoid any effect of gravity, that may lead to segregation of gas and oil in the core during experiments, the core-holder is rotated 180 degrees every 15 minutes.

The outlet end of the core-holder is attached to a visual cell. The visual cell, which is 10 cc in volume, has a long window on both sides so that the gas-oil interface is clearly visible for production measurement. The small size of the separator is selected to minimize the dead volume. This ensures that almost all of the gas collected in the visual cell is coming from the sand-pack and negligible amount of the gas is being generated in the oil in the visual cell. The picture of the visual cell is shown in Figure 5.3. The outlet, from the bottom of the visual cell, is connected to the Isco pump.

Other equipment required are a recombiner for the preparation of the live oil and a transfer cylinder for the transfer of live oil from recombiner to the Isco pump.

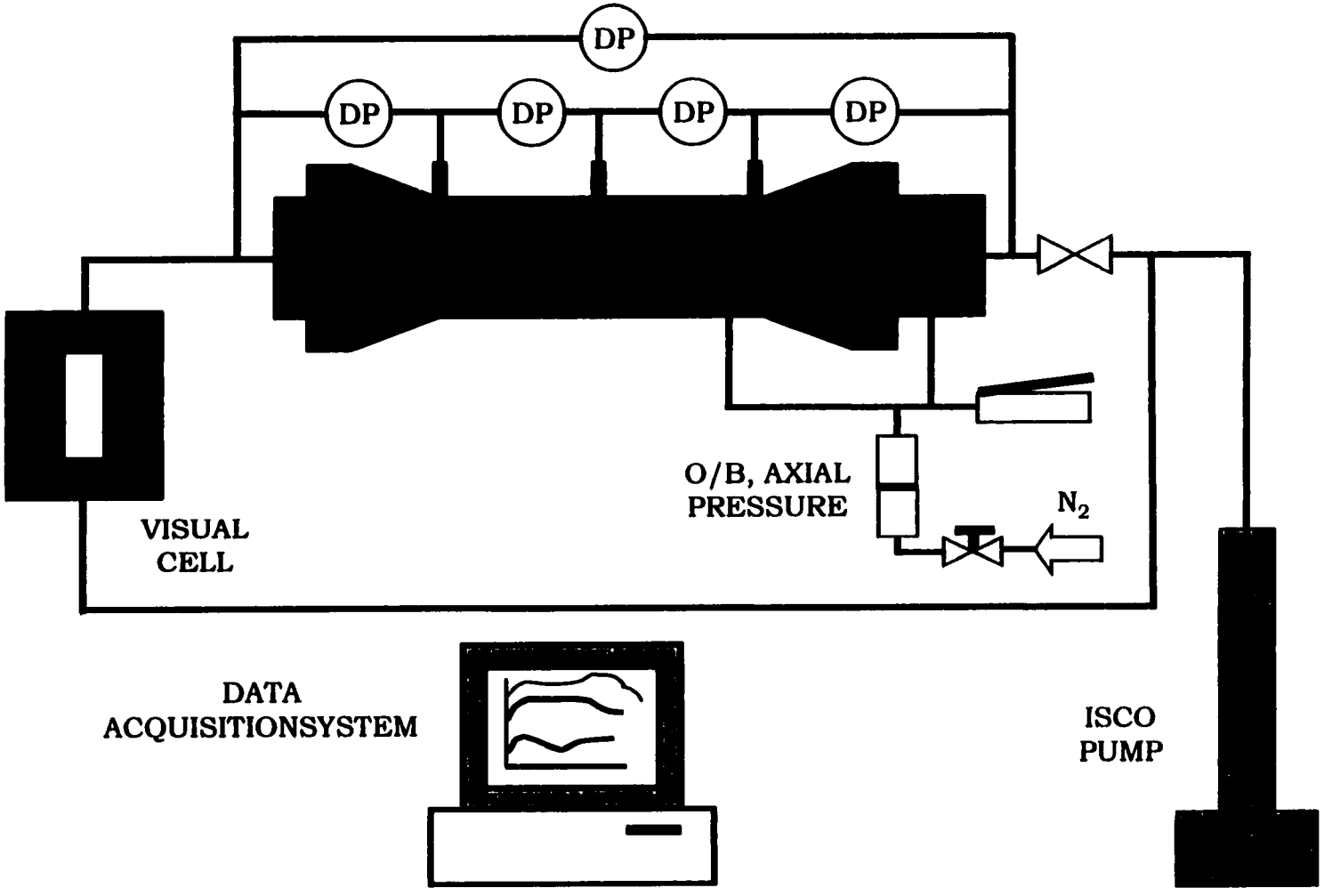

Figure 5.1: Experimental Setup

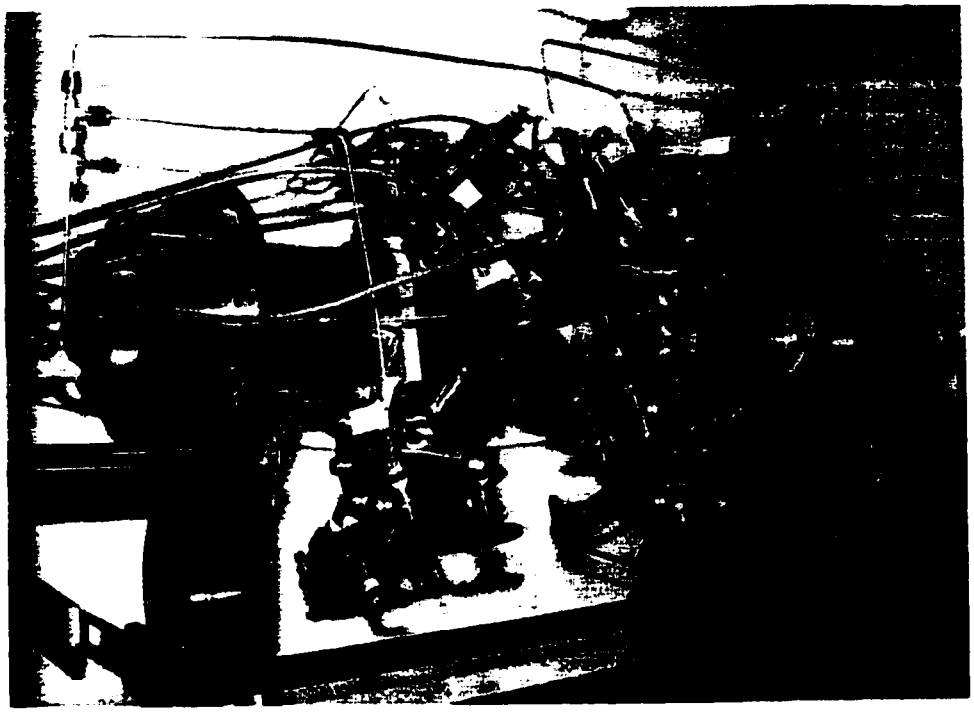

Figure 5.2: Core-holder

Figure 5.3: Visual cell (Gas-Oil separator)

The overburden and axial pressure system comprises of a hand-pump, a buffer piston vessel and a backpressure regulator. Water is used as the overburden/axial pressure medium. The hand-pump is used to build up the pressure during start-up. A buffer piston vessel with nitrogen on one side, connected through a backpressure regulator to the nitrogen supply cylinder, is used to dampen pressure fluctuations that may be introduced due to temperature fluctuations.

The core-holder and visual cell is placed in a constant temperature bath. A temperature controller acting on a hot air blower is used to control the temperature in the bath. The temperature in the bath is controlled within an accuracy of ± 0.1 Deg C.

5.3. Fluid data

A poly-alphaolefinic type (PAO-100) of synthetic hydrocarbon oil (From Nye Inc.), with specific gravity of 0.85 and dead oil viscosity of 2552 cp at 25 Deg C, is used. The dead oil viscosity is measured with a Haake-PK100 cone and plate viscometer. The GOR of the live oil was measured to be 15.57 vol/vol at 25 Deg C. Methane is used as the gas phase in all the experiments. Properties of the live oil are shown in Table-5.1

For measurement of live oil viscosity, a flow loop is made at the inlet of the sand-pack. The pressure drop across the loop is used to determine the viscosity. Thus, it is possible to measure viscosity of the fluid inline.

Table – 5.1: Property of fluid

Property	Value
Oil	PAO-100
Dead Oil Viscosity @ 25°C	2552 cp
Live Oil Viscosity @ 25°C	1100 cp
Specific Gravity	0.85
GOR @ 25°C	15.57 v/v
Bubble Point	575 psia (3963 KPa)

5.4. Experimental procedure

5.4.1. Hydro-testing of the vessels

All the vessels to be used in the experiment were hydro-tested to a pressure equal to 1.5 times the maximum operating pressure in the system. This was done to ascertain the mechanical health of the vessel and avoid any leakage or failure of the vessels during experimental run.

5.4.2. Calibration of transducers

The absolute pressure transducers and digital pressure gauges were calibrated using dead weight tester. The Sensotech differential pressure transducer was calibrated using the calibration method specified in instruction manual. The range of measurement of differential pressure transducer is 10-15 psid and reading accuracy is ± 0.025 psi (0.17 KPa). The differential pressure transducer is designed to operate with liquid on both the sides, so it was made sure that both the chambers were free of air (completely liquid filled). This was done by filling it with Bayol (A light oil) prior to connecting it to the system.

5.4.3. Over pressure controls

The running of experiments required safety to be one of the major concerns. The system was equipped with proportional pressure relief valves, set at relieving pressure depending on the maximum operating pressure and design pressure of the equipment and piping/fitting. The Isco pump control software also has an inherent feature through which the safety pressure setting can be set. The outlet piping of the pump is equipped with pressure relief device to ensure additional safety. All the pressure safety valves were set at the proper relieving pressure by flowing light oil (Bayol) through them using the

Quizix pump, at constant flow rate. The discharge pressure was adjusted by tightening or loosening the spring of the pressure relief valve. This pressure then becomes the relieving pressure.

5.4.4. Data acquisition and control

A Labtech notebook (1994) was used for data acquisition from the various pressure transducers and thermocouples. A program was written to acquire the required data and display it on the screen in digital as well as graphical form. Further, this data was also recorded in a file that could be read on a worksheet.

5.4.5. Temperature control

The oil used in the experiment, being highly incompressible, exhibits a significant change in pressure due to small change in temperature. So it was imperative to maintain a constant temperature during the experiments.

The big cabinet housing the core-holder is equipped with a temperature controller acting on a heater. The temperature in the smaller Blue-M oven was controlled by a temperature controller acting on In-car heater that was placed in the oven. Both the ovens were equipped with circulating fans to have a uniform temperature across the oven. The temperature of the fluid in Isco pump barrel was controlled by a similar controller acting on a heating tape that was wound around the pump barrel. Further, the pump barrel was insulated to avoid any heat loss. The flow lines were insulated to prevent any heat loss. The temperature controllers were equipped with over temperature control that trips the system if the temperature exceeds the safety set point.

5.4.6. Calibration of visual cell

The gas and oil produced from the core is separated in the visual cell. The amount of gas or oil produced is measured by measuring the gas-oil

interface. So it is necessary that the visual cells be calibrated. The height of the interface was measured with a cathetometer, which was mounted outside the oven. A high intensity light was thrown from the rear window of the visual cell which facilitated the measurement of gas-oil interface in visual cell. The visual cell was calibrated with the Quizix pump. The calibration was done by recording the reading on the Cathetometer scale against the volume of the fluid injected in the visual cell, which was measured by Quizix pump. A plot was generated with the above data of volume vs. height on the cathetometer.

5.4.7. Sand preparation and packing

Prior to packing in the core, the desired sand was sieved with a sieve shaker through 200 mesh screen. The undersize was then sieved through 325 mesh screen. The oversize from this screen was taken as the product sand to be used in packing of the core. The grain size distribution of the sand thus obtained was between 50 and 75 μm. The desired sand was then extracted for five days using a 1:1 mixture of Methylene Chloride and Methanol. This was done to remove any impurities and have a total water wet sand. This was carried out in a round bottom flask, where the liquid mixture was at the bottom and the sand was held in the neck of the flask in cylindrical cellulose containers. The flask was then heated by providing controlled heat through a rheostat. The vapours from the bottom of the flask extracted the sand and then were condensed at the top in a total condenser. The condensed liquid would then flow back into the bottom of the flask. The setup is shown in Figure 5.4. Once the extraction was over the sand was taken out and dried to remove traces of solvents.

The sand is then packed in Viton sleeve, which is inserted into the core-holder prior to packing. The main body of the coreholder consists of five basic parts: the pressure cell body, the stationary end, the piston end and two collars. The sleeve material used for the coreholder was viton.

Figure 5.4: Sand extraction setup

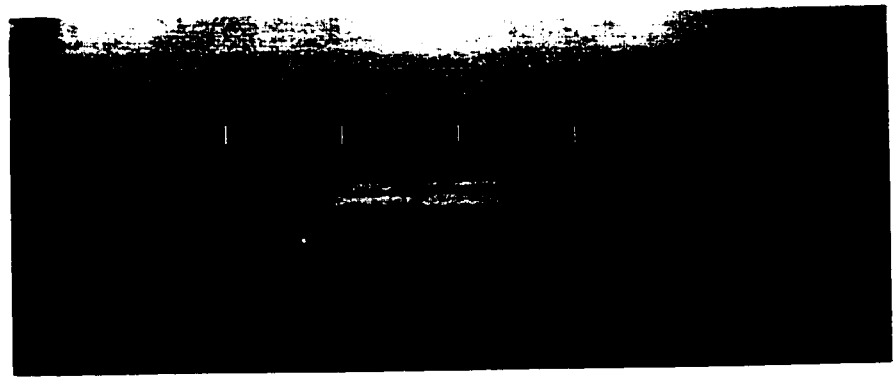

Figure 5.5: Viton sleeve with multiple pressure taps

Table – 5.2: Property of Sand-Pack

Property	Value
Length of the Sand-Pack	60 cm
Pore Volume	487 cc
Porosity	38.6 %
Absolute Permeability	1.24 Darcy
Effective Permeability	1.18 Darcy
Connate Water Saturation	2.1 %
Sand Grain Size	50 – 75 Micron
Overburden/Axial Pressure	1120 psig (7720 KPa)
Compressibility	2.2×10^{-5} psi^{-1}
	(3.2×10^{-6} KPa^{-1})

To pack the coreholder with sand, first the collar was installed on one end of the sleeve. Subsequently, the pressure cell was mounted on to the rotating stand. The sleeve and stationary end was then inserted into the pressure cell, aligning pressure port on sleeve with those on core-holder. A picture of sleeve is shown in Figure 5.5. The stationary end was locked in place. The dry sand was then vibrated into place leaving room at the top for the piston end. A thin layer of coarser sand grains was used at either end while packing the sand. This is done so that a screen larger than the grain size of the sand-pack can be used and yet migration of sand into the outlet stream can be avoided. The larger screen size prevents build-up of gas at the outlet due to trapping of gas bubbles [Pooladi-Darvish and Firoozabadi (1999)], which could happen if screen size smaller than the sand grain size is used. The property of the sand-pack is given in Table-5.2.

The sand used in filling was weighed to measure the length of the sand pack. Any sand particles that may have accumulated on the upper portion of the sleeve material were removed to ensure proper seal. The second collar was inserted into the end of the sleeve. Carefully the piston end was inserted into the collar and sleeve and locked in place.

5.4.8. Rotating Core-holder

It was decided to rotate the core-holder to minimise the gravity effects. For this purpose, the core-holder was mounted on swivel joints on both ends. A DC motor with gear box having a gear ratio of 15125:1 was attached to rotate the core-holder approximately 180 degrees once every 15 minutes.

5.4.9. De-aerating water

It is important to ensure that the water, to be used in leak test and in flooding the core, contains no air (free of compressible fluid). This was done to avoid any confusion arising during leak test, because of pressure drop due to dissolution of air in water. The de-aeration was done with bench vacuum in the lab and agitating liquid in the flask by magnetic stirrer.

5.4.10. Applying Overburden and Axial Pressure

Once the sand-pack was prepared, overburden and axial pressure was applied simultaneously with a hand-pump, by teeing off the line from the pump outlet to overburden and axial pressure connection on the core-holder. The overburden and axial pressure was built-up to 1120 psig (7720 KPa) in steps of 50 psig (345 KPa). Water was used as the fluid for applying overburden and axial pressure. Once the pressure was built, a piston vessel containing water on one side and nitrogen on other side was used as a buffer vessel. The nitrogen in the buffer vessel was attached to the nitrogen tank through a back pressure regulator. Buffer vessel was used to dampen pressure fluctuations, if any, that occur from temperature fluctuations. The pressure set point, of the back pressure regulator, was set equal to the overburden/axial pressure. The back pressure regulator helped in maintaining a constant overburden/axial pressure on the sand-pack.

5.4.11. Leak test

Once all the piping and core-holder was set in-place, the next step was to leak test the system. For the piping, this was done by isolating a section of piping, pressuring it up with water and observing the pressure in the section, under isothermal condition. A leak free system would indicate no pressure drop with time. The leak test in the sand-pack was done with nitrogen gas. This was done to avoid wetting of the sand-pack prior to measurement of pore volume.

5.4.12. Vacuuming of pumps/system/sand pack

Once the whole system including the core-holder was leak tested, the water from piping was drained. A vacuum pump was then used to draw vacuum of 10 mTorr. The catch-pot before the vacuum pump inlet was kept in dry ice to achieve such high vacuum. The vacuum pump was run for 24 hours to achieve such high vacuum. The vacuum was pulled to remove any air that might get trapped during flooding of the system, while measuring the dead volume. The trapping of air has two-fold affect. One, it increases the compressibility of the fluid and secondly, it gives erroneous estimation of dead volumes.

5.4.13. Volume measurement by water

Once the system was vacuumed, the water was introduced into the system by pumping with Isco pump. To measure the volume in each section of the piping the water was introduced into the system section by section; isolating a particular section from rest of the vacuumed system by closing the valve. Once a particular section was filled with water, the pressure was raised to 100 psig (689 KPa). The difference in volumetric reading indicated the volume in that section.

5.4.14. Porosity and absolute permeability measurement (saturation of core)

Next, the vacuumed sand pack was flooded with water to measure the pore volume and hence the porosity of the sand-pack. The porosity was found to be 38.6%.

Once the sand-pack was flooded with water, the valves connecting to the pressure transducers were opened. Water was flowed through the sand-pack at a known rate and the pressure drop across the core was measured for determining absolute permeability of the sand-pack. This was done at several flow rates to have an average value. The Darcy's equation in the following form was used to determine permeability

$$k = \frac{q\mu / A}{\Delta P / L} \tag{5.1}$$

Here, q is the flow rate, ΔP is the pressure drop across the sand-pack, L is the length, A is the cross sectional area and μ is the viscosity. A plot was generated, shown in Figure 5.6, and the slope was found to determine permeability. The value of the absolute permeability was found to be 1.24 Darcy.

5.4.15. Connate water saturation and effective permeability measurement (flooding with dead oil)

Once the sand-pack was flooded with water and absolute permeability was determined, the dead oil was flooded into the sand-pack displacing the water. The dead oil was injected until no additional water was produced from the outlet end. The oil and water thus produced were measured to determine the connate water saturation in the sand-pack. The connate water saturation was found to be 2.1%.

Once the inlet piping to the core-holder and the sand-pack was flooded with dead oil, the dead oil was flowed through the sand-pack at a known flow rate and the differential pressure across the core measured to determine the

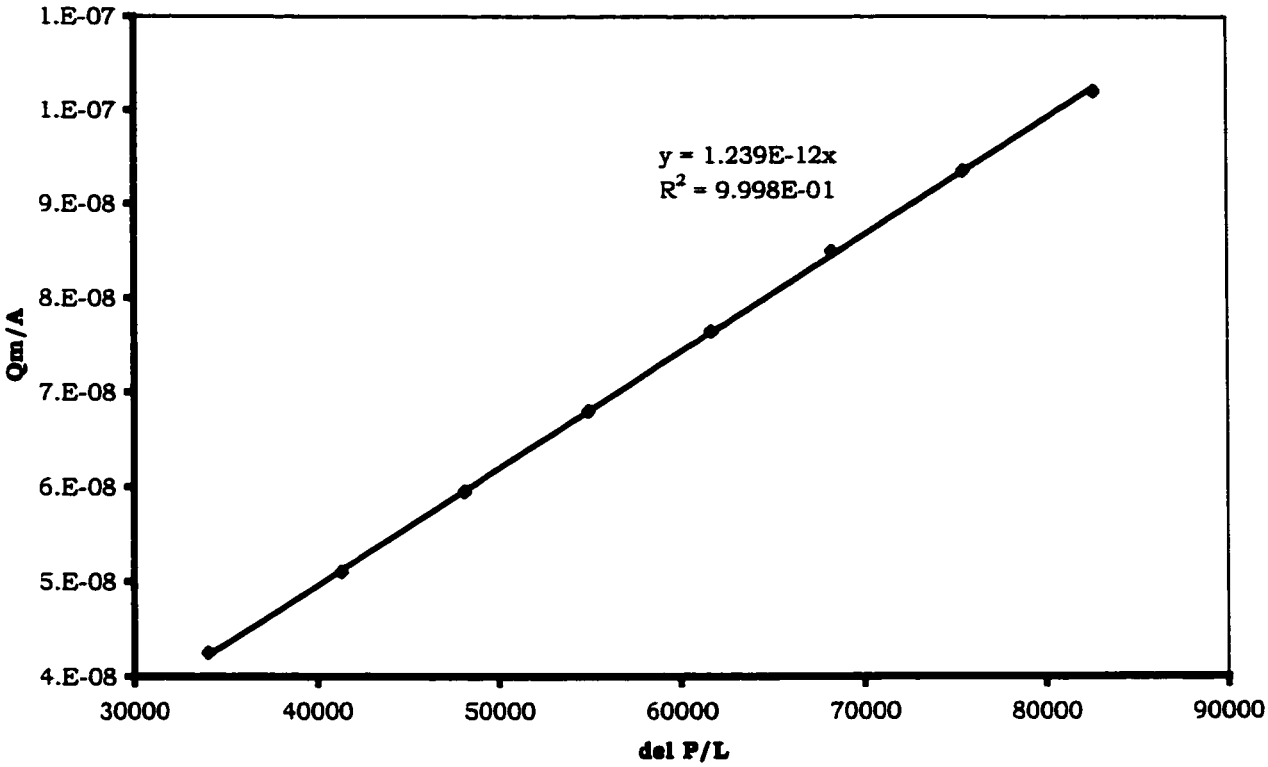

Figure 5.6: Determination of absolute permeability

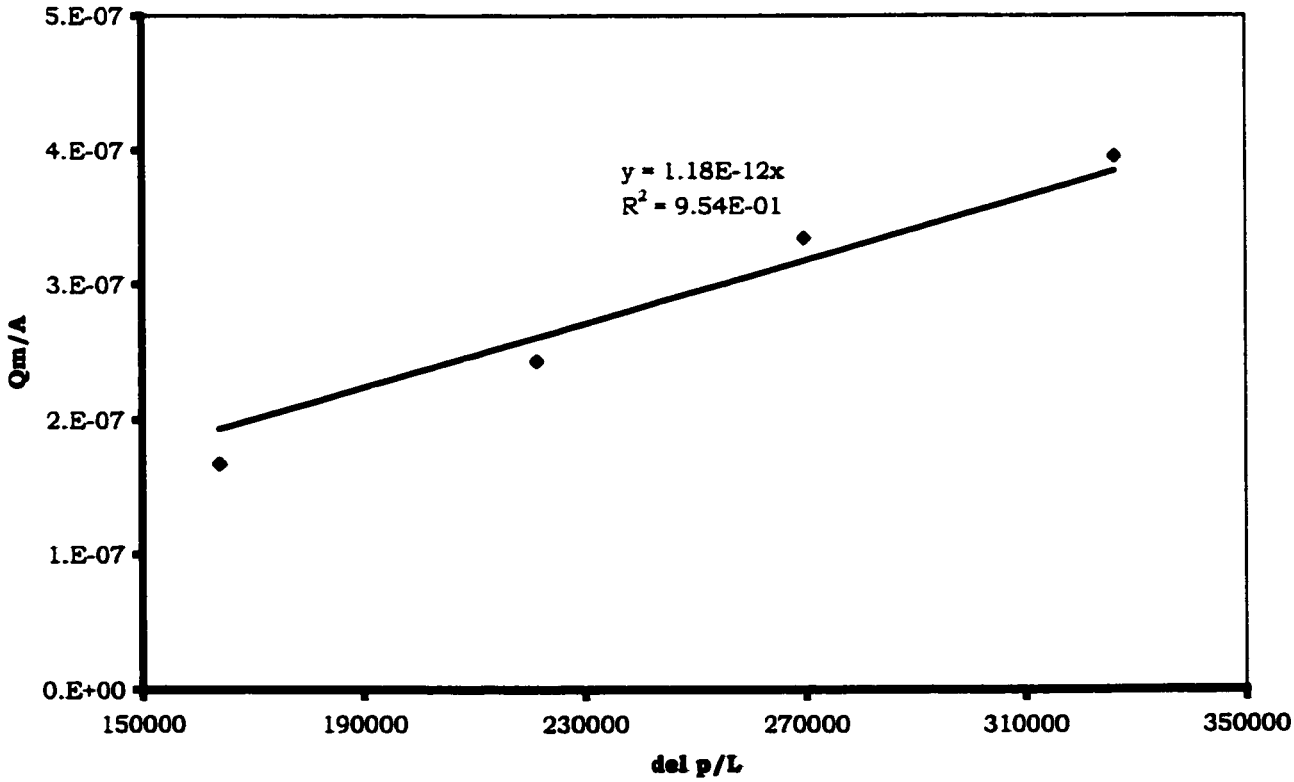

Figure 5.7: Determination of Effective Permeability

effective permeability of the sand-pack. A similar plot as discussed for absolute permeability was generated. The plot is shown in Figure 5.7. The effective permeability of the sand-pack was found to be 1.18 darcy.

Once the core was flooded with dead oil, the rest of the system comprising of visual cell and piping was flooded with dead oil displacing water.

5.4.16. Measurement of dead oil viscosity

The viscosity of the dead oil was measured at various temperatures using a Haake PK-100 cone and plate viscometer. The picture of the equipment is shown in Figure 5.8. The viscometer was first calibrated with a fluid of known standard viscosity at a given temperature. The temperature was maintained by a heating/cooling bath. Next, the dead oil sample was put under the disc and the torque measured at a specified RPM. This data was used to calculate the viscosity. This was done at various temperatures. Further, a log-log viscosity vs. temperature graph was plotted to predict viscosity of the dead oil with temperature. The experimental data is given in Table 5.3 and the result graph is shown in Figure 5.9.

5.4.17. Viscosity loop calibration

It was desired to measure in-line viscosity of live oil during the experimental run. The viscosity was measured in-line by measuring the pressure drop in a certain section of a coiled tube and then calculating the viscosity using the Hagen-Pouisille Equation [McCabe, Smith and Harriot (1990)] for flow through pipes which is expressed as

$$\Delta P = \frac{4\rho L f u^2}{2D} \qquad (5.2)$$

where f is the friction factor. For laminar flow $f = \frac{16}{Re}$ where Re is the Reynolds number which is expressed as

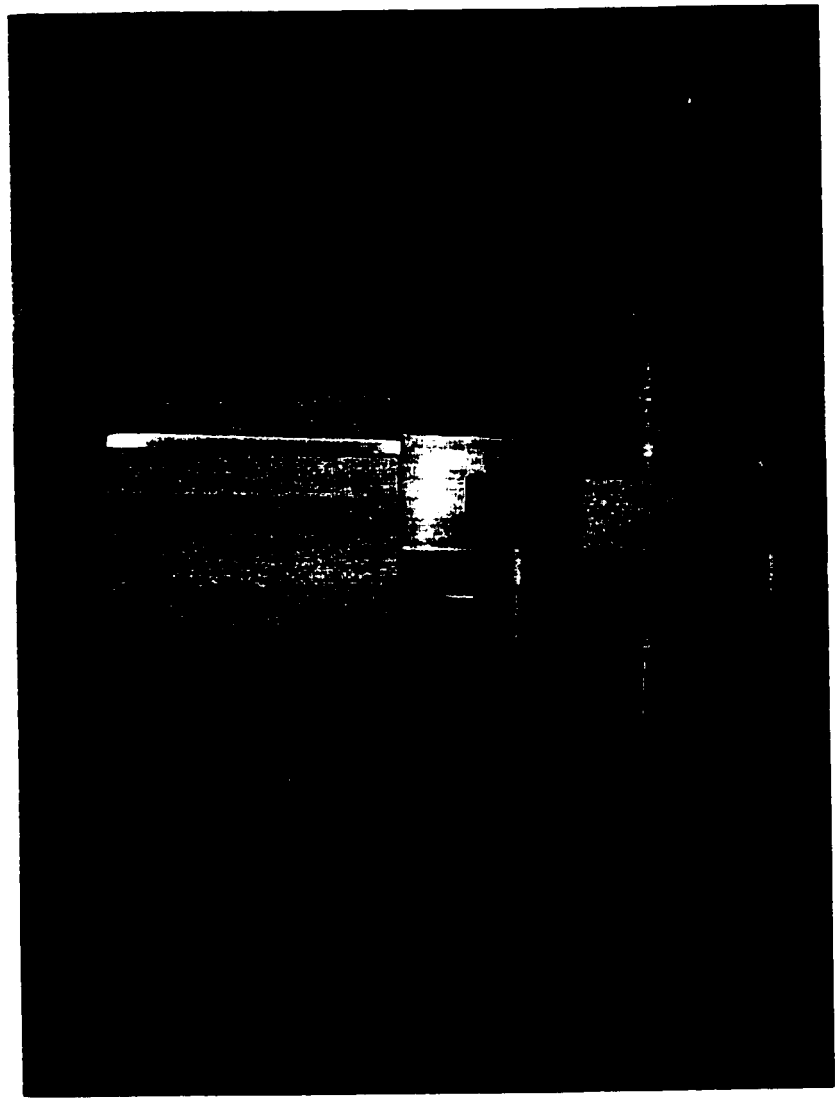

Figure 5.8: Haake PK-100 viscometer

Table 5.3: Experimental data for measurement of dead oil viscosity

Temperature, Deg C	Viscosity, cp	
Standard sample	**Standard**	**Measured**
20	720.5	722
25	478.5	477
40	166.8	166.5
Dead oil		
20	3575	
25.2	2654	
38.8	970.1	

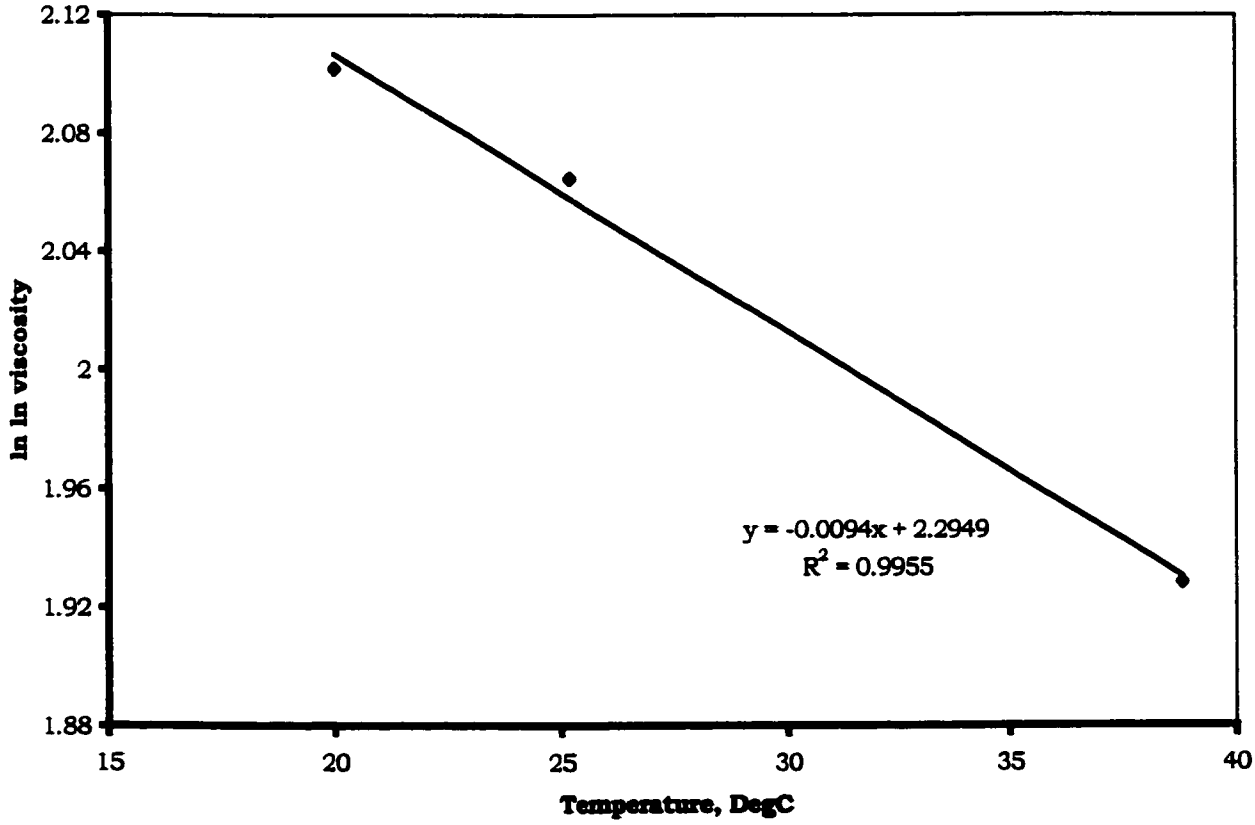

Figure 5.9: Viscosity vs temperature for dead oil

$$\mathrm{Re} = \frac{Dup}{\mu} \tag{5.3}$$

substituting this in Equation 5.2 and simplifying we get

$$\mu = \left(\frac{\pi D^4}{128L}\right)\frac{\Delta P}{q} \tag{5.4}$$

Here, the initial part on the RHS in the parenthesis is a constant and depends on the geometry of the flow loop (geometric factor). This constant was determined by calibrating the flow loop with fluid of known viscosity viz. water and dead oil.

The dead oil and water of known viscosity were flown through the loop and the pressure drop across the loop was measured. Knowing the viscosity, this data was then used to determine the geometric constant of the loop.

5.4.18. Measurement of compressibility of dead oil

The compressibility of the dead oil was determined by compressing it in the cylinder of the Isco Pump and recording pressure versus the volume data (P-V data). The data was then plotted on a graph and the slope of the line was used to calculate the compressibility using the following formula:

$$\kappa_{do} = -\frac{1}{V}\frac{\partial V}{\partial P} \tag{5.5}$$

The P-V graph for determination of dead oil compressibility is shown in Figure 5.10. The dead oil compressibility was found to be 7 x 10^{-6} psi^{-1} (1.01 x 10^{-6} KPa^{-1}).

5.4.19. Live oil preparation

The live oil was prepared in a rocker cell. The cell was first half filled with dead oil. Then methane gas was introduced into the rocker cell at the desired bubble point pressure of the oil. The cell was then rocked to dissolve the gas into the oil. Once the pressure dropped below the desired bubble point

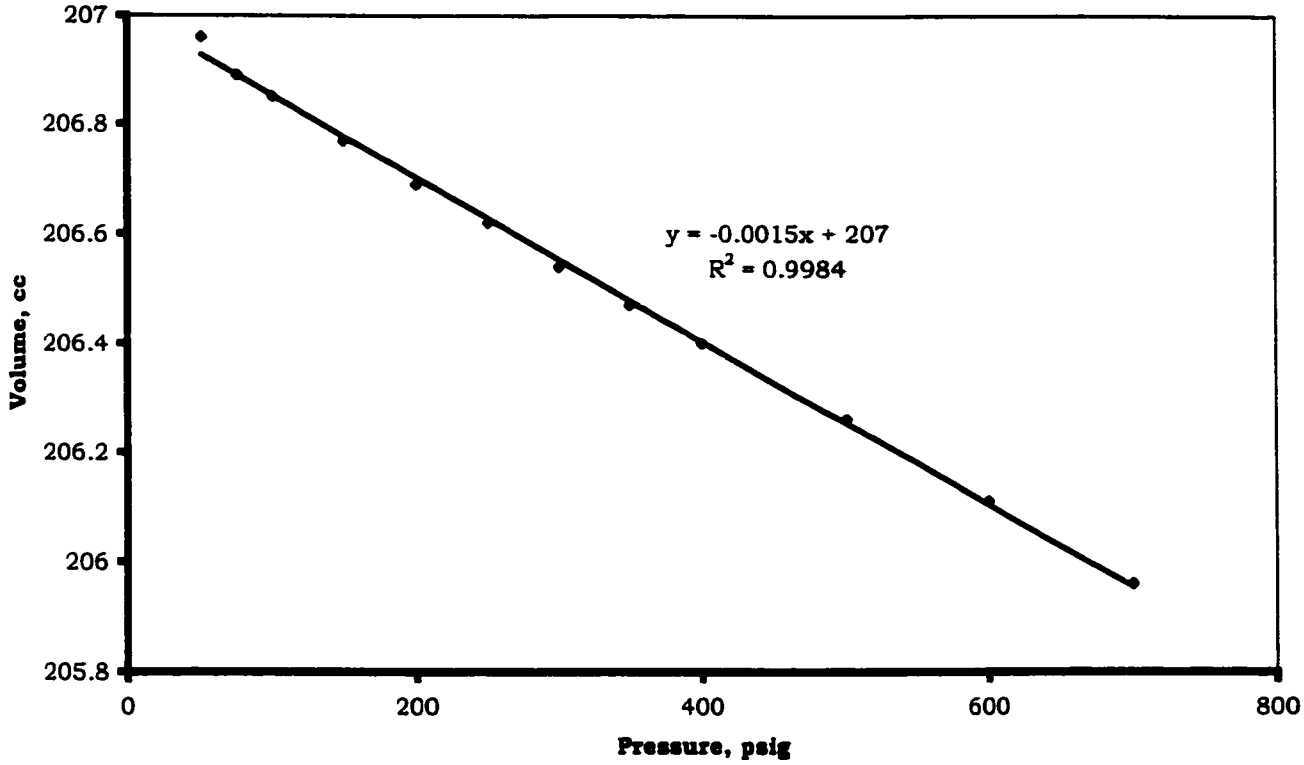

Figure 5.10: P-V graph for determination of dead oil compressibility

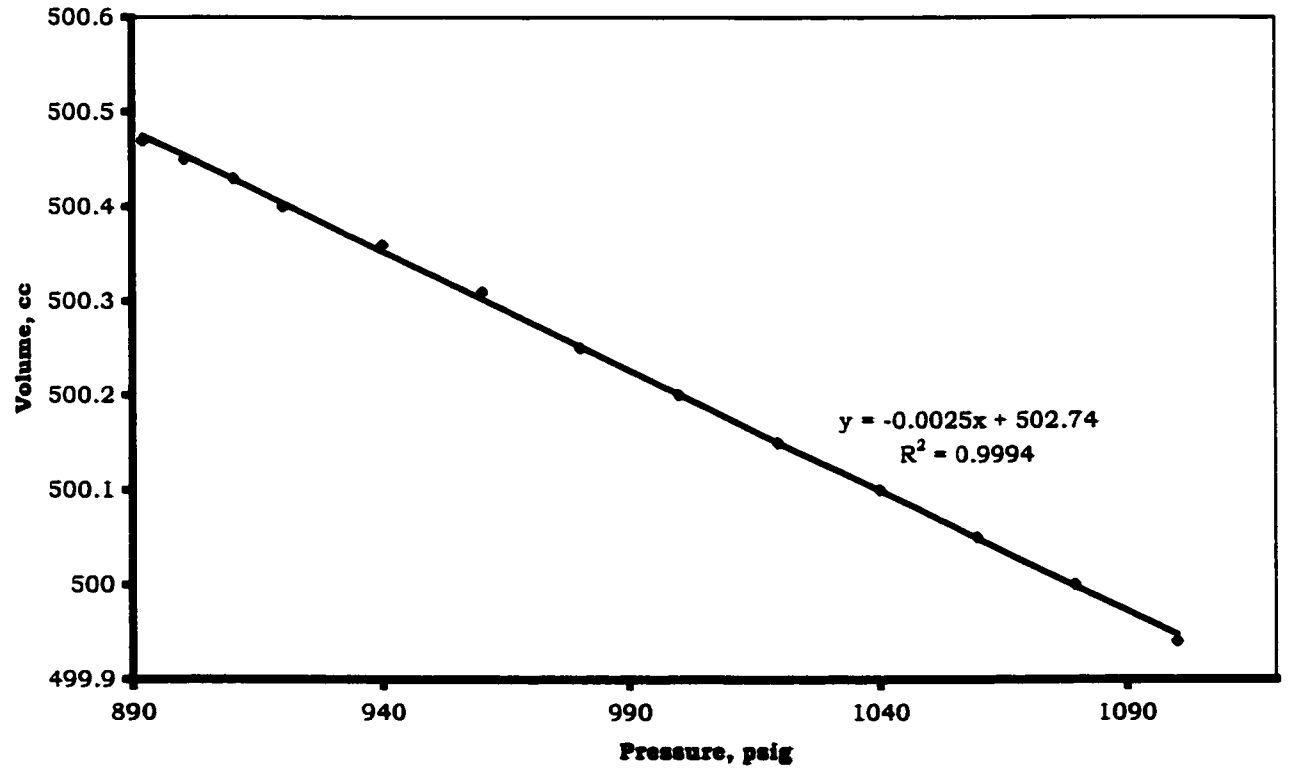

Figure 5.11: Determination of compressibility of live oil

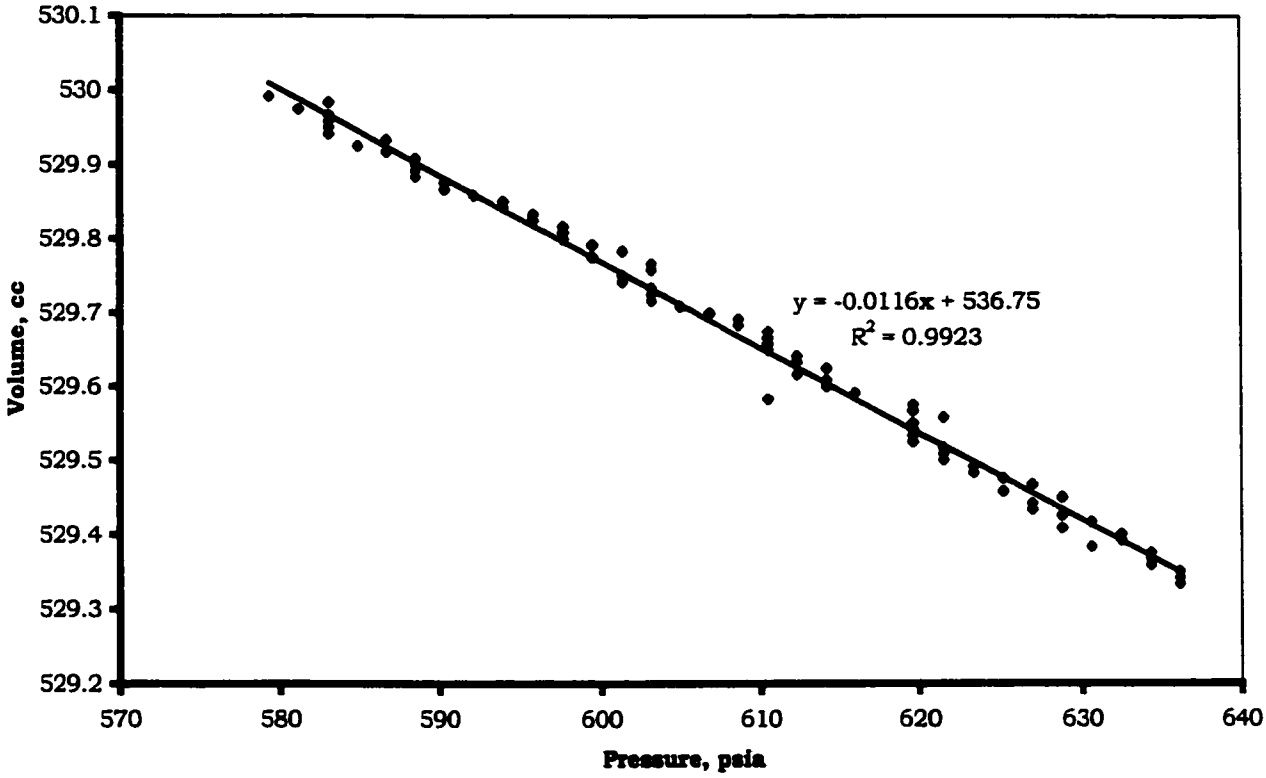

Figure 5.12: Determination of compressibility of sand-pack

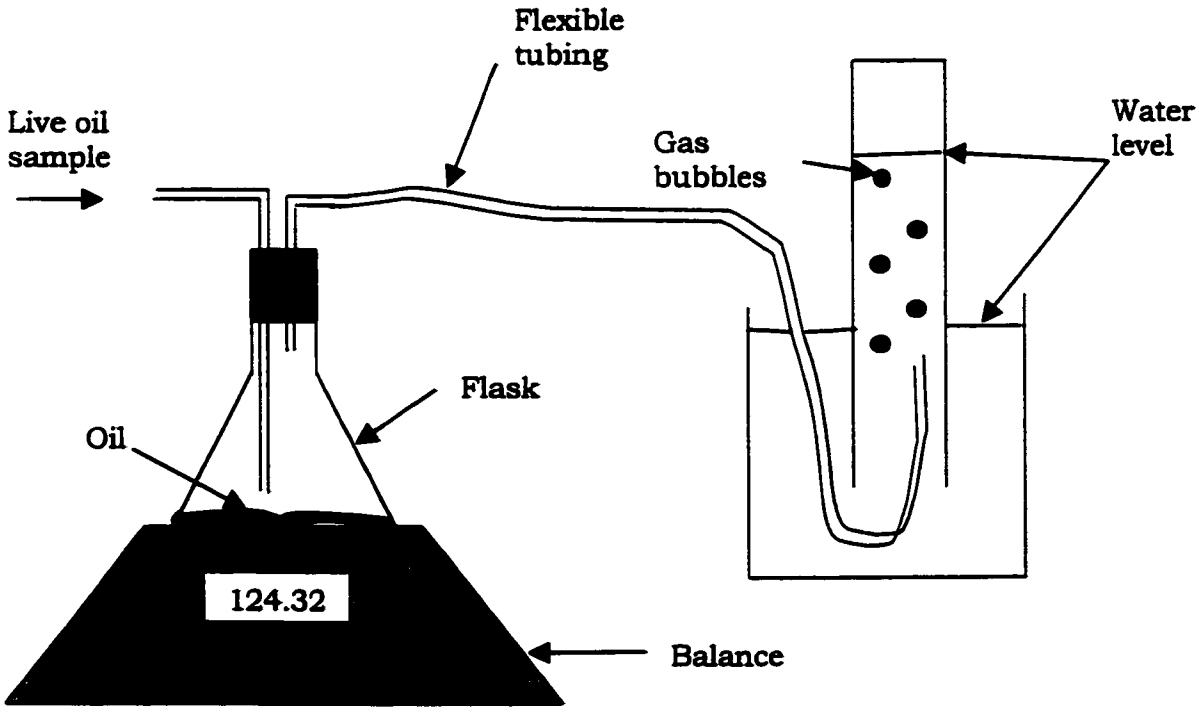

Figure 5.13: Setup for measurement of gas-oil ratio

more methane gas was introduced and the pressure was again brought up to the desired bubble point pressure. This was done until the pressure stabilised, i.e. no more gas was getting dissolved into the oil. Once this happened the cell was rocked for another 48 hours to ensure complete dissolution.

5.4.20. Determination of live oil and sand-pack compressibility

Once the live oil was prepared it was transferred into the transfer vessel by applying pressure in the rocker cell with nitrogen. Next, the live oil was transferred into Isco pump. The compressibility of the live oil was measured using the same procedure as that used for dead oil. The P-V graph for live oil compressibility determination is shown in Figure 5.11. The live oil compressibility was found to be 5×10^{-6} psi^{-1} (7.2×10^{-7} KPa^{-1}).

The compressibility of the sand-pack using dead oil was measured in a similar way. The inlet of the core was connected to the pump and the outlet was closed. The fluid was then injected into the core and pressure versus the volume injected was recorded and then plotted to determine the slope. This was further used to determine the core compressibility using the above equation. The P-V plot is shown in Figure 5.12. The sand-pack compressibility was found to be 22×10^{-6} psi^{-1} (3.2×10^{-6} KPa^{-1}).

5.4.21. Gas-Oil Ratio (GOR) determination

The gas-oil ratio of the live oil was determined by taking a sample of live oil into a flask whose outlet was connected to an inverted glass graduated cylinder filled with water. This was done to collect the gas produced in the inverted cylinder by bubbling it over water. The weight of the flask was measured to determine the oil volume. The measured quantities were then brought to standard condition to calculate the Gas-Oil Ratio (GOR). A schematic of the setup is shown in Figure 5.13.

A setup is prepared to obtain the R_{so} curve for the oil and is shown in Figure 5.14. The cylinder was first filled with methane gas to a pressure equal

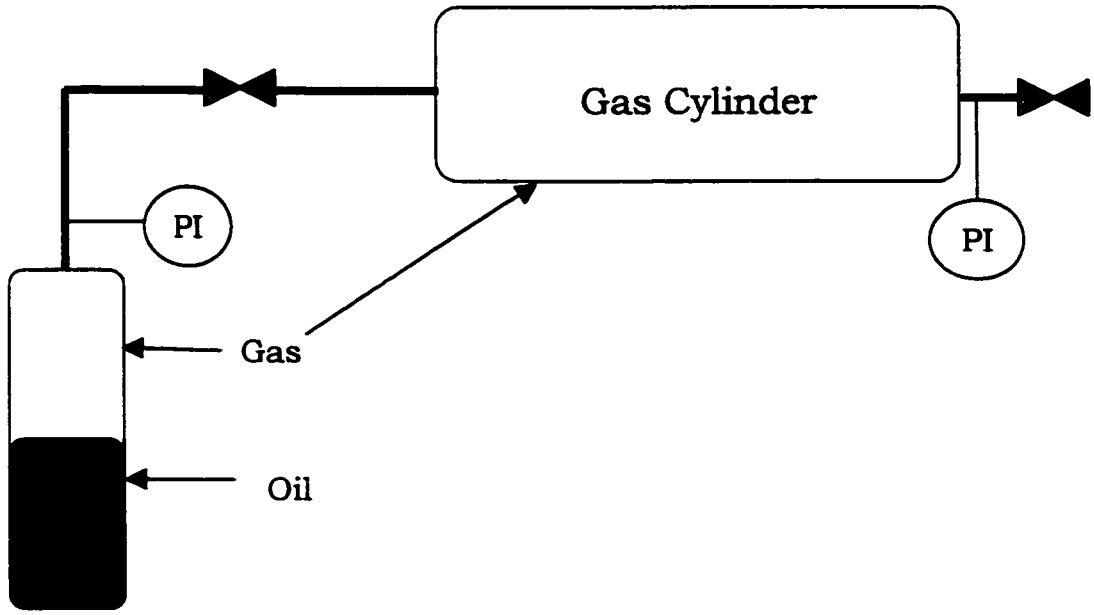

Figure 5.14: Setup for solution gas-oil ratio (R_{so}) measurement

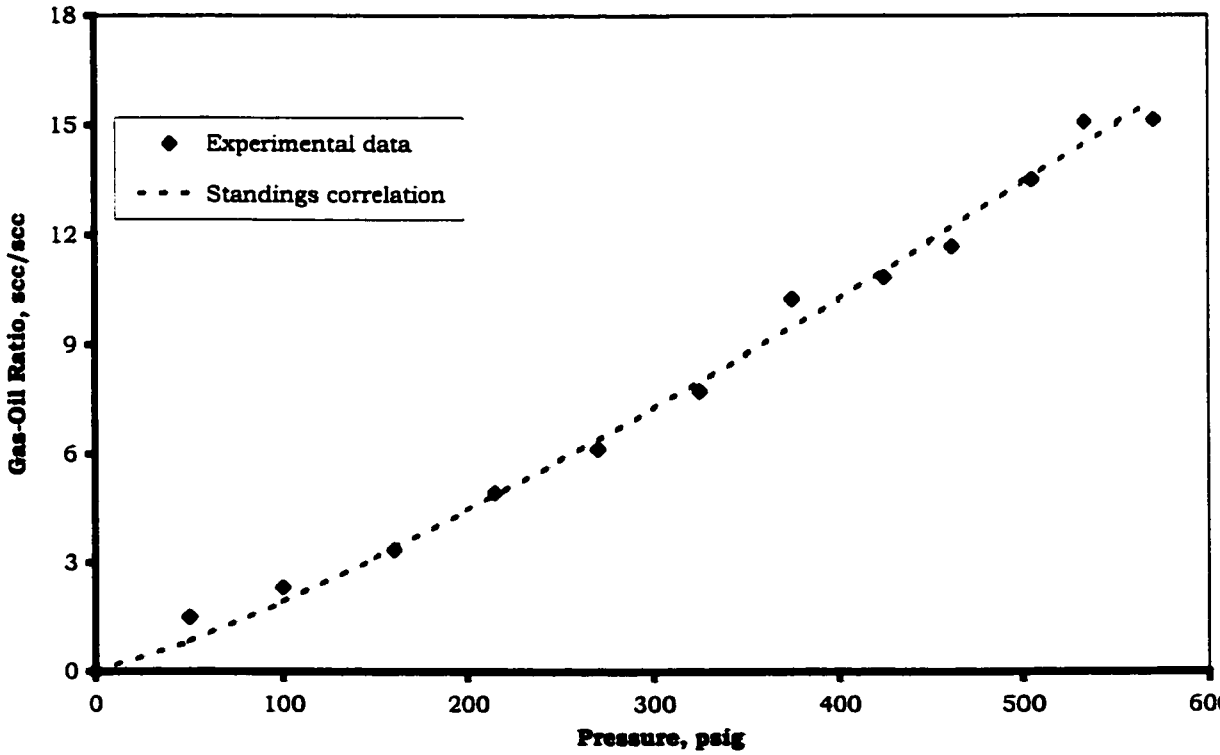

Figure 5.15: Measured solution gas-oil ratio (Rso) for oil

to bubble point of live oil. A known volume of live oil (about half the volume of the cylinder) was then injected into the cylinder with Isco pump. The resultant pressure was brought to the bubble point of live oil by bleeding off some methane gas. The system was then stabilised for 24 hours. The pressure in the cylinder was then lowered, by bleeding off methane into the gas cylinder. The pressure in both the cylinders was allowed to stabilise.

The resultant pressure in the cylinders is an indication of the gas left in respective cylinders. This value is then used to calculate the solution gas-oil ratio at various pressures. The R_{so} curve obtained is shown in Figure 5.15. R_{so} curve matches well with the Standing's correlation (Craft and Hawkins (1992)), depicted in Figure 5.15, hence Standing's correlation was used in all the calculations

5.4.22. Live oil flooding

Once the system was flooded with dead oil and the Isco pump was charged with live oil, the next step was to inject live oil into the system. The dead oil, displaced due to flooding of system by live oil, was produced through a back-pressure regulator. The pressure of the back-pressure regulator was set above bubble point pressure of live oil. This was done to ensure that pressure is above the bubble point and second phase is not generated in the system. Samples were drawn from the produced oil periodically and GOR was measured. It was assumed that all of dead oil was displaced when the GOR of the produced oil became equal to the GOR of the live oil being injected. This required flooding of about 1.5 - 2 pore volumes of live oil.

5.5 Running experiments

5.5.1. Depletion runs

Once the sand-pack is filled with live oil and pressurised, it is ready for depletion to be performed. The Isco pump is operated at constant flow refill

mode. The oil is withdrawn into the pump through the visual cell. The inlet to the visual cell is from the top and the outlet is from the bottom. The depletion was done at rates of 0.08, 0.37, 3 and 12 cc/hr.

Before start of a new run, the core was thoroughly flushed with about 2 pore volumes of live oil at pressure higher than the bubble point. This was done to guarantee complete dissolution of the gas into the oil. Once this was done, the system was left for 24 hours and pressure was recorded to ensure that there was no free gas dissolving into the oil. Presence of free gas is reflected by fall in pressure in the sand-pack. The compressibility of the sand-pack was also measured before start of the run to ensure single phase in the sand-pack.

5.5.2. Production measurement

The critical gas saturation is marked by sustained gas production in the visual cell. After reaching critical gas saturation, produced free gas starts accumulating at the top of the visual cell. The small size of the visual cell minimizes the dead volume and ensures that the gas being accumulated is coming from the sand-pack rather than being generated from the oil in the visual cell. The amount of free gas produced is measured with a Cathetometer, that is mounted outside the oven, by measuring the gas-oil interface. For slower runs, the run is stopped when the visual cell is full with gas, whereas, for the faster runs, run is stopped after depleting the sand-pack up to a certain volume (nearly equivalent to that in slower runs).

All other parameters viz. temperatures, pressures, differential pressures etc. were recorded on the Labtech notebook.

5.6 Results

Table 5.4 shows the summary of results for the various runs. Run 5 is performed to check the reproducibility of the runs. Reproducibility run was found to duplicate the data of original run quite well. The system pressure

result of Run 5 is presented in inset in Figure 5.16, which exhibits a fairly good reproducibility. Other results of Run 5 henceforth shall not be presented in the chapter.

Table 5.4: Summary of results

Test	Depletion Rate, cc/hr	Bubble Point Pressure, psia (KPa)	Critical Gas Saturation, %	Final Gas Saturation, % (After 29 cc depl.)	End Point value
Run 1	0.08	575 (3963)	3.0	3.85	0.0015
Run 3	0.37	575 (3963)	3.4	4.3	0.0009
Run 4	3.0	575 (3963)	4.2	4.8	0.0005
Run 5	3.0	575 (3963)	4.15	4.7	0.0005
Run 6	12.0	575 (3963)	7.0	5.6	0.00005

5.6.1. Pressure

Figure 5.16 shows the P-V data for the various depletion runs. A constant volumetric rate depletion is carried out. The average pressure in the sand-pack is plotted against the volume of fluid withdrawn. The volumetric average pressure is calculated using the Simpson's $1/3^{rd}$ rule, using the pressure at some points along the length of the sand-pack. The initial pressure for all the runs was approximately 606 psig (4177 KPa). It can be seen in the figure that during the initial part of depletion process, the pressure in the system falls sharply. The slope is representative of the single-phase compressibility of the sand-pack, which was determined before start of the run. Even after reaching the bubble-point, the pressure keeps on falling at the same rate (exhibiting single-phase compressibility). Here, the system is in non-equilibrium condition. The curve reaches a minimum pressure, known as the "Critical Supersaturation", before system pressure starts to rebound.

In Chapter 4, it was shown that this minimum point on the P-V curve does not need to correspond to the nucleation point or "Critical

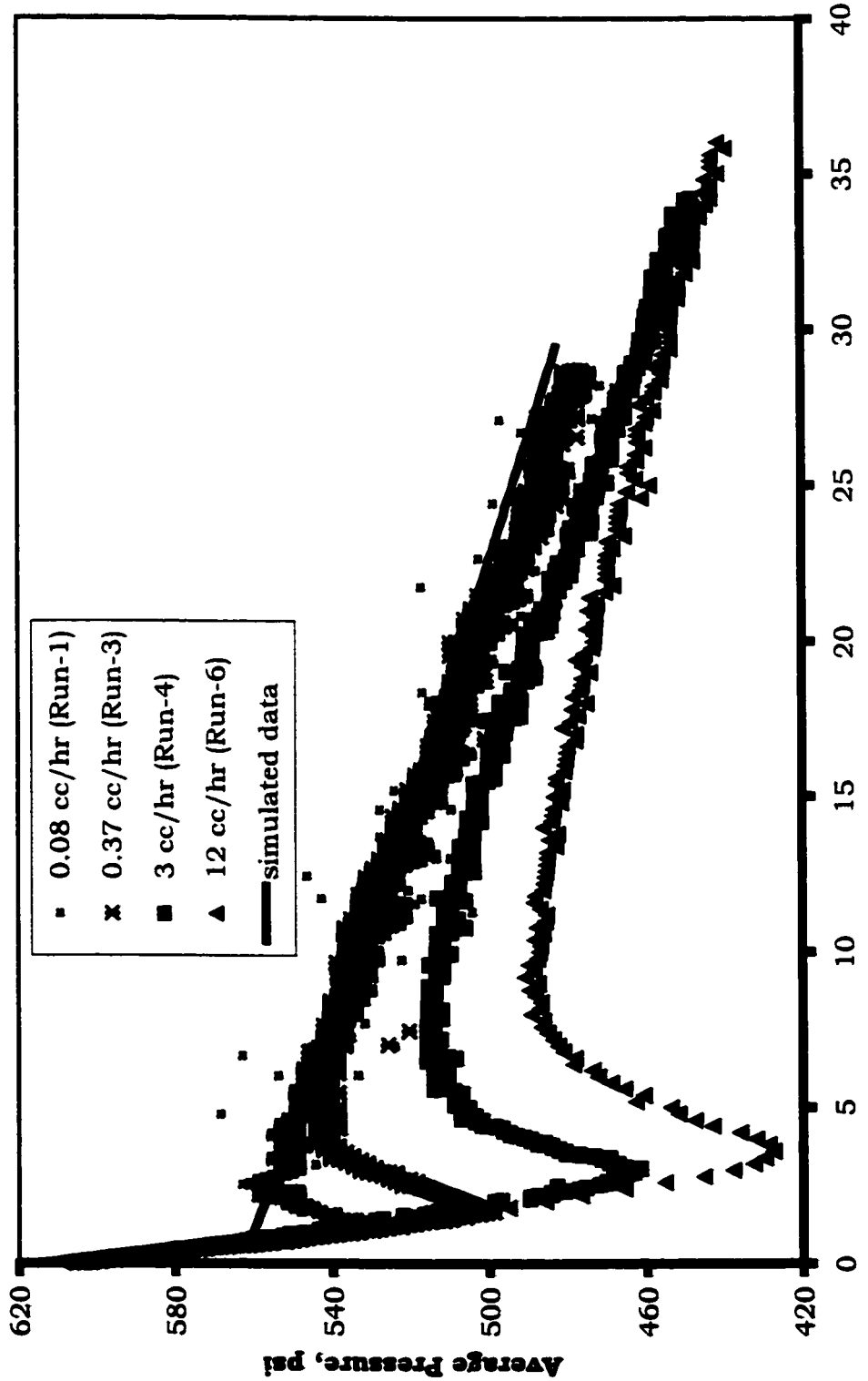

Figure 5.16: Average Pressure vs. Depletion - Experimental and Simulated Data

Supersaturation", as assumed earlier. Rather, the system pressure can keep on falling with the compressibility of the single even after bubbles nucleate. A term "Apparent Critical Supersaturation" was assigned to the lowest point on the P-V graph. The study concluded that the minimum point on the P-V graph may be partly attributed to growth kinetics as opposed to nucleation kinetics proposed in earlier studies. Henceforth, in rest of this chapter we would refer to the lowest point on P-V graph as "Apparent Critical Supersaturation".

Coming back to Figure 5.16, once the pressure starts to rebound, it reaches a certain maximum value before it starts to fall again, this time with a much smaller slope. All the curves approach a single value asymptotically at late times. This is the equilibrium value. The slower runs (Run 1 and 3) reach this value quickly. However, the faster runs (Runs 4 & 6) approach the equilibrium value gradually at late times. Some non-equilibrium effect is apparent in the faster runs even after the end of run. This was evident in run 5, where the pressure went up by 15 psi (103.4 KPa), after the run was stopped.

It can also be observed that as the depletion rate is increased, the non-equilibrium portion of the curve dips further down. This indicates increase in "Apparent Critical Supersaturation" with depletion rate. Explanation of this behaviour was given in the previous chapter.

5.6.2. Differential pressure

The differential pressures across the sand-pack for various runs are plotted in Figures 5.17 and 5.18. For the slower depletion rates (0.08 and 0.37 cc/hr), the differential pressure first rises sharply during the transient phase, then becomes constant for some time, as would be expected during the single-phase flow. Following this, the differential pressure across the sand-pack starts rising, indicating generation of gas phase and lowering of oil relative permeability. This can be seen in Figures 5.17 (ΔV= 2-14 cc) and 5.18 (ΔV= 2-12 cc), for Runs 1 and 3, respectively. This indicates that the oil phase

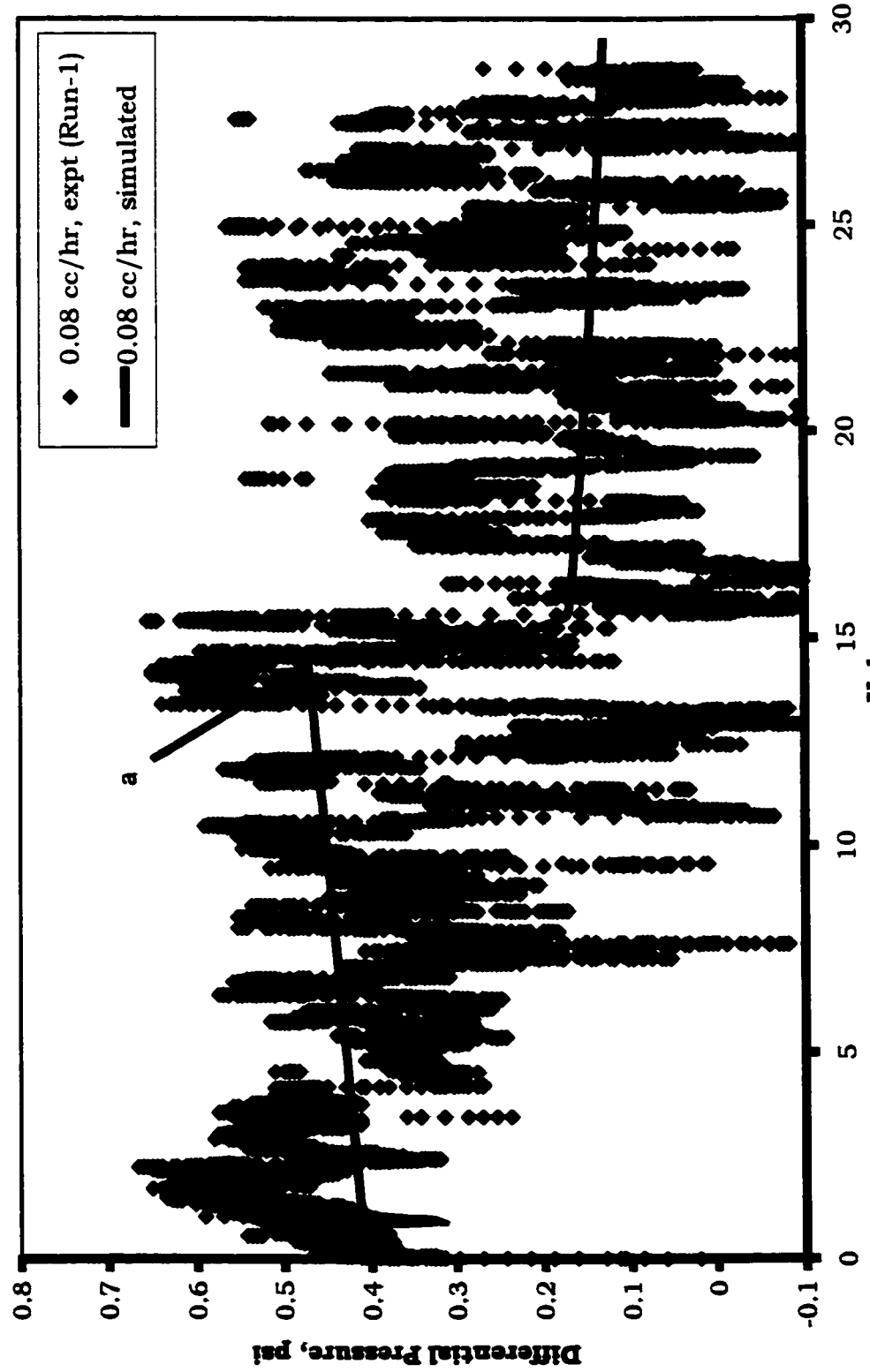

Figure 5.17: Differential Pressure for Run 1

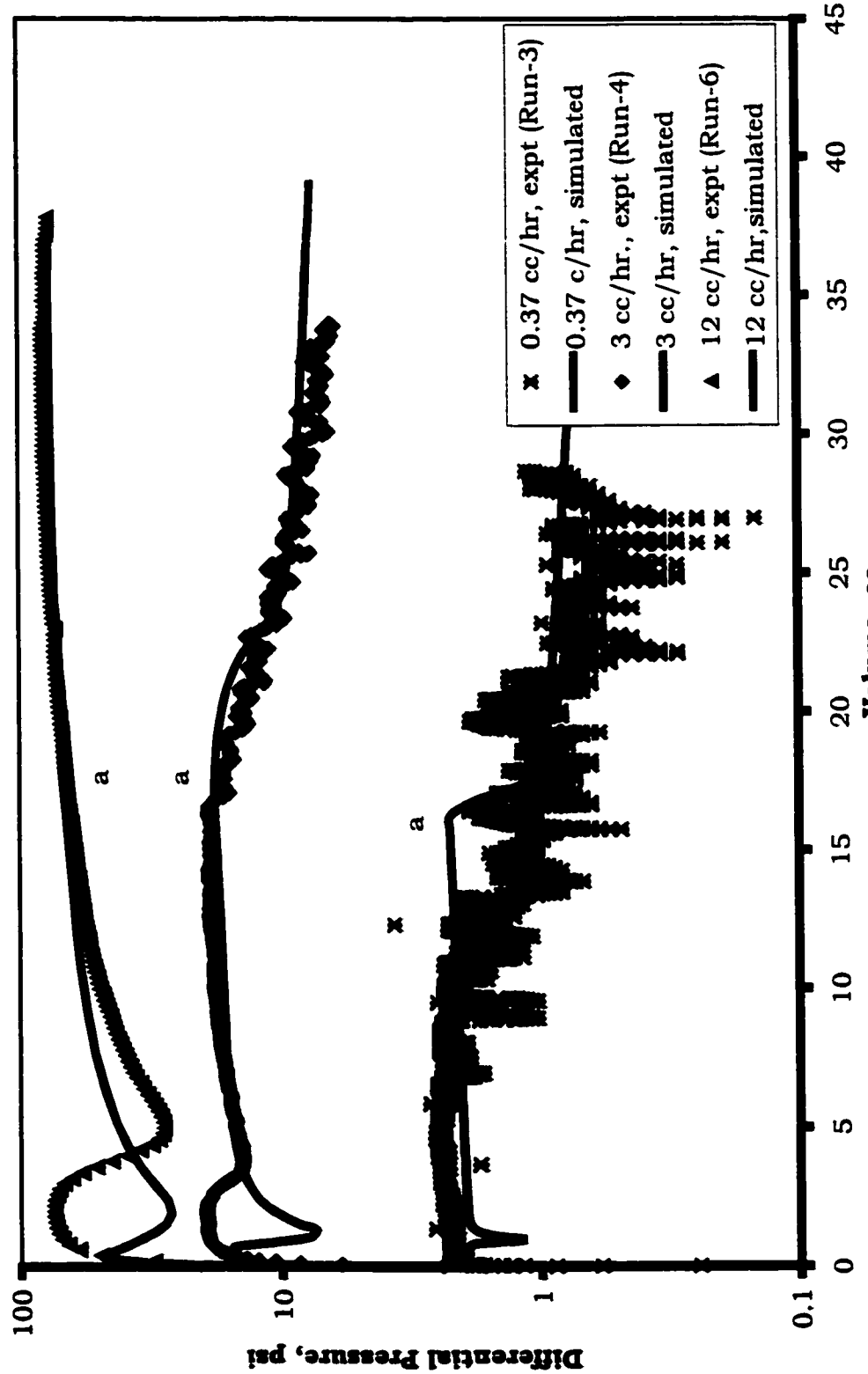

Figure 5.18: Differential Pressures for Run 3, 4 and 6

mobility is not increased due to generation of gas bubbles. This observation negates one of the theory [Shen and Batycky (1999)], attributing the favourable behaviour of heavy oil reservoirs to increase in oil mobility due to nucleation of gas bubbles at pore walls. A similar behaviour was previously reported in the work of Pooladi-Darvish and Firoozabadi (1999).

The fluctuations in differential pressure, once the gas is generated in the sand-pack and starts to move, could be due to other factors besides gas movement in the sand-pack. The random measurement of gas and oil pressure may be a factor for fluctuation in differential pressure. The onset of gas production, in all Figures, is indicated by the letter *'a'*. Once critical gas saturation is reached, which is indicated by sustained gas production in the visual cell, the differential pressure becomes more chaotic and fluctuates with greater frequency and higher amplitude. This indicates that gas is flowing out intermittently rather than flowing out continuously. This has been visually observed in some other works [Pooladi-Darvish and Firoozabadi (1999), Guo-Quig and Firoozabadi (1999)], where similar experiments were performed in a transparent system. After start of gas production, the differential pressure in the system starts to go down monotonously for the remaining part of the experimental run.

The behaviour of differential pressure for 3 cc/hr run (Run 4), shown in Figure 5.18, is slightly different in the beginning. Initially, the differential pressure rises and then becomes constant during the single-phase flow. Following this, the differential pressure falls sharply (ΔV= 2.4 cc). This can be explained by the fact that since the differential pressure is higher, (approx. 20 psi (138 KPa)) the gas is first generated at the outlet end, whereas there is still single-phase at the no-flow boundary. The nucleation of gas phase decreases the rate of pressure drop at the outlet end, thereby decreasing the differential pressure across the sand-pack. This is shown in Figure 5.19, where the pressure at the production end and no-flow boundary is plotted for Run 4. After 2.4 cc production, the tangents to the pressure data (No. 1/2) tend to converge, indicating decrease in differential pressure which complies with the

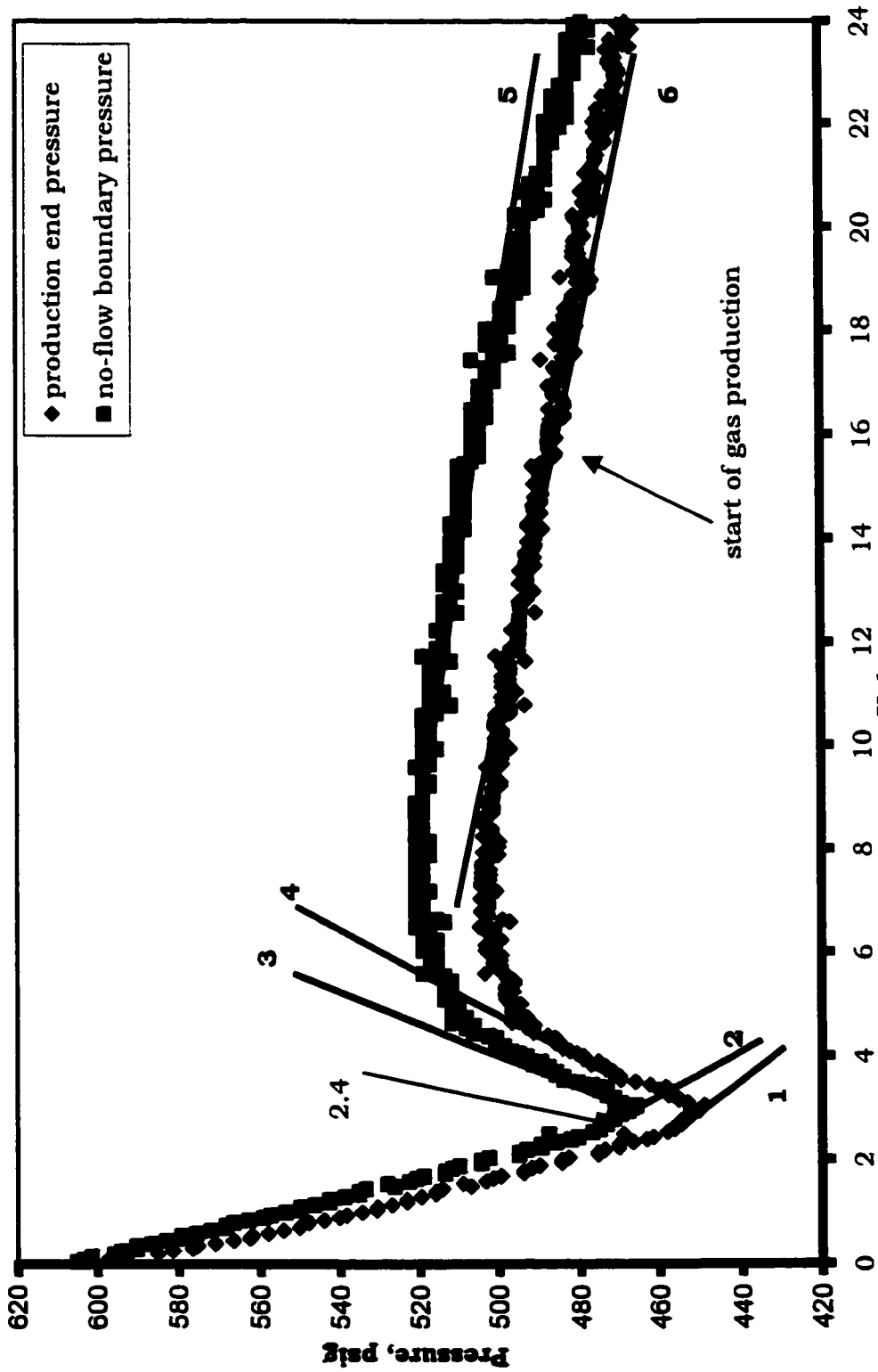

Figure 5.19: Experimental production-end and no-flow boundary pressure (Run 4)

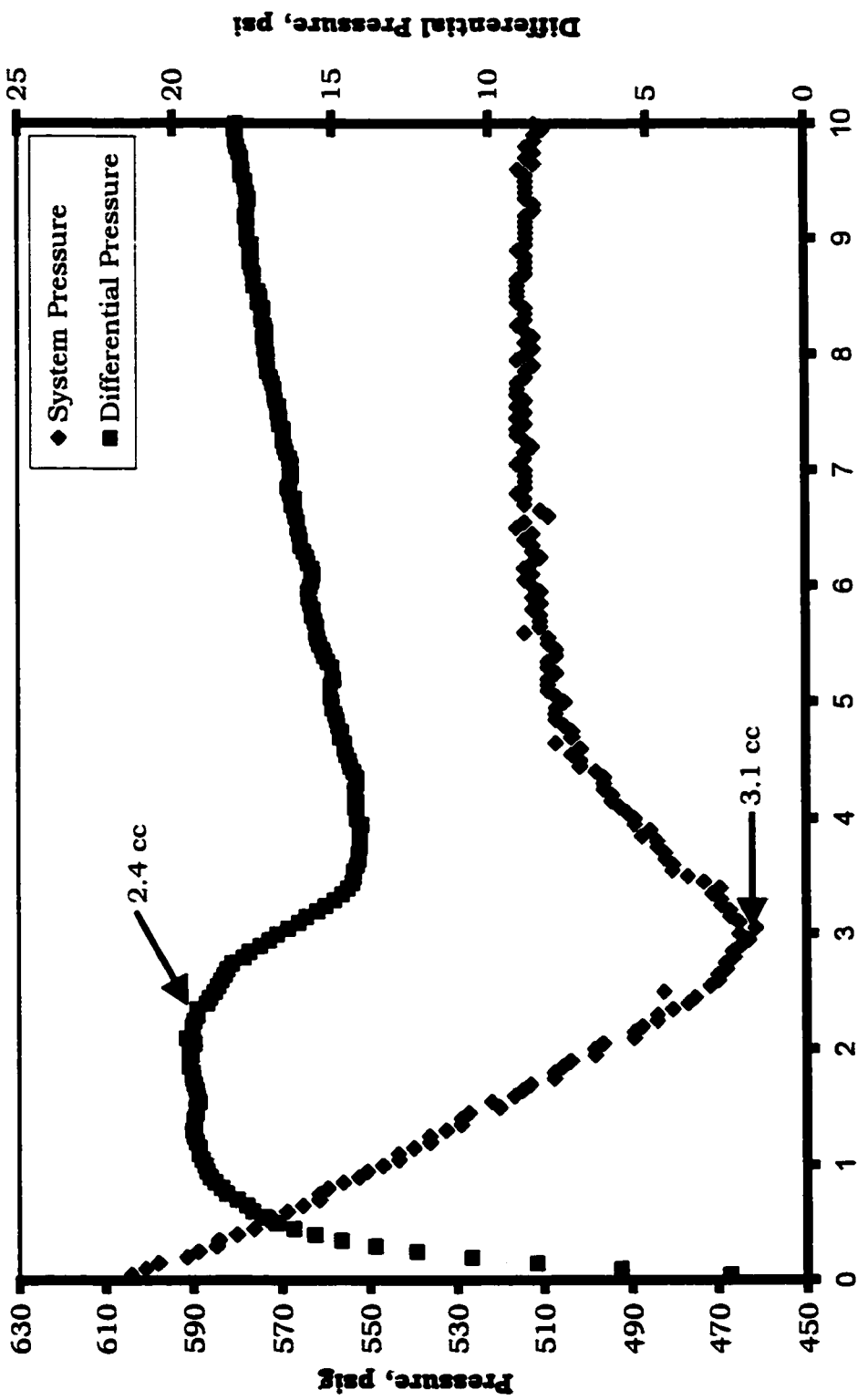

Figure 5.20: System and Differential Pressure: 3 cc/ hr (Run-4)

differential pressure data (Figure 5.20). This is the transition time when the slope of the P-V graph is changing and the pressure in the system is rebounding. This effect is not evident in the slower runs since the pressure drop is much lower (0.5– 2 psi (3.4-13.8 KPa)). Hence, the gas might generate anywhere in the sand-pack. Moreover, the similar depleted volume in slower runs corresponds to a much longer time than in faster runs, thereby allowing more time in the slower runs for the pressure to reach the no-flow boundary. Once the gas is generated at the no-flow boundary, the differential pressure in the system starts to rise again (indicated by difference in slope of line 3/4 and 5/6 in Figure 5.19); a behaviour similar to the one observed in slower runs discussed earlier. Once the critical gas saturation is reached the differential pressure starts decreasing due to flow of a less viscous fluid in the porous medium.

The behaviour of 12 cc/hr (Run 6), shown in Figure 5.18, run is similar to that of 3 cc/hr at early times, but at late times it has a different behaviour. Once the differential pressure starts to rise (ΔV= 4.5 cc) it does not decrease, rather it increases for the duration of the experimental run. One of the possible explanations could be that the gas phase saturation near the no-flow boundary has not reached critical gas saturation and the gas phase is still building up there. Hence, the pressure at the far boundary decreases at a slower rate than pressure at the production end. Further, very little gas is being produced and liquid flow rate is the same whereas the gas saturation in the sand-pack is increasing, resulting in higher pressure drop.

One of the observations, that is not quite conspicuous in the slower runs (Test 1 and 3), but is evident in faster depletion runs, (Test 4 and 6) is that, the depleted volume, at which the differential pressure starts falling down (corresponding to nucleation of bubbles as discussed earlier), does not correspond to "Apparent Critical Supersaturation". The depleted volume at which the differential pressure starts falling is 2.4 cc for Runs 4 & 6. Whereas, the depleted volume, for "Apparent Critical Supersaturation", is 3.1 & 3.6 cc for Run 4 & 6 respectively. For Run 4 this discrepancy can be seen in Figure 5.20,

where the early time data for system and differential pressure is plotted together. This observation further confirms the theory presented in chapter 4 that the bubbles do not nucleate at "Apparent Critical Supersaturation" but rather somewhere below bubble-point and before "Apparent Critical Supersaturation".

5.6.3. Average gas saturation and production

For Run 1 (0.08 cc/hr) the first gas bubble was observed after 14 cc of depletion. This corresponds to roughly 3 % average gas saturation. The run was stopped after 15 days when the visual cell was full with gas. For Run 3 (0.37 cc/hr) the steady gas production started after 17.3 cc of depletion, corresponding to 3.4 % average gas saturation. In these slower runs, there was a clearly distinguishable gas-oil interface in the visual cell. For Run 4 (3 cc/hr), the gas production started after 18.8 cc of depletion which corresponds to 3.85 % average gas saturation. The gas production during this run was in form of slightly foamy and frothy fluid. A not-so-distinct gas-oil interface was observed. Tiny gas bubbles on the surface marked the interface. For the fastest depletion rate (Run 6; 12 cc/hr), swarms of very tiny bubbles were observed initially (ΔV=14 cc). After this, there was no gas production for some time. Then after some time, another swarm of bubbles was observed at ΔV=15 cc. The sustained production of gas started at ΔV=18 cc. This was ascertained to be the critical gas saturation, corresponding to 3.7 % average gas saturation. In this run, a very unclear gas-oil interface was observed in the visual cell. The gas space was completely filled with gas bubbles with liquid lamella separating them. The gas bubbles did not coalesce rapidly. It was difficult to ascertain the amount of gas produced which lead to some error while calculating the amount of produced gas. Observance of a more dispersed gas phase in oil at higher depletion rate has also been reported in some previous studies [Bora and Maini (1997)]. The duration of run 4 and 6 were 12 and 3 hours, respectively.

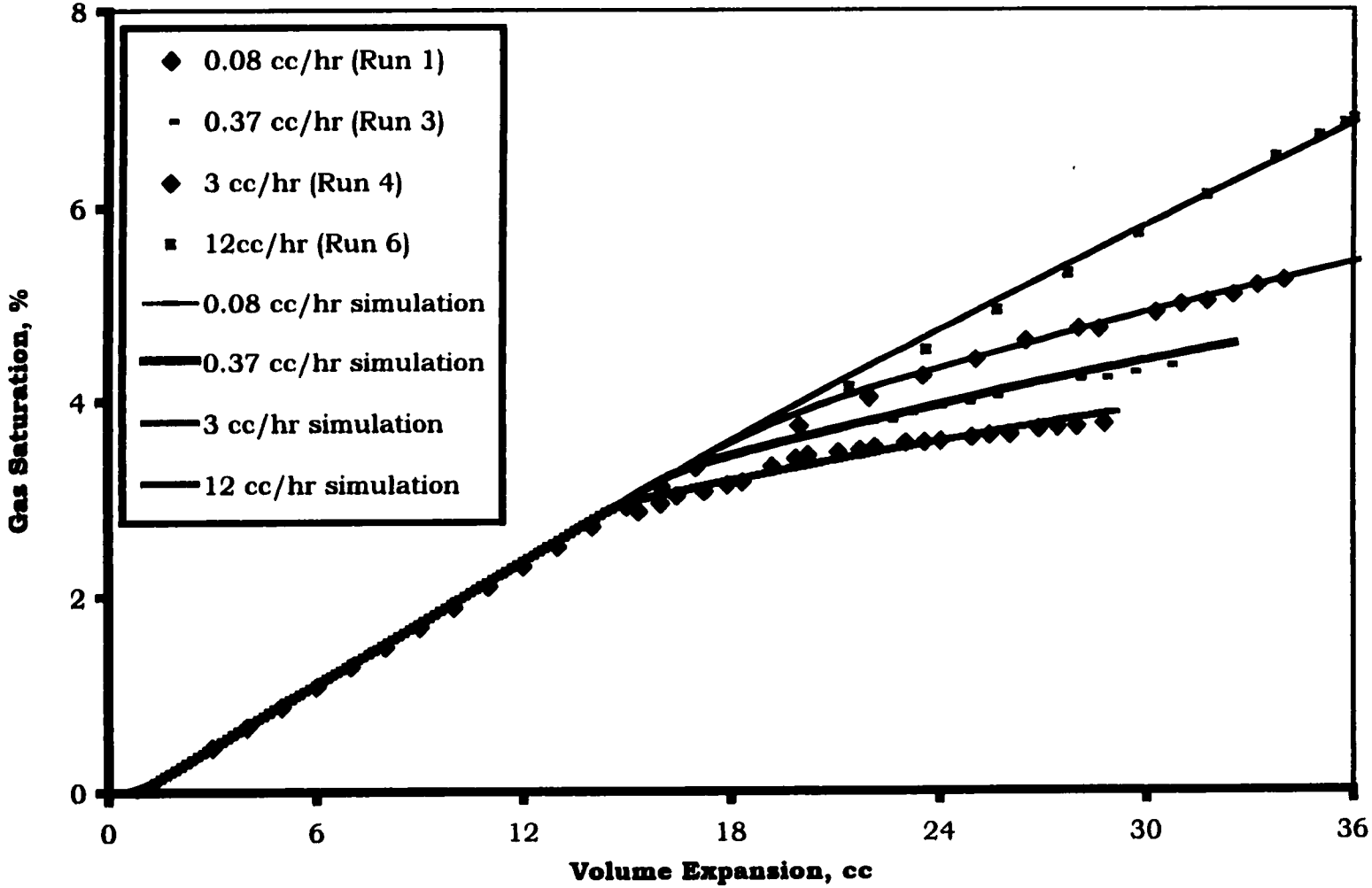

Figure 5.21:. Gas Saturation - Experimental vs. Simulated Data

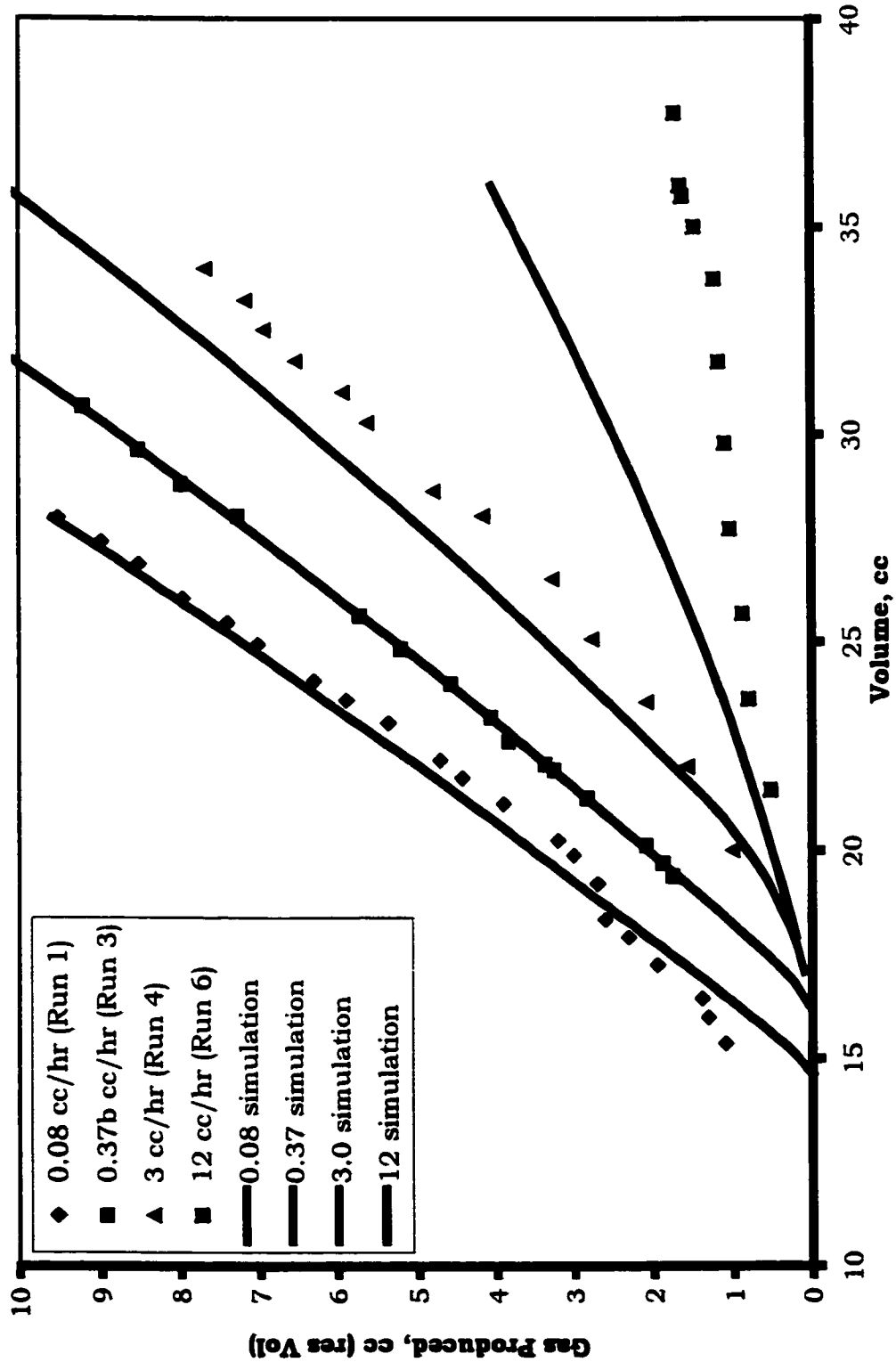

Figure 5.22: Produced Gas - Experimental vs. Simulated Results

Figure 5.21 and 5.22 show the average gas saturation and free gas production during the runs. The gas saturation was determined by finding the difference between free gas produced and total volumetric depletion. The changes in slope of line, in Figure 5.21, indicate establishment of critical gas saturation. Although the average gas saturation, at the onset of free gas flow, for all the runs is around 3-4%, the critical gas saturation for the faster depletion cases are much higher. This is due to high pressure gradient that exists across the core, which results in saturation gradient.

In the above figure, it can be clearly noted that the average gas saturation keeps on increasing with depletion rate. As the depletion rate was increased, lesser amount of free gas was produced as shown in Figure 5.21. As stated earlier, increase in depletion rate is accompanied by production of fluid with entrained dispersed gas. Figures 5.21 and 5.22 when read in conjunction indicate that faster depletion rate results in lesser free gas production and higher retention of gas-phase in the sand-pack.

The above results indicate that for gas-phase, the resistance to flow increases with depletion rate, which is reflected in lesser gas production. Further, the faster runs, as discussed earlier, were accompanied by frothy and foamy fluid production. Considering all the results together, inference can be drawn that, faster depletion rate results in higher average gas saturation in sand-pack, lower free gas production and higher resistance to flow of gas (lower gas relative permeability). This may be due to more dispersed gas phase flow.

5.7 Analysis and Discussion

5.7.1 Simulation of the experiments

The above experiments were simulated on an Eclipse-100 Black oil simulator [Schlumberger *GeoQuest*]. The objective was to match the experimental data to determine the gas relative permeability. The known variables are the fluid properties, sand-pack properties, average gas saturation,

average pressure in sand-pack, differential pressure across the sand-pack and free gas produced.

A Corey type of model [Honarpour *et al.* (1994)] was used to represent the relative permeability curve.

$$k_{ro} = k_{ro}^{0} S^{n_o}$$

$$k_{rg} = k_{rg}^{0} (1 - S)^{n_g}$$

$$S = \frac{S_o - S_{org}}{1 - S_{org}}$$

The Hagoort (1980) type of function was used to represent the capillary pressure.

$$P_c = 0.005 + 0.02 \frac{(1.01 - S)^{0.2} - (0.01)^{0.2}}{S^{0.3}}$$

The capillary end effect [Richardson (1952)] was introduced into the simulation by assigning zero capillary pressure to the grid block near to the well bore. The data used for simulation is shown in Table 5.5. Other combinations also could have been possible. The critical gas saturation and gas relative permeability were modified to match the experimental data.

Table 5.5: Data used in simulation of experiments

No. of grid blocks	100, 1, 1
Live Oil viscosity, cp	1100
Oil FVF, rm^3/sm^3	1.04 (at 620 psia (4273 KPa))
Gas FVF, rm^3/scm^3	$\beta_g = P_{sc}T/(zPT_{sc})$, $z=0.96$
Bubble point pressure, psia	575 (3963 KPa)
n_o , n_g	2, 1.5
k_{ro}^{0}	1
S_{org}	40%

5.7.2 Analysis of the results

The match for the simulated run with the experimental data is shown in Figures 5.16 - 5.18 and 5.21 - 5.22. Figure 5.16 shows the simulated data of average pressure in the core. The initial and the later part of the data match quite well. The non-equilibrium data cannot be matched as the simulator runs on equilibrium assumption.

Figure 5.17 and 5.18 matches the differential pressure data. The dip in the differential pressure in all the cases is an indication of gas being formed at outlet end, whereas there is still single-phase at the no flow boundary. This results in sudden decrease of differential pressure. This effect had been discussed earlier in the chapter. This behaviour in the simulation run at early time is shown in Figure 5.23, where the production-end pressure and no-flow boundary pressure is plotted for Run 4. The change in slope of the lines occurs at the different depletion volumes, which correspond to bubble point pressure. This results in drop in the differential pressure in the sand-pack. This phenomenon happens in the simulator at the bubble-point, since equilibrium assumption is considered in a simulator. This does not match with the experimental results where the bubbles nucleate after achieving a certain supersaturation. For example, in Figure 5.18 for Run 4, this happens at ΔV= 0.7 cc for simulation run and at ΔV= 2.4 cc for experimental run. Beyond this point, the experimental data matches quite well with the simulated results. A discrepancy is observed in Run 3 (0.37 cc/hr) where, near ΔV=14 cc the differential experimental pressure drops whereas in the simulation results it increases slightly. This may be due to coalescence/movement of gas inside the sand-pack. Once critical gas saturation is reached and the gas production starts, the simulated results match the experimental data well again.

Figure 5.21 shows the match of gas saturation in the sand-pack. Actually, this was the data, which was matched on the simulator to determine the relative permeability values. As is evident, a very satisfactory match has been obtained.

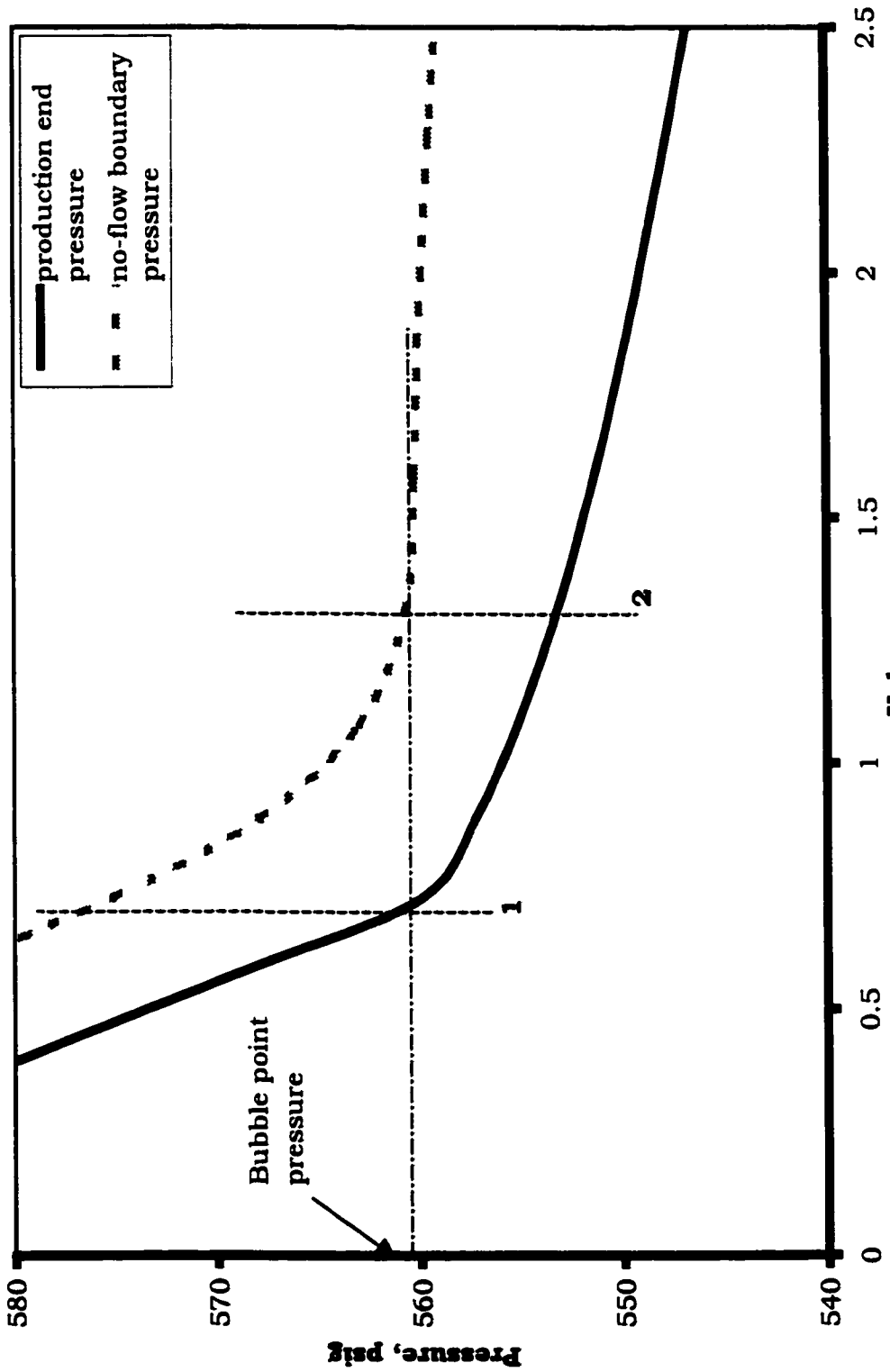

Figure 5.23: Pressure Results for Run 4 (Simulated Results)

The free gas produced is compared in Figure 5.22. A relatively satisfactory match is obtained for Run 1 and 3 (0.08 and 0.37 cc/hr). The match is not quite good for Run 4 (3 cc/hr), where the values vary slightly at higher production volumes. The simulation results do not match satisfactorily for Run 6 (12 cc/hr). Things are happening so fast that the system is not able to reach equilibrium (evident from Figure 5.16), so the free gas is expected to be less than the equilibrium value. Since the simulator runs on equilibrium assumption it is expected that it cannot model faster experiments which is dominated by non-equilibrium effects.

Figure 5.24 shows the gas relative permeability obtained from simulation. The shifting of curves downward with increasing depletion rate indicates that the relative permeability of gas decreases with increase in depletion rate. A shift in the curves to the right with increasing depletion rate connotes increase in critical gas saturation with depletion rate.

The gas relative permeability values from our runs is compared with that in light and heavy oil obtained from experiments of Pooladi-Darvish and Firoozabadi (1999). It can be seen that relative permeability for Run 1 and 6 is about 2.5 and 4 orders of magnitude lower than that in light oil. Here we have confirmed the previous observation [Pooladi-Darvish and Firoozabadi (1999)], that gas relative permeability in heavy oil is very low.

The depletion rate of the heavy oil run of Pooladi-Darvish and Firoozabadi (1999) is similar to our Run 1, i.e. about 1 pore volume every 2.5 days. The viscosity of the oil used in their runs was 38,000 cp. whereas for our runs it was 1100 cp. Comparing Run 1 with the heavy oil run of Pooladi-Darvish and Firoozabadi (1999) shows the effect of viscosity on gas relative permeability (see Figure 5.24). The gas relative permeability seems to be lowered significantly (about 2 and 4 orders of magnitude for 1100 and 38,000 cp oil, respectively) with increase in viscosity of oil. Further studies need to be done to ascertain the exact nature of effect of viscosity on gas relative permeability.

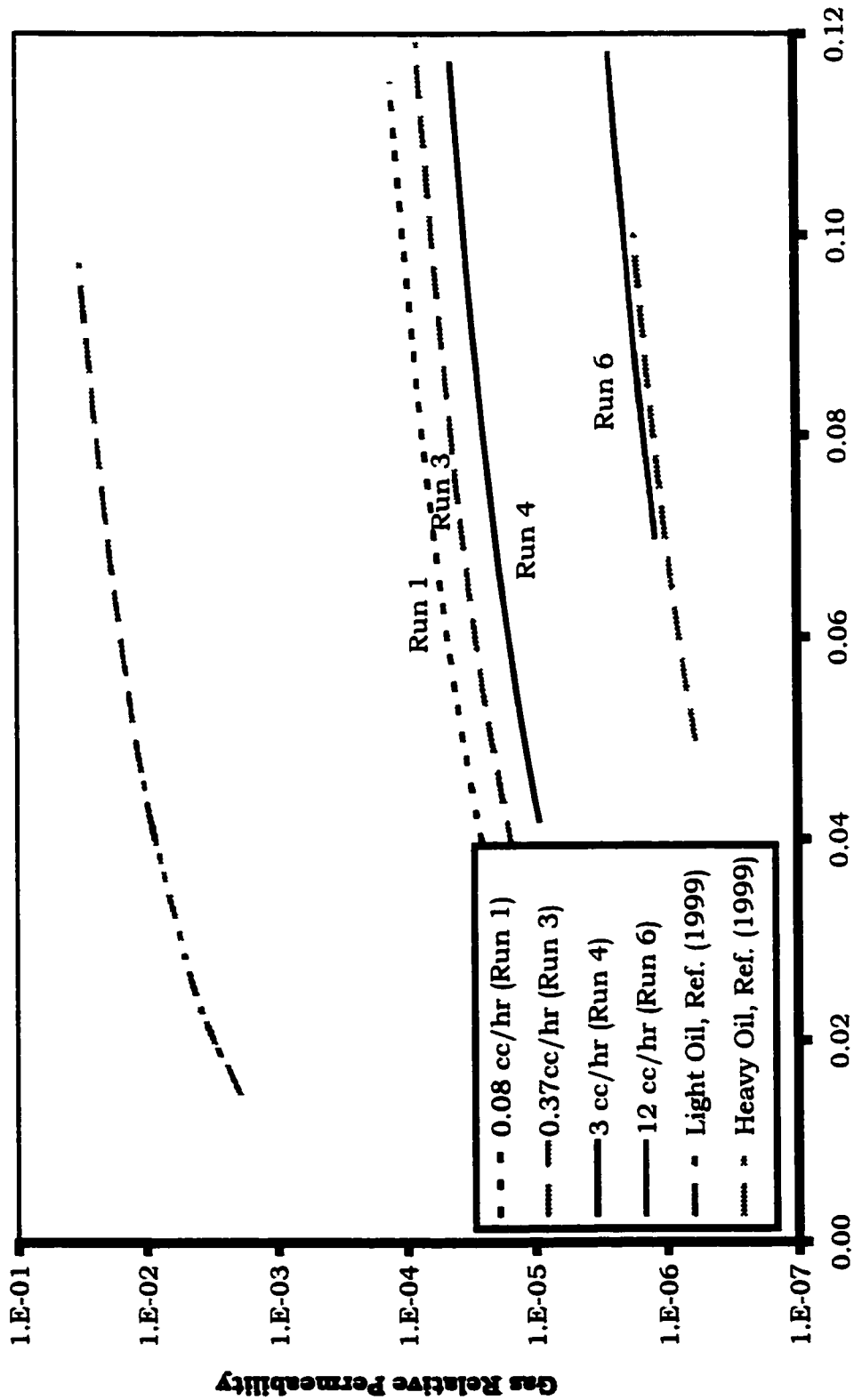

Figure 5.24: Gas Relative Permeability

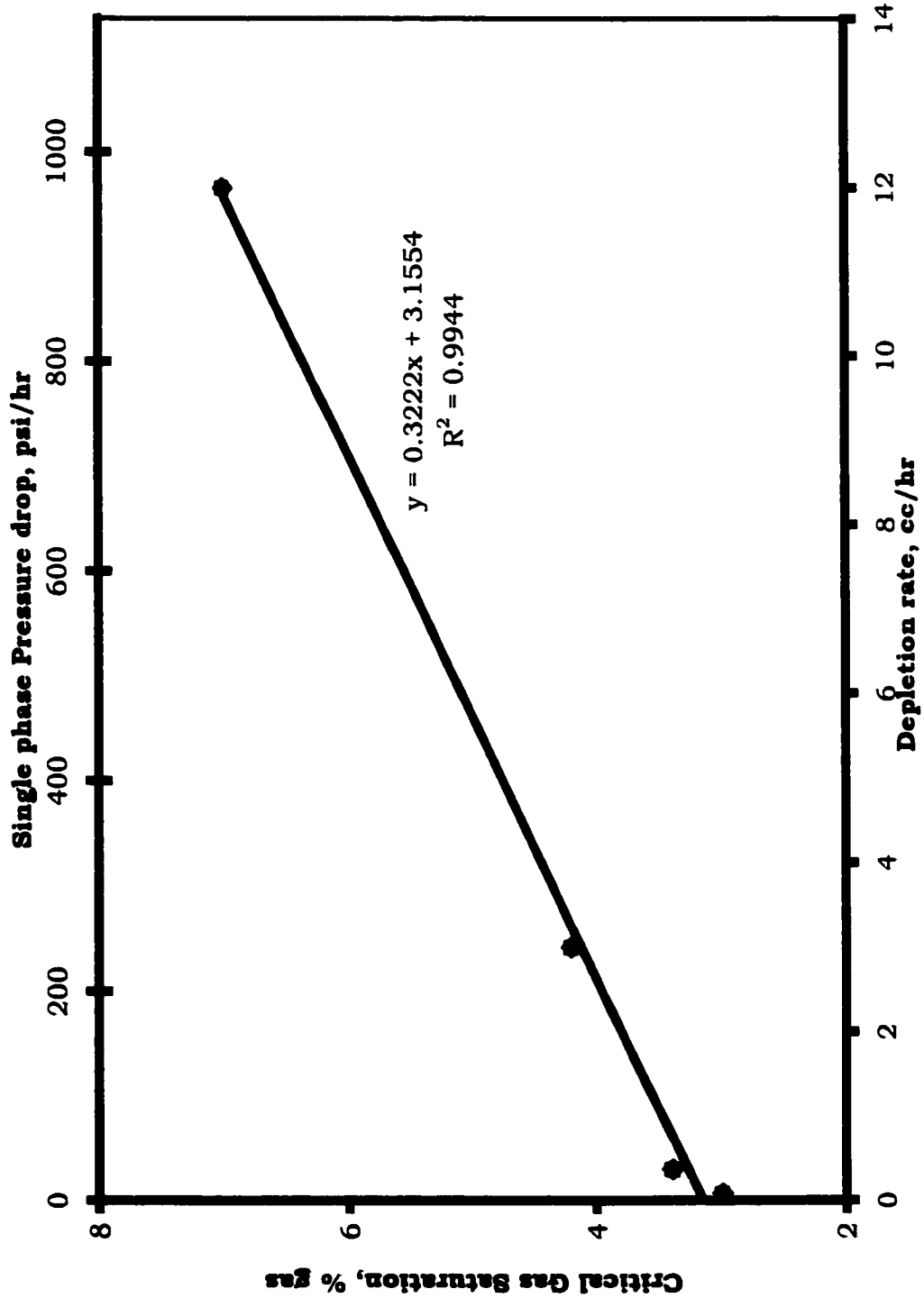

Figure 5.25: Critical Gas Saturation vs. Depletion Rate

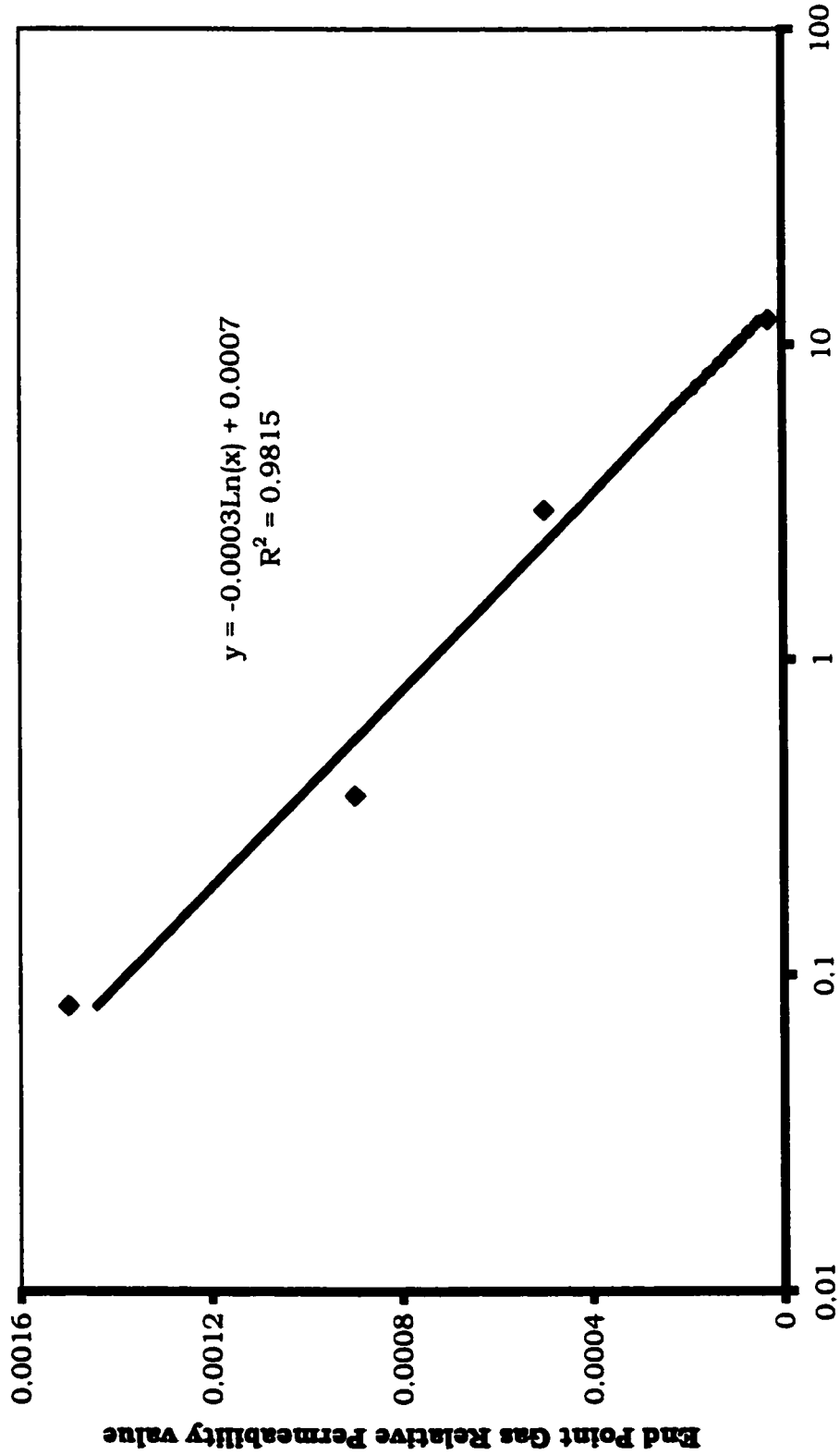

Figure 5.26: End Point Value vs. Depletion Rate

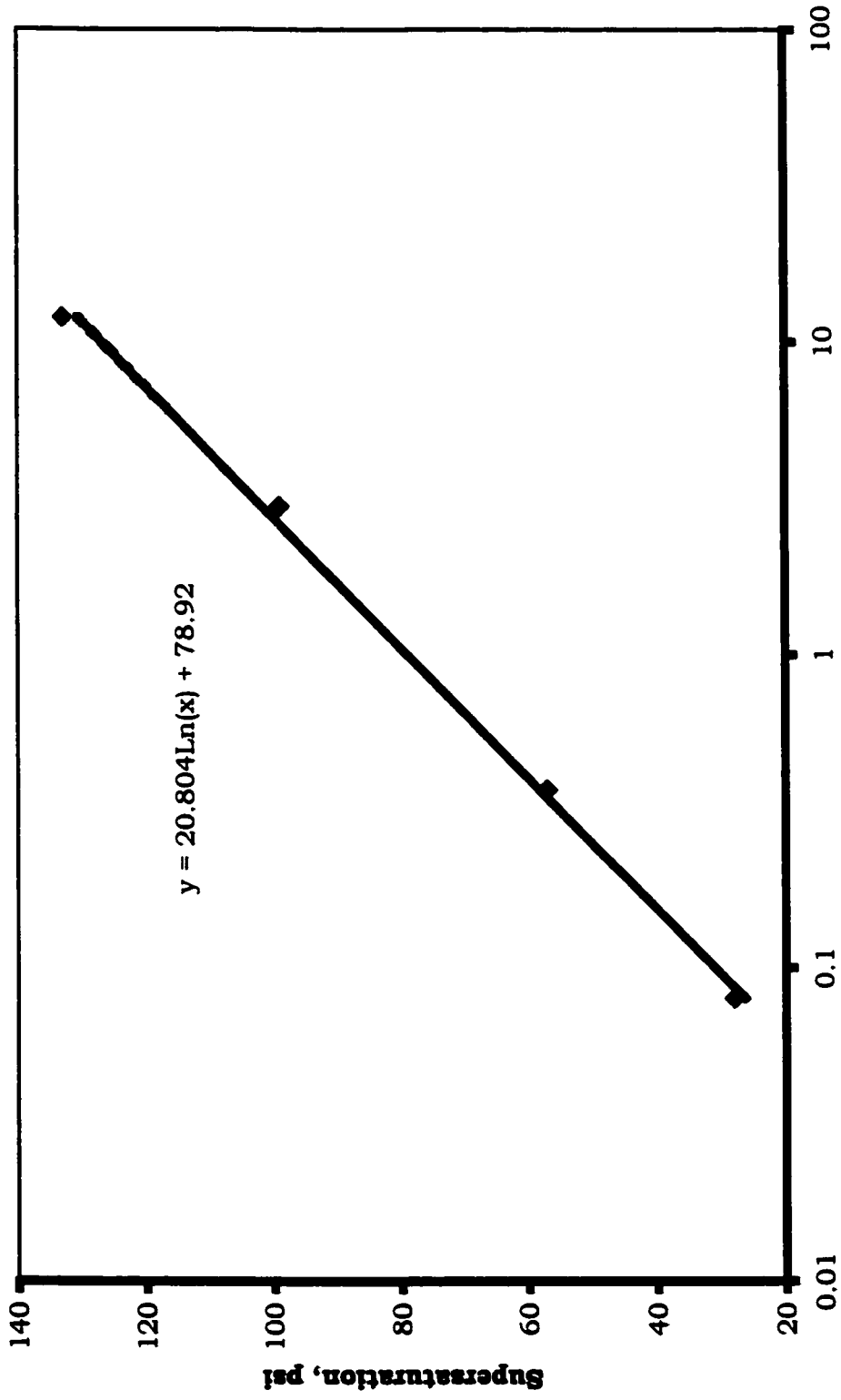

Figure 5.27: Apparent Critical Supersaturation vs. Depletion Rate

Considering the results of gas relative permeability in light of all the experimental observations and results, conclusion can be drawn that increase in depletion rate decreases the gas relative permeability, results in lower free gas production and higher gas saturation in sand-pack. The higher depletion rate was also observed to result in fluid production with more entrained and dispersed gas. Studies [Falls (1988)] have shown that more dispersed gas flow reduces the gas relative permeability. Hence, this could be one of the factors contributing to lower gas phase mobility.

In Figure 5.25 Critical Gas Saturation, as obtained from the simulation, is plotted against depletion rate. Although the average gas saturation in the sand-pack for all the runs, when the critical gas saturation is reached, is 3-4%, it was found that to match the experimental results, the critical gas saturation had to be significantly increased for the faster depletion runs. This is because a saturation gradient exists along the sand-pack due to high pressure gradient in faster depletion runs. Higher gas saturation at the outlet end, at higher depletion rates, has been observed in some of the previous works [Sarma and Maini (1992)]. A critical gas saturation of 3% was obtained for Run 1 (0.08 cc/hr.), whereas a critical gas saturation of 7% was obtained for Run 6 (12 cc/hr). A straight line can be fitted through the data.

Figure 5.26 shows the effect of depletion rate on K_{rg}^{0}; the end point value of gas relative permeability. A semi-log model can be fitted into the experimental data.

In Figure 5.27 "Apparent Critical Supersaturation" is plotted against depletion rate. Here again a semi-log model can be developed to predict "Apparent Critical Supersaturation".

Correlations developed in Figures 5.25 - 5.27 are only applicable for the system under study and depend on the choice of our model (Corey model). They indicate the trend observed by the parameter due to change in depletion rate. The coefficients of the model may not be suitable to predict the parameter in other systems, since the values of the parameter might depend on a number of factors other than depletion rate e.g. viscosity, porous media, oil type etc. A

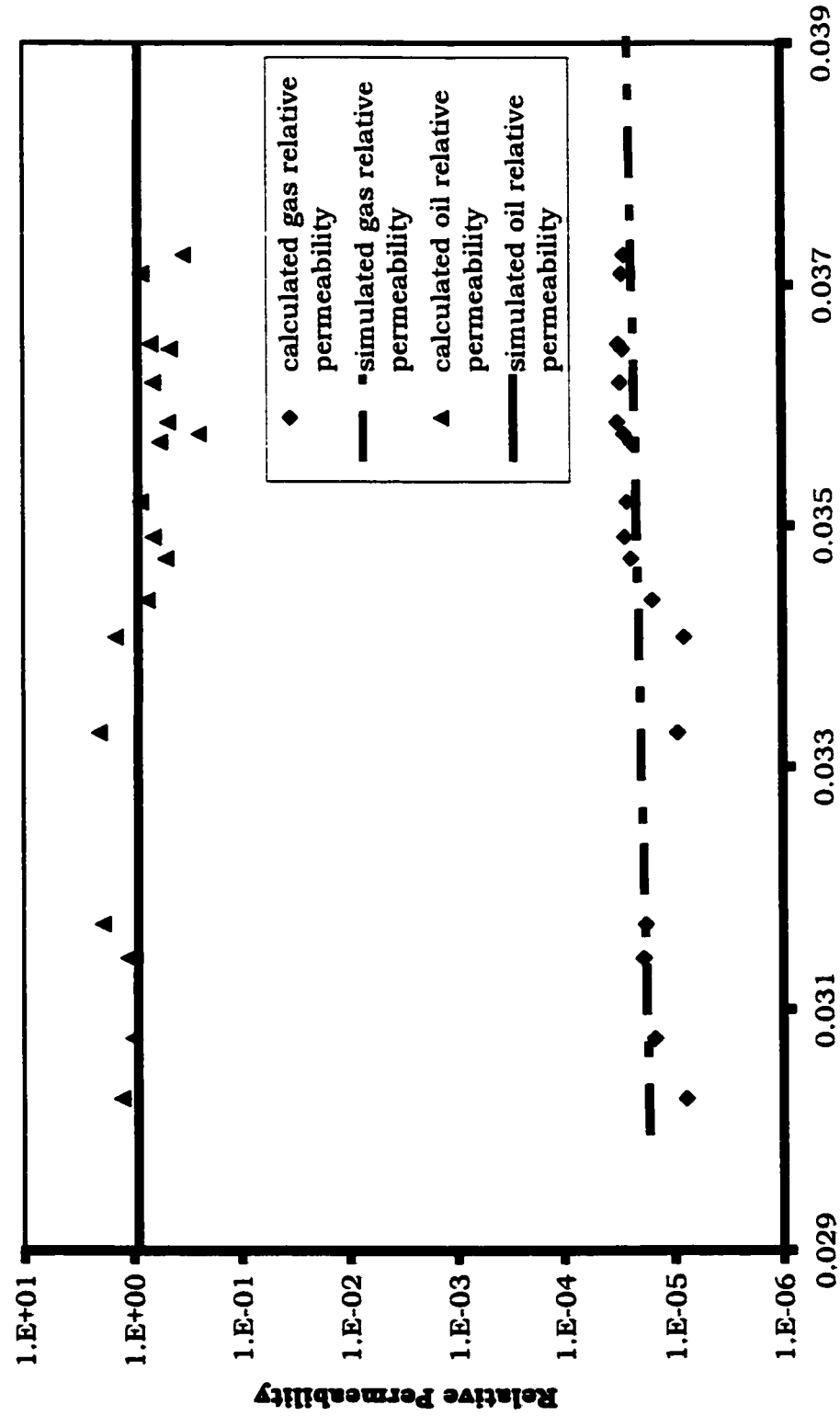

Figure 5.28: Gas Relative Permeability for 0.08 cc/hr

detailed study needs to be done, considering all the factors, to develop a comprehensive model, which can predict these parameters for any system, and examine the applicability of semi-log and linear relationships, suggested here.

5.7.3 Discussion

Recently, in a similar study [Guo-Quig and Firoozabadi (1999)] the relative permeability was calculated based on Darcy's law. The analysis considered negligible saturation gradient across the core. This may be true for the case where there is negligible pressure drop across the sand-pack. This approach is not applicable for Runs 3, 4 and 6 since there is considerable pressure drop across the sand-pack which results in a saturation gradient. However, this analysis can be applied for Run 1 where there is negligible pressure drop across the sand-pack.

Figure 5.28 shows the comparison of gas and oil relative permeability values as obtained from calculation [Guo-Quig and Firoozabadi (1999)] with the one generated using the Corey model used in the simulation of experiments. A fair match could be obtained.

5.8. Conclusions

1. Experiments were carried out to investigate the factors leading to favourable behaviour in heavy oil reservoirs under solution gas drive. Further, the effect of rate of depletion on solution gas drive process was also studied. The observations from the experiments indicated that:
   - Average gas saturation in the sand-pack increased with depletion rate, hence the produced free gas volume decreased.
   - Oil phase mobility did not increase upon formation of gas bubbles.
   - Fluid, with more entrained dispersed gas phase, was produced as the depletion rate was increased.
   - It was clearly observed in the faster depletion runs, that the gas nucleation point did not coincide with "Critical Supersaturation".

- Higher depletion rate resulted in higher "Apparent Critical Supersaturation"
- After the runs were terminated the non-equilibrium effects were absent in the slower depletion rate runs but in the faster depletion rate runs the non-equilibrium effects were still present.

2. The experiment was successfully simulated on Eclipse-100 Black oil simulator. All the data were matched satisfactorily. The results from the simulation indicate that:

- The critical gas saturation was not very high (3-7%)
- Gas phase relative permeability decreases with increase in depletion rate.
- The gas relative permeability in heavy oil under study was low (10^{-6} to 10^{-4}, depending upon depletion rate) for gas saturation upto 12%.
- Critical gas saturation was observed to vary linearly with depletion rate.
- A semi-log empirical model was developed to predict "Apparent Critical Supersaturation" and end point with depletion rate for the system studied.

Chapter 6

SUMMARY AND RECEOMMENDATIONS

6.1. Summary

A study on the bubble growth and gas mobility measurement in heavy oil was done. The following main findings were made from the study:

1. From the bubble growth study it was found that hydrodynamic forces do not play a major role in bubble growth at late times and diffusion forces alone may be adequate for modelling gas phase growth. It was found that a single value of coefficients 'a' and 'b', in the growth model at^b, may not be valid at all times; especially at early time. Further, the coefficients differ for infinite and no-flow boundary growth cases. The subsequent modelling of the constant volumetric rate depletion process in a closed system, showed that the nucleation of bubbles may not coincide with lowest point on the P-V graph. In all the earlier studies, it was assumed that the bubbles nucleate at the lowest point on the P-V graph. In the present study, it was found that system pressure might fall even after nucleation of bubbles. A new term "Apparent Critical Supersaturation" was defined for lowest point on the P-V graph which was formerly termed as "Critical Supersaturation"; i.e. the supersaturation at which the bubbles nucleate. Sensitivity studies explained reasons for observance of different behaviour of heavy and light oil systems.
2. The experiments, to measure the gas relative permeability in heavy oil and study the effect of depletion rate on the solution-gas drive process were conducted successfully. The results indicated that the gas phase relative permeability is much lower in heavy oil, as compared to that in light oil. The

effect of some of the other theories, postulated to explain the favourable behaviour of heavy oil reservoirs, was not found to exist in the current experiments. The gas phase relative permeability was found to decrease with increase in depletion rate. The critical gas saturation and supersaturation were observed to increase with depletion rate. Low gas phase relative permeability, was presented as one of the reasons contributing to favourable behaviour of heavy oil reservoirs.

6.2. Recommendations

The present study does not resolve all the issues related to the favourable behaviour of heavy oil reservoirs. It is just a small contribution to explain the complex phenomenon. A lot of work still needs to be done, to address all the aspects. Some of the work recommended for future, which shall compliment the present study, is as follows:

1. The capillary forces term (incorporating the effect of porous media) needs to be included in the bubble growth model. Comprehensive modelling of gas phase growth in porous media may require network modelling.
2. The effect of oil viscosity on the solution-gas drive process needs to be explored more thoroughly. The proposed study should include observing various parameters that are affected by the change in oil viscosity. The results from this proposed study along with the results from the current study will help in developing a model to predict gas phase relative permeability as a function of viscosity and depletion rate.
3. Since the formation of *"foamy oil"* is debatable under slow depletion experiments, experiments should be done with sand production, thus simulating formation of "wormholes". The existence of high pressure gradient and formation of *"foamy oil"* should be observed in such experiments. Once again, scaled experiments simulating the field operating conditions should be performed. The results from these experiments shall confirm presence of *"foamy oil"*.

4. Last but not the least, results from comprehensive studies on phenomenon such as supersaturation, nucleation, coalescence, sand-production, rheology, thermodynamics and flow need to be assimilated, to present a model to explain favourable behaviour of heavy oil reservoirs.

REFERENCES

AEUB: "Alberta's Energy Resources-1996 in Review", Alberta Energy and Utilities Board, (1997) 6-7.

HEPTER, L. G., and HIS, C., AOSTRA Technical Handbook on Oil Sands, Bitumen and Heavy Oil; AOSTRA Technical Publication Series # 6, 1989.

BAIL, P. T. and MARSDEN, S. S., Saturation Distribution in a Linear System During Oil Displacement; *Producers Monthly*, pp. 22-32, June 1957.

BATYCKY, J. P., LEAUTE, R. P., and DAWE, B. A., A mechanistic model of Cyclic Steam Stimulation, paper SPE 37550; Presented at the International Thermal Operations and Heavy Oil Symposium, Bakersfield, CA, Feb 10-12, 1997.

BENTSEN, R. G., Conditions Under which the Capillary Term may be Neglected, *Journal of Canadian Petroleum Technology*, pp. 25-30, Oct-Nov 1978, Montreal.

BORA, R., Cold Production of Heavy Oil - An Experimental Investigation of Foamy Oil Flow in Porous Media; Ph.D. Dissertation, University of Calgary, 1998.

BORA, R. and MAINI, B. B., Flow Visualisation Studies of Solution Gas Drive Process In Heavy Oil Reservoirs Using a Glass Micromodel; SPE 37519 Presented at the SPE International Thermal Operations and Heavy Oil Symposium, Bakersfield, CA, Feb. 10-12, 1997.

BOYER, R. L., MORGAN, F., and MUSKAT, M., A New Method for Measurement of Oil Saturations in Core; TP 2124 in Petroleum Technology, January 1947.

BRENNEN, C. E., *Cavitation and Bubble Dynamics*; Oxford University Press, 1995.

BUTLER, R. M., *Thermal Recovery of Oil and Bitumen;* Prentice-Hall Inc., 1991.

CARMAN, P.C., Fluid Flow Through Granular Beds. *Trans. Inst. Chem. Eng.*, Vol. 15, 150-166, 1937.

CHARDAIRE, C., Simultaneous Estimation of Relative Permeabilities and Capillary Pressures; presented at the 64th Annual Technical Conference and Exhibition of the SPE held in San Antonio, TX, October 8-11, 1989.

CIVAN, F, and DONALDSON, E. C., Relative Permeability from Unsteady-State Displacements: An Analytical Interpretation; SPE 16200, presented at the SPE Production Operations Symposium held in Oklahoma city, Oklahoma, March 8-10, 1987.

CLARIDGE, E. L. and PRATS, M., A Proposed Model and Mechanism for Anomalous Foamy Heavy Oil Behaviour; SPE 29243 Presented at the International Heavy Oil Symposium held in Calgary, AB, Canada, June 19-21, 1995.

COLES, R., "Boiling Nucleation"; *Advanced Heat Transfer*, 10, pp. 24-26, 1974.

CRAFT, B. C., and HAWKINS, M. F., *Applied Petroleum Reservoir Engineering*; Prentice Hall Inc., 19

CRUM, L., Nucleation and Stabilization of Microbubbles in Liquids; *Applied Scientific Research*, 38, pp. 101-115, 1982.

DANESH, A., PEDEN, J. M., KRINIS, D., and HENDERSON, D., Pore Level Investigation of Oil Recovery by Solution Gas Drive and Gas Injection; SPE 16956, presented at the 62 Annual Technical Conference and Exhibition, Dallas, TX, September 27-30, 1987.

DUMORE, J. M., Development of Gas-Saturation During Solution-Gas Drive in an Oil Layer Below a Gas Cap; *Society of Petroleum Engineers Journal*, pp. 211-218, September 1970.

DUSSEAULT, M., Cold Production and Enhanced Oil Recovery; *Journal of Canadian Petroleum Technology*, pp. 16-18, November 1993.

ECLIPSE 100 Reference Manual; Version 96A, *Schlumberger, GeoQuest.*

FALLS, D. H., HIRASAKI, G. J., PATZEK, T. W., GAGLITZ, D. A., MILLER, D. D. and RATULOWSKI, T., Development of a Mechanistic Foam Simulator: Population Balance and Generation by Snap-off; *SPE Reservoir Engineering*, pp 884-892, 1988.

FATT, J. and DYKSTRA, H., Relative Permeability Studies; *Trans* AIME, Vol. 192, pp. 249 - 256, 1951.

FIROOZABADI, A., and KASHCHIEV, D., Pressure and Volume Evolution During Gas Phase Formation in Solution Gas Drive Process; *Society of Petroleum Engineers Journal*, pp. 219-227, September, 1996.

FIROOZABADI, A., OTTENSEN, B., and MIKKELSEN, M., Measurements of Supersaturation and Critical Gas Saturation; *SPE Formation Evaluation*, pp. 337-344, December 1992.

GEFFEN, T. M., and GLADFELTER, R. E., A Note on the X-Ray absorption Method of Determining Fluid Saturations in Cores; *Trans* AIME, Vol. 195, pp. 322-323, 1952.

GEILIKMAN, M. B., DUSSEAULT, M. B., and DULLIEN, F. A. L., Dynamic Effects of Foamy Fluid Flow In Sand Production Instability; SPE 30251 Presented at the International Heavy Oil Symposium held in Calgary, AB, Canada, June 19-21, 1995.

GUO-QUIG, TANG., and FIROOZABADI, A., Gas and Liquid Phase Relative Permeabilities for Cold Production from Heavy Oil; SPE 56540 Presented at the SPE Annual Technical Conference and Exhibition, Houston, TX, 3-6 October 1999.

HAGOORT, J., Oil Recovery by Gravity Drainage; *Society of Petroleum Engineers Journal*, pp. 139-150, June 1980.

HANDY, L. L., A Laboratory Study of Oil Recovery by Solution Gas Drive; *Trans AIME*, Vol. 213, pp. 310-315, 1958.

HELSET, H. M., NORDTVEDT, J. E., SKJOEVELAND, S. M., and VIRNOVSKY, G. A., Relative Permeabilities from Displacement Experiments with Full Account for Capillary Pressure; *SPE Reservoir Engineering and Evaluation*, pp. 92-98, April 1998.

HEMMINGSEN, E. A., Cavitation in Gas-Saturated Solutions; *Journal of Applied Physics*, 46, 1, January 1975.

HOFFMAN, J. D., *Numerical Methods for Engineers and Scientists*; McGraw Hill Inc., 1992.

HOLM, L. W., The Mechanism of Gas and Liquid Flow Through Porous Media in Presence of Foam; *Society of Petroleum Engineers Journal*, pp. 359-369, December 1968.

HONARPOUR, M, KOEDERITZ, L., and HARVEY, A. H., *Relative Permeability of Petroleum Reservoirs*, Society of Petroleum Engineers Inc. Publication, 1994.

HOYOS, M., MOULU, J. C., DEFLANDRE, F., and LENORMAND, R., Ultrasonic Measurements of the Bubble Nucleation Rate During Depletion Experiments in a Rock Sample; SPE 20525, presented at the 65th Annual Technical Conference and Exhibition of the SPE held in New Orleans, LA, September 23-26, 1990.

HUANG, W. S., MARCUM, B. E., CHASE, M. R., and YU, C. L, Cold Production of Heavy Oil from Horizontal Wells in the Frog Lake Field; SPE 37545, Presented at the SPE International thermal Operations and heavy Oil Symposium, Bakersfield, CA, 10-12 February, 1997.

HUERTA, M., TICO, A., JIMENEZ, I., MIRABAL, M. DE., and ROJAS, G., Understanding Foamy Oil Mechanism for Heavy Oil Reservoirs During Primary Production; SPE 36749, Presented at the 1996 SPE Annual Technical Conference and Exhibition, Denver, CO, October 6-9, 1996.

HUNT, E. B., and BERRY, V. J., Evolution of Gas From Liquid Flowing Through Porous Media; *AIChE Journal*, Vol. 2, No. 4, pp. 560-567, 1956.

ISLAM, M. R. and CHAKMA, A., Mechanics of Bubble Flow in Heavy Oil Reservoirs; SPE 20070 Presented at the 60th California Regional Meeting, Ventura, CA, April 4-6, 1990.

ISLAM, M. R., and PADDOCK, J., A New Equation of State for Crude Oils with Microbubbles; 99-43, presented at the CSPG and Petroleum Society Joint Convention, Calgary, AB, June 14-18, 1999.

JOHNSON, E. F., BOSSLER, D. P., and NAUMANN, V. O., Calculation of Relative Permeability from Displacement Experiments; *Trans AIME*, Vol. 216, pp. 370-372, 1959.

JONES, S. F., EVANS, G. M., and GALVIN, K. P., Bubble Nucleation form Gas Cavities - A Review; *Advances in Colloid and Interface Science*, 80, pp. 27-50, 1999.

KALAYDJIAN, F. J. M., Dynamic Capillary Pressure Curve for Water/Oil Displacement in Porous Media: Theory Vs. Experiment; SPE 24813, presented at the 67th Annual Technical Conference and Exhibition of the SPE held in Washington, DC, October 4-7, 1992.

KAMATH, J., and BOYER, R. E., Critical Gas Saturation and Supersaturation in Low-Permeability Rocks; SPE 26663, *SPE Formation Evaluation*, pp 247-253, December 1995.

KASHCHIEV, D., and FIROOZABADI, A., Kinetics of Initial Stage of Isothermal Gas Phase Formation; *J of Chem. Phys.*, 98, 6, pp. 4690-4699, March 5, 1993.

KENNEDY, H. T., and OLSON, C. R., Bubble Formation in Supersaturated Hydrocarbon Mixtures; *Trans* AIME, Vol. 195, pp. 271-278, 1952.

KOVSCEK, A. R., and RADKE, C., Fundamentals of Foam Transport in Porous Media; chapter 3 of "Foams: Fundamental and Application in the Petroleum Industry", Schramm, L. L., Ed.; *Advances in Chemistry Series 242, American Chemical Society, Washington D.C.*, 1994.

KRAUS, W. P., McCAFFREY, W. J., and BOYD, G. W., Pseudo-Bubble Point Model for Foamy Oils; presented at the Annual Technical Conference of The Petroleum Society of CIM, Calgary, AB, May 9-12, 1993.

LABTECH, *User's Guide*, Laboratory Technologies Corporation; 1994.

LAIRD, A. D. K. and PUTNAM, J. A., Fluid Saturation in Porous Media by X-Ray Techniques; *Trans* AIME, Vol. 192, pp. 275-284, 1951.

LAIRD, A. D. K. and PUTNAM, J. A., Three Component Saturation in Porous Media by X-Ray Techniques; *Trans* AIME, Vol. 216, pp. 216-220, 1959.

LEAS, W. J., JENKS, L. H., and RUSSEL, CHARLES. D., Relative Permeability to Gas; *Trans* AIME, Vol. 189, pp. 65-72, 1950.

LEVERETT, M.C., Flow of Oil Water Mixture Through Unconsolidated Sands; *Trans* AIME, Vol. 132, 149, 1939.

LEVERETT, M.C., Capillary Behaviour in Porous Solids; *Trans* AIME, Vol. 142, 152-169, 1941.

LI, X. and YORTSOS, Y. C., Theory of Multiple Bubble Growth in Porous Media by Solute Diffusion; *Chem. Engg. Sci.*, Vol. 50, pp. 1247-1271, 1995.

LOUGHEAD, D. J. and SALTUKLAROGLU, M., Lloydminster Heavy Oil Production - Why so Unusual?; Ninth Annual Heavy Oil Sands Technology Symposium, Calgary, March 11, 1992.

MAINI, B. B., Foamy Oil Flow in Primary Production of Heavy Oil under Solution Gas Drive; SPE 56541, presented at the SPE Annual Technical Conference and Exhibition, Houston, TX, 3-6 October, 1999.

MAINI, B. B., Laboratory Evaluation of Solution Gas Drive Recovery Factors in Foamy Heavy Oil Reservoirs; presented at the CSPG and Petroleum Society Joint Convention, Calgary, AB, 14-18 June, 1999.

MAINI, B. B., Foamy Oil Flow in Heavy Oil Production; *Journal of Canadian Petroleum Technology*, pp. 21-24, June 1996.

MAINI, B. B., Is it Futile to Measure Relative Permeability for Heavy Oil Reservoirs; Presented at the 46th Annual Technical Meeting of the Petroleum Society of CIM, Banff, AB, Canada, May 14-17, 1995.

MAINI, B. B., SARMA, H. K., and GEORGE, A. E., Significance of Foamy-oil Behaviour in Primary Production of Heavy Oils; *Journal of Canadian Petroleum Technology*, pp. 50-54, November 1993.

McCABE, SMITH and HARRIOT; *Unit Operations in Chemical Engineering*; McGraw Hill Publication, 1990.

METWALLY, M. and SOLANKI, S. C., Heavy Oil Reservoir Mechanisms, Lindbergh and Frog Lake Fields, Alberta Part I: Field Observations and Reservoir Simulation; presented at the 46th Annual Technical Meeting of the Petroleum Society of CIM, Banff, AB, Canada, May 14-17, 1995.

MIRABAL, M. DE., RODRIGUEZ, H., and GORDILLO, R., Impact of Foamy Oil Mechanism on the Hamaca Oil Reserves, Orinoco Belt - Venezuela; SPE 36140, Presented at the Fourth Latin American and Caribbean Petroleum Engineering Conference, Port of Spain, Trinidad and Tobago, 23-26 April 1996.

MIRABAL, M. DE., RODRIGUEZ, H., and GORDILLO, R., Production Improvement Strategy for Foamy Hamaca Crude Oil; SPE 37544, Presented at

the SPE International Thermal Operations and Heavy Oil Symposium, Bakersfield, CA, 10-12 February, 1997.

MORGAN, F., McDOWELL, J. M., and DOTY, E. C., Improvements in the X-Ray Saturation Techniques of Studying Fluid Flow, *Trans* AIME, Vol. 189, pp. 183-194, 1950.

MOULU, J. C., Solution-Gas Drive: Experiments and Simulation; *Journal of Petroleum Science and Engineering*, 2, pp. 379-386, 1989.

MUSKAT, M., *Physical Principles of Oil Production*, McGraw-Hill Book Co., N.Y., 1949.

OAK, M. J., BAKER, L. E. and THOMAS, D. C., Three Phase Relative Permeability of Berea Sandstone; *Journal of Petroleum Technology*, pp. 1054-1061, August 1990.

OAK, M. J. and EHRLICH, R., A New X-Ray Absorption Method for Measurement of Three Phase Relative Permeability; *SPE Reservoir Engineering*, pp. 199-206, February 1998.

ODEH, A. S., Effect of Viscosity Ratio on Relative Permeability; *Trans* AIME, Vol. 216, pp. 346-353, 1959.

OSOBA, J. S., RICHARDSON, J. G., KERVER, J. K., HAFFORD, J. A., and BLAIR, P. M., Lab Measurement of Relative Permeability; *Trans* AIME, Vol. 192, pp. 47-56, 1951.

PARSONS, R. W., Microwave Attenuation - A New Tool for Monitoring Saturations in Laboratory Flooding Experiments; *Society of Petroleum Engineers Journal*, pp. 302-310, August 1975.

PATEL, R. D., Bubble Growth in Viscous Newtonian Liquid; *Chem. Engg. Sci.*, Vol. 35, pp. 2352-2356, 1980.

POOLADI-DARVISH, M. and FIROOZABADI, A., Solution Gas Drive in Heavy Oil Reservoirs; *Journal of Canadian Petroleum Technology*, pp. 54-61,April 1999.

POON, D., and KISMAN, K., Non-Newtonian Effects on the Primary Production of Heavy Oil Reservoirs; *Journal of Canadian Petroleum Technology*, pp. 55-59, September 1992.

RAMEY, H. J., Rapid Methods for Estimating Reservoir Compressibilities; *Journal of Petroleum Technology*, pp. 447-454, April 1964.

RAPOPORT, L. A., and LEAS, W. J., Relative Permeability to Liquid in Liquid Gas Systems; *Trans* AIME, Vol. 192, pp. 83 - 98, 1951.

RICHARDSON, J. G., KERVER, J. K., HAFFORD, J. A., and OSABA, J. S., Laboratory Determination of Relative Permeability; *Trans* AIME, Vol. 195, pp. 187-196, 1952.

ROSE, W., Theoretical Generalizations Leading to the Evaluation of Relative Permeability; *Trans.* AIME, pp. 111-126, 1949.

ROSNER, D. E. and EPSTEIN, M., Effect of Interface Kinetics, Capillarity and Solute Diffusion on Bubble Growth Rates in Highly Supersaturated Liquids; *Chem. Engg. Sci.*, Vol. 27, pp. 69-88, 1972.

SARMA, H. K., and BENTSEN, R. G., A New Method for Estimating Relative Permeabilities from Unstabilised Displacement Data; *Journal of Canadian Petroleum Technology*, Vol. 28, No. 4, pp. 118-128, July-Aug 1989.

SARMA, H. K., and BENTSEN, R. G., Further Experimental Validation of the External-Drive Technique; *Journal of Canadian Petroleum Technology*, Vol. 29, No. 4, pp. 75-83, July-Aug 1990.

SARMA, H., and MAINI, B., Role of Solution Gas in Primary Production of Heavy Oils; SPE 23631, presented at the Second Latin American Petroleum Engineering Conference, Caracas, Venezuela, March 8-11, 1992.

SCRIVEN, L. E., On the Dynamics of Phase Growth; *Chem. Engg. Sci.*, Vol. 10, pp. 1-13, 1959.

SHEN, C. and BATYCKY, J., Some Observations of Mobility Enhancement of Heavy Oils Flowing Through Sand Pack Under Solution Gas Drive; *Journal of Canadian Petroleum Technology*, pp. 46-53, April 1999.

SHENG, J. J., MAINI, B. B., HAYES, R. E., and TORTIKE, W. S., Experimental Study of Foamy Oil Stability; *Journal of Canadian Petroleum Technology*, pp. 31-37, April 1997.

SHENG, J. J., HAYES, R. E., MAINI, B. B., and TORTIKE, W. S., Modelling Foamy Oil Flow in porous Media; *Transport in Porous Media*, 35, pp. 227-258, 1999.

SHENG, J. J., HAYES, R. E., MAINI, B. B., and TORTIKE, W. S , A Non Equilibrium Model to Calculate Foamy Oil Properties; *Journal of Canadian Petroleum Technology*, pp. 38-45, April 1999.

SMITH, G. E., Fluid Flow and Sand Production in Heavy Oil Reservoirs Under Solution Gas Drive; SPE 15094, *SPE Production Engineering*, pp 169-179, May 1988.

STEWART, C. R., CRAIG, F. F. Jr., and MORSE, R. A., Determination of Limestone Performance Characteristic by Model Flow Tests; *Trans AIME,* Vol. 198, pp. 93-102, 1953.

STEWART, C. R., HUNT, E. B., SCHNEIDER, F. N., GEFFEN, T. M., and BERRY, V. J., The Role of Bubble Formation in Oil Recovery by Solution Gas Drives in Limestones; *Trans AIME,* Vol. 201, pp. 294, 1954.

SZEKELY, J. and MARTINS, G. P., Non Equilibrium Effects in the Growth of Spherical Gas Bubbles due to Solute Diffusion; *Chem. Engg. Sci.,* Vol. 26, pp. 147-159, 1971.

SZEKELY, J. and FANG, S. D., Non Equilibrium Effects in the Growth of Spherical Gas Bubbles due to Solute Diffusion - II; *Chem. Engg. Sci.,* Vol. 28, pp. 2127-2140, 1973.

TAXLER, R.N., and BAUM; L.A.H., Permeability of Compacted Powder - Determination of Average Pore size. *Physics,* 7, pp. 9 - 14, 1936.

TREMBLAY, B., SEDGWIK, G.and VU, D., CT Imaging of Sand Production in a Horizontal Sand Pack Using Live Oil; Presented at the 49th Annual Technical Meeting of The Petroleum Society in Calgary, AB, Canada, June 8-10, 1998.

TREINEN, R. J., RING, W. W., SPENCE, A. P., MIRABAL, M. DE. and HUERTA, M., Hamaca: Solution Gas Drive Recovery in Heavy Oil Reservoir, Experimental Results; SPE 39031, Presented at the Fifth Latin American and Caribbean Petroleum Engineering Conference and Exhibition, Rio de Janeiro, Brazil, August 30-September 3, 1997.

WALL, C. G., and KHURANA, A. K., The Effects of Rate of Pressure Decline and Liquid Viscosity on Low-Pressure Gas Saturations in Porous Media; *Journal of the Institute of Petroleum*, pp. 335-345, November 1972.

WARD, C. A., TIKUISIS, P., and VENTER, R. D., Stability of Bubbles in Closed Volume of Liquid-gas Solution; *Journal of Applied Physics*, 53(9), pp. 6076-6084, September 1982.

WARD, C. A., and LEVART, E., Conditions for Stability of Bubble Nuclei in Solid Surface Contacting a liquid-gas Solution; *Journal of Applied Physics*, 56(2), pp. 491-500, July 1984.

WATSON, A. T., RICHMOND, P. C., KERIG, P. D., and TAO, T. M., A Regression-Based Method for Estimating Relative Permeabilities From Displacement Experiments; *SPE Reservoir Engineering*, pp. 953-958, August 1988.

WILT, P. M., Nucleation Rates and Bubble Stability in Water-Carbon Dioxide Solutions; *Journal of Colloid and Interface Science*, 112, 2, August 1986.

WONG, R. C. K., GUO, F., WEAVER, J. S., and BARR, W. E., Heavy Oil Flow Under Solution-gas Drive: Pressure Depletion Tests; *Journal of Canadian Petroleum Technology*, pp. 31-37, April 1999.

YOUSFI, A. El., ZARCONE, C., BORIES, S., and LENORMAND, R., Physical Mechanisms for Bubble Growth during Solution Gas Drive; SPE 38921, presented at the Annual Technical Conference and Exhibition, San Antonio, TX, October 5-8, 1997.

ZHANG, Y., Temperature Effects on Foamy Solution-Gas Drive; M. Sc. Thesis, University of Calgary, 1999.

APPENDIX – I

SOLUTION FOR BUBBLE GROWTH

AI.1. Formulation of the Problem

Consider a stationary spherical gas bubble in a quiescent supersaturated liquid. It grows due to the transfer of a dilute component from the supersaturated liquid to the gas (vapour) inside the bubble. The density and viscosity of the liquid is assumed to be constant and the system isothermal. It is assumed that thermodynamic equilibrium exists at the gas-liquid interface.

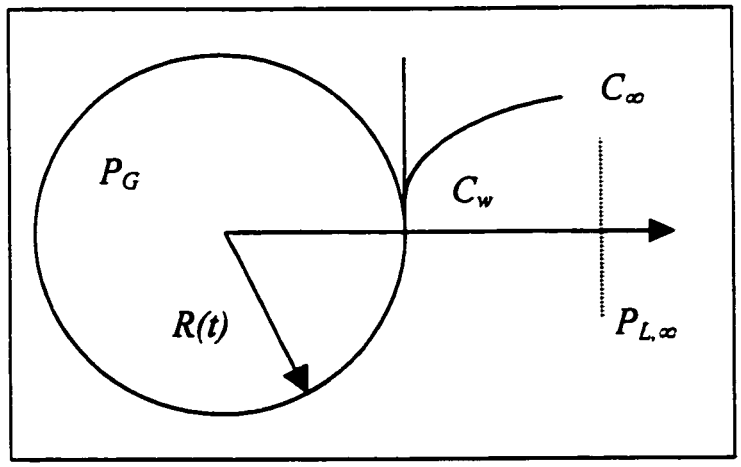

Figure A1: Schematic representation of the bubble growth system (Modified from Szekely and Fang (1973))

By using these assumptions, the equations of continuity and motion may be combined in spherical co-ordinate system to obtain the following equation for bubble growth [Brennen (1995)] (see Figure A1).

$$R\frac{d^2R}{dt^2}+\frac{3}{2}\left(\frac{dR}{dt}\right)^2=\frac{1}{\rho_L}\left[P_{L,R}-P_{L,\infty}\right] \qquad \text{(I-1)}$$

where, R is the bubble radius.

$P_{L,R}$ is related to $P_{G,R}$ through the continuity of the normal stress on the surface of the bubble. This relationship is expressed as [Brennen (1995)]

$$P_{L,R} = P_{G,R} - \frac{2\sigma}{R} - \frac{4\mu}{R}\frac{dR}{dt} \tag{I-2}$$

In Equation (I-2), the difference in pressure in the bubble and at its surface is the driving force for growth and has to overcome the viscous momentum transfer and the work done by surface tension forces. The above two equations can be combined to give:

$$R\frac{d^2R}{dt^2} + \frac{3}{2}\left(\frac{dR}{dt}\right)^2 = \frac{1}{\rho_L}\left[P_{G,R} - \frac{2\sigma}{R} - 4\mu\frac{(dR/dt)}{R} - P_{L,R}\right] \tag{I-3}$$

For transfer of the solute from the liquid phase to the gas phase by diffusion a mass conservation equation can be written in spherical co-ordinates [Brennen (1995)] as:

$$\frac{\partial C}{\partial t} = D\left[\frac{\partial^2 C}{\partial r^2} + \frac{2}{r}\frac{\partial C}{\partial r}\right] - \left(\frac{R}{r}\right)^2 \frac{dR}{dt}\frac{\partial C}{\partial r}, \quad r > R \tag{I-4}$$

where the above equation utilises the fact that:

$$u_r|_{r=R} \equiv \frac{dR}{dt} \quad \text{and} \quad u_r r^2 \equiv R^2 \frac{dR}{dt} \tag{I-5}$$

Next the initial and the boundary conditions are written. For initial conditions specifying an initial bubble size (R_0), zero initial growth rate, and uniform solute distribution in the liquid we can write:

$$R = R_0, \quad t = 0 \tag{I-6}$$

$$\frac{dR}{dt} = 0, \quad t = 0, \tag{I-7}$$

$$C = C_0, \quad t = 0, \quad r \geq R \tag{I-8}$$

We assume bubble to be already nucleated and in thermodynamic and physical equilibrium with the surrounding liquid, so an initial zero growth rate is valid. Regarding the boundary conditions for the infinite case, we consider concentration of solute far from the bubble remains constant:

$$C = C_0 \ at \quad r \to \infty \quad \text{at all times} \tag{I-9}$$

For the case of finite domain

$$\frac{\partial C}{\partial r} = 0 \quad \textit{at outer boundary} \tag{I-10}$$

During the growth of the bubble, the pressure within the bubble and hence gas density changes. The equation of continuity at the bubble surface can be expressed as:

$$4\pi R^2 D \frac{\partial C}{\partial r} = \frac{d(\rho_G \frac{4}{3}\pi R^3)}{dt}; \quad r = R$$

which relates the mass flux at the surface to rate of increase in diameter. This simplifies to the following form:

$$3DR^2 \frac{\partial C}{\partial r} = \frac{d(\rho_G R^3)}{dt}; \quad r = R \tag{I-11}$$

Finally, the statement of thermodynamic equilibrium relationship at the bubble surface is represented as:

$$P_G = f(C), \quad r = R \tag{I-12}$$

which states that the pressure within the bubble is some function of the concentration of the solute in the liquid at the interface. We use Henry's law for thermodynamic equilibrium relationship, which is a good model for heavy oil-gas mixtures.

It can be observed that the equation of motion (I-3) and the diffusion equation (I-4) are mutually coupled through the boundary conditions contained in equations (I-10) and (I-12) for regimes where both the forces dominate. It is expected that the solutions to equations I-3 and I-4 with their initial and boundary conditions for growth rate will give asymptotic solutions when the process is controlled either by hydrodynamic forces or by diffusion [Szekely and Martins (1971), Szekely and Fang (1973)].

AI.2. Dimensionless Formulation

To solve the problem, the governing equations were put in a dimensionless form and then integrated in co-ordinate system moving with gas-

oil interface through the use of finite difference method. The dimensionless parameters used are defined in Table 4-1.

Application of dimensionless number into the model equations is given below. Defining the derivatives of dimensionless parameters for incorporation into equations results in:

$$\frac{dt}{d\tau} = \frac{R_0^2}{D} \tag{I-13}$$

$$\frac{dR}{d\xi} = R_0 \tag{I-14}$$

$$\frac{dP_G}{d\Pi} = P_0 \tag{I-15}$$

$$\frac{\partial C}{\partial C^*} = C_0 \tag{I-16}$$

$$\frac{\partial r}{\partial \eta} = R_0 \tag{I-17}$$

AI.2.1. Hydrodynamic Growth Model

In the process of conversion to dimensionless form, the hydrodynamic equation (I-3) can be written as:

$$\frac{R}{R_0} R_0 \left[\frac{d}{d\tau}\left(\frac{d\xi}{d\tau}\frac{d\tau}{dt}\frac{dR}{d\xi} \right)\frac{d\tau}{dt} \right] + \frac{3}{2}\left[\frac{d\xi}{d\tau}\frac{d\tau}{dt}\frac{dR}{d\xi} \right]^2 =$$

$$\frac{1}{\rho_L}\left[\frac{P_0}{P_G}\frac{P_G}{P_0} - \frac{2\sigma}{R_0 P_0}\frac{P_0 R_0}{R_0 \xi} \right] - 4\frac{\mu}{\rho_L D}\frac{\rho_L D}{R_0 \xi}\frac{d\xi}{d\tau}\frac{d\tau}{dt}\frac{dR}{d\xi} - P_{L,\infty}$$

Substituting the dimensionless parameters from Table 4.1, derivatives values from equations I-13 to I-17 and simplifying we get above the equation in the following form:

$$\xi\frac{d^2\xi}{d\tau^2} + \frac{3}{2}\frac{D^2}{R_0^2}\left(\frac{d\xi}{d\tau}\right)^2 = \frac{1}{\rho_L}\left[P_0\left(\Pi - \frac{\phi}{\xi} \right) - 4Sc\frac{\rho_L D^2}{\xi R_0^2}\frac{d\xi}{d\tau} - P_{L,\infty} \right]$$

this further can be simplified to

$$\xi\frac{d^2\xi}{d\tau^2}+\frac{3}{2}\left(\frac{d\xi}{d\tau}\right)^2+\frac{4Sc}{\xi}\frac{d\xi}{d\tau}=G\left[\Pi-\frac{\phi}{\xi}\right]-\frac{G}{P_o}\left[P_{L,\infty}\right] \qquad \text{(I-18)}$$

Since, equation I-18 is a non-linear equation it needs to be linearised before being solved by finite difference method. Newton's linearisation method is used for this purpose.

AI.2.2. Diffusion Growth Model

Since bubble growth is a moving boundary problem, a new set of co-ordinates are defined that move with the bubble boundary. The new co-ordinate is defined in Table - 4.1 and is represented by η.

Below we define dimensionless terms, that are affected by moving boundary, for diffusion equation:

$$\left(\frac{\partial C}{\partial t}\right)_r=\frac{\partial C}{\partial \eta}\frac{\partial \eta}{\partial t}+\left(\frac{\partial C}{\partial t}\right)_\eta=\frac{\partial C}{\partial C^*}\frac{\partial C^*}{\partial \eta}\left(-\frac{\partial \xi}{\partial t}\right)+\frac{\partial C^*}{\partial \tau}\frac{\partial \tau}{\partial t}\frac{\partial C}{\partial C^*}$$

Substituting value of derivatives from equation I-13 to I-17, the above equation simplifies to,

$$\frac{\partial C}{\partial t}=-C_0\frac{D}{R_0^2}\left(\frac{\partial C^*}{\partial \eta}\right)\left(\frac{d\xi}{d\tau}\right)+C_0\frac{D}{R_0^2}\left(\frac{\partial C^*}{\partial \tau}\right) \qquad \text{(I-19)}$$

By substituting equation I-19 and other dimensionless parameters into equation I-4, we get the following form of diffusion equation,

$$-C_0\frac{D}{R_0^2}\left(\frac{\partial C^*}{\partial \eta}\right)\left(\frac{d\xi}{d\tau}\right)+C_0\frac{D}{R_0^2}\left(\frac{\partial C^*}{\partial \tau}\right)+\left[\frac{R_0\xi}{(\eta+\xi)R_0}\right]^2\left(\frac{d\xi}{d\tau}\frac{dR}{d\xi}\frac{d\tau}{dt}\right)\left(\frac{\partial C^*}{\partial \eta}\frac{\partial C}{\partial C^*}\frac{\partial \eta}{\partial r}\right)=$$

$$D\left[\frac{\partial}{\partial \eta}\left(\frac{\partial C^*}{\partial \eta}\frac{\partial \eta}{\partial r}\frac{\partial C}{\partial C^*}\right)\frac{\partial \eta}{\partial r}+\frac{2}{R_0(\eta+\xi)}\frac{\partial C^*}{\partial \eta}\frac{\partial \eta}{\partial r}\frac{\partial C}{\partial C^*}\right]$$

which simplifies to,

$$\frac{\partial C^*}{\partial \tau}=\frac{\partial^2 C^*}{\partial \eta^2}+\frac{d\xi}{d\tau}\left[1-\frac{1}{(1+\eta/\xi)^2}\right]\frac{\partial C^*}{\partial \eta}+\frac{2}{\xi(1+\eta/\xi)}\frac{\partial C^*}{\partial \eta} \qquad \text{(I-20)}$$

AI.2.3. Equilibrium at the interface

Henry's law is used to express equilibrium condition at the interface. This is represented as:

$$P_G = KC_w \tag{I-21}$$

Where, P_G is the pressure inside the bubble, C_w is the interface solute concentration and K is the Henry's constant. Writing the above correlation for initial condition:

$$P_0 = KC_0 \tag{I-22}$$

Dividing equation I-21 by I-22 we have the following expression

$$\frac{P_G}{P_0} = \frac{C_w}{C_0} \quad \text{or} \quad \Pi = C_w^* \tag{I-23}$$

This is substituted in equation I-18 to eliminate Π from the equation. C_w^*, is the concentration at the interface and is also expressed as C_1^*.

AI.2.4. Initial and Boundary Conditions

(i) For hydrodynamic growth model

The initial conditions, I-6 and I-7, can be written in dimensionless form as,

$$\xi = 1 \quad at \quad \tau = 0 \tag{I-24}$$

$$\frac{d\xi}{d\tau} = 0 \quad at \quad \tau = 0 \tag{I-25}$$

The hydrodynamic model is solved with the above initial condition to arrive at the bubble growth solution limited by hydrodynamic forces only.

(ii) For diffusion growth model

The initial and boundary conditions (I-8 and I-9) in dimensionless form can be written as,

$$C^*(0,\eta) = 1 \tag{I-26}$$

$$C^*(\tau,\infty)=1 \qquad \text{(I-27)}$$

For diffusional growth model it is assumed that there is no pressure driving force (or $P_{L,\infty}$ equals pressure in the bubble, P_G). So,

$$C_w=\frac{P_{L,\infty}}{K} \quad \text{or} \quad C_w^*=\frac{P_{L,\infty}}{KC_0} \qquad \text{(I-28)}$$

The above boundary conditions are solved with the initial condition I-24 and I-25 to arrive at the solution. The above formulation is valid for infinite domain. For finite domain the boundary condition I-27 changes. The formulation for finite domain is given later.

(iii) For general growth model

The mass flux at the boundary is represented by equation I-11. The gas density is not assumed to be constant and changes with the change in pressure. Equation I-11 can be expanded as follows:

$$\rho_G 3R^2\frac{dR}{dt}+R^3\frac{d\rho_G}{dt}=3DR^2\left(\frac{\partial C}{\partial r}\right)_{r=R}$$

The ideal gas law is assumed. Thus, $\rho_G=\frac{MP_G}{\gamma T}$

Where, M is the molecular mass, γ is the gas constant and T is the temperature. Converting the above equation into dimensionless form by applying dimensionless parameters, the equation can be written as:

$$\frac{MP_o\Pi}{\gamma T}\frac{d\xi}{d\tau}\frac{d\tau}{dt}\frac{dR}{d\xi}+\frac{R_o\xi}{3}\frac{M}{\gamma T}\frac{d\Pi}{d\tau}\frac{dP_G}{d\Pi}\frac{d\tau}{dt}=D\left(\frac{\partial C^*}{\partial\eta}\frac{\partial\eta}{\partial r}\frac{\partial C}{\partial C^*}\right)_{\eta=0}$$

Simplifying the above equation and substituting

$$\rho_{G,0}=\frac{MP_0}{\gamma T}$$

in the equation, we end up with the following form of above equation,

$$\left(\frac{\partial C^*}{\partial\eta}\right)_{\eta=0}=\frac{\rho_{G,0}}{C_0}\left(\Pi\frac{d\xi}{d\tau}+\frac{\xi}{3}\frac{d\Pi}{d\tau}\right) \text{ or,}$$

$$\left(\frac{\partial C^*}{\partial \eta}\right)_{\eta=0} = Ja\left(\Pi\frac{d\xi}{d\tau} + \frac{\xi}{3}\frac{d\Pi}{d\tau}\right) \qquad \text{(I-29)}$$

In the general growth model, the hydrodynamic (I-18) and diffusion (I-20) equation are solved along with initial condition I-24 to I-26, boundary condition I-27 or I-30 (as the case may be), I-29 and equilibrium assumption (I-23).

(iv) For finite domain

The infinite source of solute condition (boundary condition I-27) is no more valid. Instead, the boundary condition equation I-10 is applied at the far boundary, that can be written in dimensionless form as:

$$\left(\frac{\partial C^*}{\partial \eta}\right)_{\eta = far\ boundary} = 0 \qquad \text{(I-30)}$$

This reflects that there is zero influx of solute at the far boundary. The far boundary is fixed and stationary, whereas the bubble interface is moving outwards. This results in shrinkage of space between bubble interface and fixed outer boundary. This can be viewed as inward movement of the far boundary, as the bubble grows. This during simulation, translates into renewal of number of grid blocks at each time step.

AI.2.5. Constant rate of pressure drop

A function is defined for pressure variation in the field with respect to time, which is expressed as:

$$P_{L,\infty} = P_0 - ct \qquad \text{(I-31)}$$

Where, c is the rate of pressure drop. The above equation implies that pressure is dropping at a constant rate in the system. This is substituted in equation I-18 for $P_{L,\infty}$ to get the solution.

AI.2.6. Solution gas drive model

Since a direct relation of pressure with time is not available for constant volumetric rate depletion, the following additional equation is solved along with the above equations for solution:

$$\kappa_o = -\frac{1}{V}\frac{\partial V}{\partial P}$$

Where, κ_o is the compressibility of oil. This is the compressibility equation, that relates volume depleted to the pressure in the system. This in difference form results in

$$P_f = P_l - \frac{(V_f - V_l)}{\kappa_o V_l} \tag{I-32}$$

Where, the subscript f denotes the resultant value and l, the value at previous time step. V_f is given by

$$V_f = V_p - \left(\frac{4}{3}\pi(\xi R_0)^3\right)B_{no} \tag{I-33}$$

Where, B_{no} and V_p are number of bubbles and pore volume respectively. The equation implies that final volume oil volume is equal to pore volume minus the volume of gas phase. Substituting equation I-33 into I-32 results in

$$P_f = P_l - \frac{\left(V_p - \left(\frac{4}{3}\pi(\xi R_0)^3\right)B_{no}\right) - V_l}{\kappa_o V_l} \tag{I-34}$$

The value of P_f is equivalent to $P_{L,\infty}$ in equation I-18. Equation I-34 defines pressure in terms of radius of bubble and fluid withdrawn (known value). Substituting this expression in equation I-18 eliminates $P_{L,\infty}$ and gives equation I-18 in terms of ξ.

$$\xi\frac{d^2\xi}{d\tau^2}+\frac{3}{2}\left(\frac{d\xi}{d\tau}\right)^2+\frac{4Sc}{\xi}\frac{d\xi}{d\tau}=G\left[\Pi-\frac{\phi}{\xi}\right]-\frac{G}{P_o}\left[P_l-\frac{\left(V_p-\left(\frac{4}{3}\pi(\xi R_0)^3\right)B_{no}\right)-V_l}{\kappa_o V_l}\right] \quad \text{(I-35)}$$

Equation I-35 is solved with equations I-20, boundary conditions I-23, I-29, I-30 or I-27, and initial conditions I-24, I-25, I-26 to obtain the solution for constant volumetric rate depletion problem.

For constant pressure drop probelm, equation I-31 is substituted for $P_{L,\infty}$ and the problem is solved similarly.

AI.3. Numerical Solution

For solution of the bubble growth problem, all the equations were put in finite difference form and solved numerically. Since the hydrodynamic and the diffusional growth model equations are non-linear, they were linearised before obtaining finite difference form.

Newton's method [Hoffman, (1992)] was used for linearisation. This involves guessing the value of the solution and substituting into the equation. The solution is assumed to be represented as,

$$\xi^n=\xi_e^n+\delta^n \quad \text{(I-36)}$$

$$C_i^{*,n}=C_{e,i}^{*,n}+\alpha_i^n \quad \text{(I-37)}$$

where subscript e denotes the estimated (guessed) value of the solution, and i, the position in space. Superscript n is the time step number, in the solution process. δ and α are the errors in the guess value of the solution. The errors are assumed to be very small. While linearising any second order term of error is neglected in the equation, and hence we obtain a linearised equation for solution. So now, since the solution is guessed, the linear equation is solved for the errors instead of unknowns. The solution for unknowns is arrived at, by substituting errors into equation I-36 and I-37.

The following equations for derivatives can be obtained from above equations

$$\frac{d\xi^n}{d\tau} = \frac{d\xi_e^n}{d\tau} + \frac{d\delta^n}{d\tau} \tag{I-38}$$

$$\frac{d^2\xi^n}{d\tau^2} = \frac{d^2\xi_e^n}{d\tau^2} + \frac{d^2\delta^n}{d\tau^2} \tag{I-39}$$

$$\frac{\partial C_i^{*,n}}{\partial\tau} = \frac{\partial C_{e,i}^{*,n}}{\partial\tau} + \frac{\partial\alpha_i^n}{\partial\tau} \tag{I-40}$$

$$\frac{\partial C_i^{*,n}}{\partial\eta} = \frac{\partial C_{e,i}^{*,n}}{\partial\eta} + \frac{\partial\alpha_i^n}{\partial\eta} \tag{I-41}$$

$$\frac{\partial^2 C_i^{*,n}}{\partial\eta^2} = \frac{\partial^2 C_{e,i}^{*,n}}{\partial\eta^2} + \frac{\partial^2\alpha_i^n}{\partial\eta^2} \tag{I-42}$$

AI.3.1. Finite Difference form of Dimensionless Equations

All the dimensionless equations are put in finite difference form, to obtain a set of linear algebraic equations that are then put into a matrix and solved simultaneously at a particular time step. An LU decomposition method is used to solve the equation. An implicit method is used while writing the equation in finite difference form, thus eliminating stability problem in the solution.

Backward Time Centred Space (BTCS) method is used while discretising the equations. The finite difference form of the derivatives of δ, α, ξ_e^n and $C_{e,i}^{*,n}$ is as follows:

$$\frac{d\delta^n}{d\tau} = \frac{\delta^n - \delta^{n-1}}{\Delta\tau}$$

$$\frac{d^2\delta^n}{d\tau^2} = \frac{\delta^n - 2\delta^{n-1} + \delta^{n-2}}{\Delta\tau^2}$$

Since the solution at previous time is known, the errors for previous time steps are assumed to be zero. So the above equations can be written as

$$\frac{d\delta^n}{d\tau} = \frac{\delta^n}{\Delta\tau} \tag{I-43}$$

$$\frac{d^2\delta^n}{d\tau^2} = \frac{\delta^n}{\Delta\tau^2} \tag{I-44}$$

Similarly,

$$\frac{\partial\alpha_i^n}{\partial\tau} = \frac{\alpha_i^n}{\Delta\tau} \tag{I-45}$$

for derivative of the space co-ordinate

$$\frac{\partial\alpha_i^n}{\partial\eta} = \frac{\alpha_{i+1}^n + \alpha_{i-1}^n}{2\Delta\eta} \quad \text{and} \tag{I-46}$$

$$\frac{\partial^2\alpha_i^n}{\partial\eta^2} = \frac{\alpha_{i+1}^n - 2\alpha_i^n + \alpha_{i-1}^n}{\Delta\eta^2} \tag{I-47}$$

Similarly, the guessed (known) quantities are put into finite difference form as follows:

$$\frac{d\xi_e^n}{d\tau} = \frac{\xi_e^n - \xi_e^{n-1}}{\Delta\tau} \tag{I-48}$$

$$\frac{d^2\xi_e^n}{d\tau^2} = \frac{\xi_e^n - 2\xi_e^{n-1} + \xi_e^{n-2}}{\Delta\tau^2} \tag{I-49}$$

$$\frac{\partial C_{e,i}^{*,n}}{\partial\tau} = \frac{C_{e,i}^{*,n} - C_{e,i}^{*,n-1}}{\Delta\tau} \tag{I-50}$$

$$\frac{\partial C_{e,i}^{*,n}}{\partial\eta} = \frac{C_{e,i+1}^{*,n} - C_{e,i-1}^{*,n}}{2\Delta\eta} \tag{I-51}$$

$$\frac{\partial^2 C_{e,i}^{*,n}}{\partial\eta^2} = \frac{C_{e,i+1}^{*,n} - 2C_{e,i}^{*,n} + C_{e,i-1}^{*,n}}{\Delta\eta^2} \tag{I-52}$$

AI.3.1.1. Hydrodynamic growth equation

For Solution Gas Drive Model

Equations I-36 to I-39 are substituted into I-35. The higher order terms of δ are neglected to make the final equation linear with respect to the errors.

Finally, the finite difference approximation equations I-43 and I-44 are substituted into the equation to get the following form:

$$\left[\frac{d^2\xi_e^n}{d\tau^2}+\frac{\xi_e^n}{\Delta\tau^2}+\frac{3}{\Delta\tau}\frac{d\xi_e^n}{d\tau}+\frac{4Sc}{\xi_e^n\Delta\tau}-\frac{4Sc}{(\xi_e^n)^2}\frac{d\xi_e^n}{d\tau}-\frac{G\phi}{(\xi_e^n)^2}+\frac{4G\pi(\xi_e^n)^2R_0^3B_{no}}{P_0\kappa_oV_l}\right]\delta^n-G\alpha_1^n$$

$$=-\xi_e^n\frac{d^2\xi_e^n}{d\tau^2}-\frac{3}{2}\left(\frac{d\xi_e^n}{d\tau}\right)^2-\frac{4Sc}{\xi_e^n}\frac{d\xi_e^n}{d\tau}+G\left[C_{e,1}^{*,n}-\frac{\phi}{\xi_e^n}-\frac{P_l}{P_0}+\left(\frac{V_p-V_l}{P_0\kappa_oV}\right)-\frac{4\pi(\xi_e^nR_0)^3B_{no}}{3P_0\kappa_oV_l}\right] \quad \text{(I-53)}$$

The terms in parenthesis on the LHS and all the terms on RHS are known values. The derivative values are calculated from equations I-48 and I-49 at each time step. The known values in the above equation I-53, can be represented by constants resulting in linear form of equation I-51, written as:

$$a_1^n\delta^n-G\alpha_1^n=b_1^n \quad \text{(I-54)}$$

As mentioned previously, for constant pressure decline model, equation I-31 is substituted into equation I-18 and a similar procedure as stated above is followed to get the finite difference form. The values of the constants change but the form of the linear equation is the same as I-54.

AI.3.1.2. Diffusive growth equation

Equations I-36 to I-38, and I-40 to I-42 are substituted into equation I-20 and the higher order terms of δ and α are neglected to obtain the linear form of diffusion equation. Further the finite difference approximation from equation I-43, I-45 to I-48, I-50 to I-52 are applied to get the following simplified form of diffusion equation.

$$\left[-\frac{1}{\Delta\eta^2}+\frac{a_{11,i}^n}{2\Delta\eta}\right]\alpha_{i-1}^n+\left[\frac{2}{\Delta\eta^2}+a_{10,i}^n\right]\alpha_i^n+\left[-\frac{1}{\Delta\eta^2}-\frac{a_{11,i}^n}{2\Delta\eta}\right]\alpha_{i+1}^n-a_{12,i}^n=a_{13,i}^n \quad \text{(I-55)}$$

where,

$$a_{13,i}^n=\frac{\partial^2C_{e,i}^{*,n}}{\partial\eta^2}-\frac{\partial C_{e,i}^{*,n}}{\partial\tau}+a_{8,i}^n\frac{\partial C_{e,i}^{*,n}}{\partial\eta}+(1-a_{6,i}^n)\frac{d\xi_e^n}{d\tau}\frac{\partial C_{e,i}^{*,n}}{\partial\eta}$$

$$a_{12,i}^{n} = \frac{\left(1-a_{6,i}^{n}\right)}{\Delta\tau}\frac{\partial C_{e,i}^{*,n}}{\partial\eta} - a_{7,i}^{n}\frac{d\xi_e^n}{d\tau}\frac{\partial C_{e,i}^{*,n}}{\partial\eta} - a_{9,i}^{n}\frac{\partial C_{e,i}^{*,n}}{\partial\eta}$$

$$a_{11,i}^{n} = \left(1-a_{6,i}^{n}\right)\frac{d\xi_e^n}{d\tau} + a_{8,i}^{n}$$

$$a_{10} = \frac{1}{\Delta\tau}$$

$$a_{9,i}^{n} = \frac{2}{\left(\xi_e^n\right)^2\left(1+\eta/\xi_e^n\right)^2}$$

$$a_{8,i}^{n} = \frac{2}{\left(\xi_e^n\right)\left(1+\eta/\xi_e^n\right)}$$

$$a_{7,i}^{n} = \frac{2\eta}{\xi_e^n\left(\eta+\xi_e^n\right)\left(1+\eta/\xi_e^n\right)^2}$$

$$a_{6,i}^{n} = \frac{1}{\left(1+\eta/\xi_e^n\right)^2}$$

Further, the terms in the parenthesis in equation I-55 can be denoted by constants to give the following final form of linear diffusion equation.

$$a_{14,i}^{n}\alpha_{i-1}^{n} + a_{15,i}^{n}\alpha_{i}^{n} + a_{16,i}^{n}\alpha_{i+1}^{n} - a_{12,i}^{n}\delta^{n} = a_{13,i}^{n} \qquad \text{(I-56)}$$

This is valid from *i=2 to p-1*, considering *p* is the outermost boundary. A schematic of the co-ordinates and equations valid is presented in Figure A2.

AI.3.1.3. Boundary Condition at the Interface

(i) At the interface

Equations I-23, I-36, I-37, I-38, I-40 and I-41 are substituted into equation I-29 and the higher order terms of δ and α are neglected to obtain the linear form of the boundary condition at the interface. Further the finite difference approximation from equation I-43, I-45 and I-46 are applied to get the following simplified form.

$$\frac{\alpha_2^n}{\Delta\eta}-\left[\frac{1}{\Delta\eta}+Ja\frac{d\xi_e^n}{d\tau}+\frac{Ja}{3\Delta\tau}\xi_e^n\right]\alpha_1^n-\left[Ja\frac{C_{e,1}^{*,n}}{\Delta\tau}+\frac{Ja}{3}\frac{\partial C_{e,1}^{*,n}}{\partial\tau}\right]\delta^n$$

$$=-\left(\frac{\partial C_e^{*,n}}{\partial\eta}\right)_{\eta=0}+Ja\left[C_{e,1}^{*,n}\frac{d\xi_e^n}{d\tau}+\frac{\xi_e^n}{3}\frac{\partial C_{e,1}^{*,n}}{\partial\tau}\right] \qquad \text{(I-57)}$$

The terms in the parenthesis are known and the derivatives can be calculated using equations I-48 to I-52. Denoting the terms in the parenthesis with constants we end up with the following form of equation I-57:

$$a_2^n\alpha_2^n-a_3^n\alpha_1^n-a_4^n\delta^n=a_5^n \qquad \text{(I-58)}$$

(ii) At far away boundary

Discretizing no-flow boundary condition (Equation I-30) at the far boundary results in:

$$-\alpha_{p-1}^n+\alpha_p^n=C_{e,p-1}^{*,n}-C_{e,p}^{*,n}=a_{17}^n \qquad \text{(I-59)}$$

AI.3.2. Matrix Formation

Writing all the linearised finite difference form of equations together

(i) Hydrodynamic Equation

$$a_1^n\delta^n-G\alpha_1^n=b_1^n \qquad \text{(I-60)}$$

(ii) Diffusive equation

$$a_{14,i}^n\alpha_{i-1}^n+a_{15,i}^n\alpha_i^n+a_{16,i}^n\alpha_{i+1}^n-a_{12,i}^n\delta^n=a_{13,i}^n \text{ for } i=2 \text{ to } p-1 \qquad \text{(I-61)}$$

Writing diffusion equation for all the co-ordinate points

for i=2 $\quad a_{14,2}^n\alpha_1^n+a_{15,2}^n\alpha_2^n+a_{16,2}^n\alpha_3^n-a_{12,2}^n\delta^n=a_{13,2}^n \qquad$ (I-61-1)

for i=3 $\quad a_{14,3}^n\alpha_2^n+a_{15,3}^n\alpha_3^n+a_{16,3}^n\alpha_4^n-a_{12,3}^n\delta^n=a_{13,3}^n \qquad$ (I-61-2)

.....

.....

for i=p-1 $\quad a_{14,p-1}^n\alpha_{p-2}^n+a_{15,p-1}^n\alpha_{p-1}^n+a_{16,p-1}^n\alpha_p^n-a_{12,p-1}^n\delta^n=a_{13,p-1}^n \qquad$ (I-61-p-2)

(iii) Boundary condition

$$a_2^n\alpha_2^n - a_3^n\alpha_1^n - a_4^n\delta^n = a_5^n \qquad \text{for } i=1 \qquad \text{(I-62)}$$

$$-\alpha_{p-1}^n + \alpha_p^n = a_{17}^n \qquad \text{for } i=p \qquad \text{(I-63)}$$

writing linear equations I-60 to I-63 in a matrix results in the following matrix:

$$\begin{bmatrix}
a_1^n & -G & 0 & 0 & 0 & 0 & \cdots & 0 & 0 \\
-a_4^n & -a_3^n & a_2^n & 0 & 0 & 0 & \cdots & 0 & 0 \\
-a_{12,2}^n & a_{14,2}^n & a_{15,2}^n & a_{16,2}^n & 0 & 0 & \cdots & 0 & 0 \\
-a_{12,3}^n & 0 & a_{14,3}^n & a_{15,3}^n & a_{16,3}^n & 0 & 0 \cdots & 0 & 0 \\
-a_{12,4}^n & 0 & 0 & a_{14,4}^n & a_{15,4}^n & a_{16,4}^n & 0 \cdots & 0 & 0 \\
\cdots & & & & & & & & \\
\cdots & & & & & & & & \\
\cdots & & & & & & & & \\
-a_{12,p-2}^n & 0 & 0 & \cdots & & a_{14,p-2}^n & a_{15,p-2}^n & a_{16,p-2}^n & 0 \\
-a_{12,p-1}^n & 0 & 0 & \cdots & & 0 & a_{14,p-1}^n & a_{15,p-1}^n & a_{16,p-1}^n \\
0 & 0 & 0 & \cdots & & 0 & -1 & 1 &
\end{bmatrix}
\begin{bmatrix} \delta^n \\ \alpha_1^n \\ \alpha_2^n \\ \alpha_3^n \\ \alpha_4^n \\ \cdots \\ \cdots \\ \cdots \\ \alpha_{p-2}^n \\ \alpha_{p-1}^n \\ \alpha_p^n \end{bmatrix}
=
\begin{bmatrix} b_1^n \\ a_5^n \\ a_{13,2}^n \\ a_{13,3}^n \\ a_{13,4}^n \\ \cdots \\ \cdots \\ \cdots \\ a_{13,p-2}^n \\ a_{13,p-1}^n \\ a_{17}^n \end{bmatrix}$$

The above matrix is solved by LU decomposition at each time step. The direct result form the matrix provides the error values, which are then used to find the solution for radius, pressure and concentrations at various points. A tolerence limit is specified for error values to ascertain that an accurate solution has been reached. The program is iterated in the same time step, renewing guess value everytime, until the tolerence limit is satisfied.

The algorithm for the solution of the problem is given in Appendix –II.

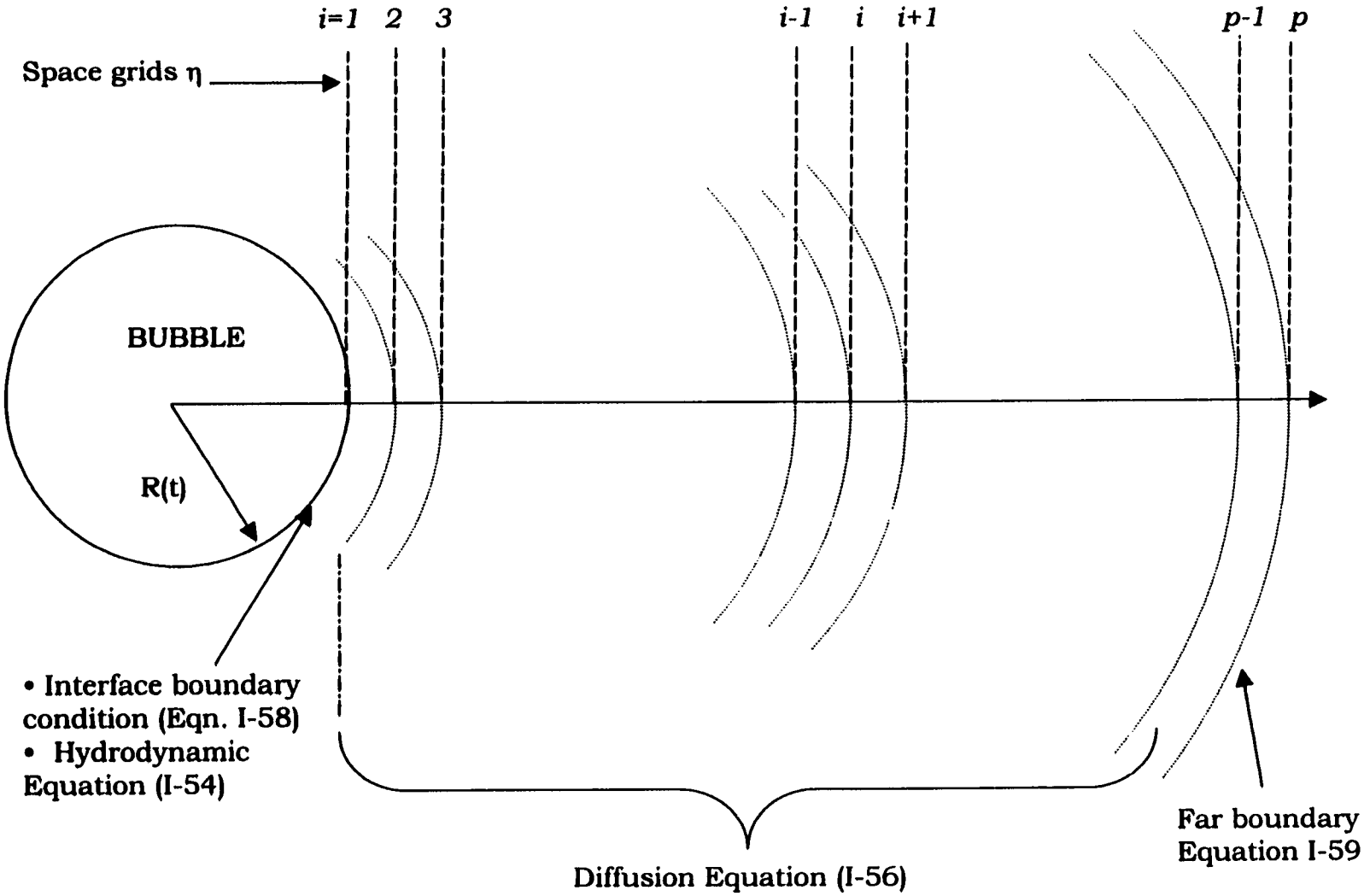

Figure A2: Schematic of the numerical solution scheme

APPENDIX - II
ALGORITHM FOR SOLUTION